The CSN-CRL pathway and two p27^{Kip1} mutations in renal cancer cells

DISSERTATION

zur Erlangung des akademischen Grades des
Doktors der Naturwissenschaften (Dr. rer. nat.)

eingereicht an der Lebenswissenschaftlichen Fakultät
der Humboldt-Universität zu Berlin

im Fach Biologie

von

M. Sc. Linda Gummlich

Präsident der Humboldt-Universität zu Berlin: Prof. Dr. Jan-Hendrik Olbertz

Dekan der Lebenswissenschaftlichen Fakultät: Prof. Dr. Richard Lucius

Gutachter/in: 1. Prof. Thomas Sommer

2. Prof. Wolfgang Dubiel

3. Prof. Carsten Stephan

Datum der Promotion: 13.07.2016

Zusammenfassung

Nierenzellkarzinome (RCC) gehören zu den häufigsten malignen Tumoren weltweit. Aufgrund der alarmierend hohen Inzidenz- und Sterberate besteht ein dringender Bedarf an neuen therapeutischen Targets zur Behandlung von RCCs. Punktmutationen in der Codesequenz von Proteinen führen zu einer Anhäufung von fehlgefalteten Proteinen in Tumorzellen und erfordern eine stärkere Kontrolle der Proteinqualität. Das Ubiquitin-Proteasome-System (UPS) bietet daher ein ideales therapeutisches Target für die RCC Therapie. Aktuelle Veröffentlichungen deuten auf eine Deregulation des COP9 Signalosome (CSN)-Cullin-RING-Ubiquitin-Ligase-(CRL)-Signalweges hin, einem Bestandteil des UPS. In der vorliegenden Arbeit wurden ausgewählte Komponenten des CSN-CRL Signalweges im RCC Gewebe und in vier RCC Zelllinien untersucht. In immunohistochemischen Studien am klarzelligen RCC-Gewebe konnte keine Hochregulierung einer einzelnen CSN-Untereinheit gezeigt werden. Höchstwahrscheinlich ist der gesamte CSN-Komplex im klarzelligen Nierenkarzinom im Vergleich zu nicht-malignem Nierengewebe stärker exprimiert. Die Untersuchung von vier RCC-Zelllinien zeigte eine interessante Deregulierung der CAND1-Skp2-p27 Achse in einer der Zelllinien. 786-O Zellen wiesen zwei $p27^{Kip1}$ (p27) Varianten (p27V109G und p27I119T), eine Erhöhung des Skp2 und eine Reduktion des CAND1 Levels auf. Die Expression und Lokalisation von CAND1 wurde weiter in einer größeren RCC-Kohorte untersucht. Dabei zeigte sich eine negative Korrelation zwischen einer hohen zytosolischen CAND1 Expression und dem Gesamtüberleben von Patienten mit klarzelligen renalen Tumoren. Beide p27 Varianten werden durch das UPS abgebaut und binden an das CSN, Skp2, Cdks sowie an Cyclin E. Interessanterweise zeigte die p27 Mutanten beinhaltende Zelllinie 786-O eine höhere Proliferationsrate als die p27-Wildtyp-Zelllinie A498. In einem im Rahmen dieser Arbeit entwickelten Genotypisierungs-Assay konnte eine große RCC-Kohorte nach den beiden p27-Mutanten untersucht werden. In 42,5% der RCC Patienten konnte die Mutante p27V109G heterozygot nachgewiesen werden. Die Präsenz der beiden Mutanten p27V109 und p27I119T im RCC-Gewebe sowie die veränderte Expression von Skp2 und CAND1 machen den CSN-CRL Signalweg zu einem attraktiven therapeutischen Target für die Behandlung von Patienten mit Nierenzellkarzinom.

Abstract

Renal cell carcinomas (RCC) belong to the most common malignant tumors worldwide. Alarming high incidence and mortality rates elucidate the urgent need for new therapeutic targets in RCCs. Point mutations in protein coding sequences lead to numerous unfolded proteins in cancer cells, requiring effective protein quality control. Therefore, components of the ubiquitin proteasome system (UPS) might be a promising new approach for RCC therapy. Recent publications in renal cancers point to a deregulated COP9 signalosome (CSN)-Cullin-RING Ubiquitin Ligase (CRL) pathway, a segment of the UPS. In the present thesis, selected components of the CSN-CRL pathway were studied in RCC tissues and four RCC cell lines. Immunohistochemistry results did not show an overexpression of a single CSN subunit in clear cell RCC tissues (ccRCC). However, it seems that the CSN holo complex is upregulated in analyzed ccRCCs. Examination of four RCC cell lines revealed a deregulation of the CAND1-Skp2-p27 axis in 786-O cells. These cells harbor two $p27^{Kip1}$ (p27) mutants (p27V109G and p27I119T), high Skp2 and decreased CAND1 levels. Expression and localization of CAND1 was studied in a larger cohort of RCC tissues and revealed high cytosolic levels of CAND1 to be negatively correlated with overall survival in ccRCC patients. Both p27 variants were found to be degraded by the UPS and bound to the CSN, Skp2, Cdks and cyclin E. Interestingly, 786-O cells appear to grow 3-fold faster than A496 cells expressing p27wt. Further, a large cohort of RCC was screened for both p27 variants using a genotyping assay, specifically designed within the present thesis. 42.5% of the RCC patients harbor p27V109G heterozygously. The occurrence of p27V109G and p27I119T in RCC tissues as well as changed expression of Skp2 and CAND1 make the CSN-CRL pathway an attractive therapeutic target for the treatment of patients with RCC.

Table of Content

1. Introduction

1.1 The Ubiquitin Proteasome System (UPS)

The ubiquitin (Ub) proteasome system (UPS) is involved in the maintenance of proteins in all eukaryotes (Hershko and Ciechanover, 1998). The UPS target proteins are labeled with K48-linked ubiquitin chains for proteolysis by the 26S proteasome (Fig. 1) (Hershko and Ciechanover, 1998). Three important enzyme families are involved in the ubiquitination cascade. First, Ub is activated by an Ub-activating enzyme (E1), then transferred by Ub-conjugating enzymes (E2s) and ligated by Ub ligases (E3s) to the protein substrate (Duda et al., 2008; Saha and Deshaies, 2008; Boh et al., 2011). Ub labeled proteins are recognized and degraded by the 26S proteasome. Single Ub is reused for further protein labeling (Fig. 1). The specificity of ubiquitination is assured by a great diversity of 600-700 E3 in human cells. Two main families of E3 exist characterized by conserved structural domains; HECT (Homology to E6AP C-terminus) and the RING (Really interesting new gene) domain containing E3 (Skaar et al., 2014).

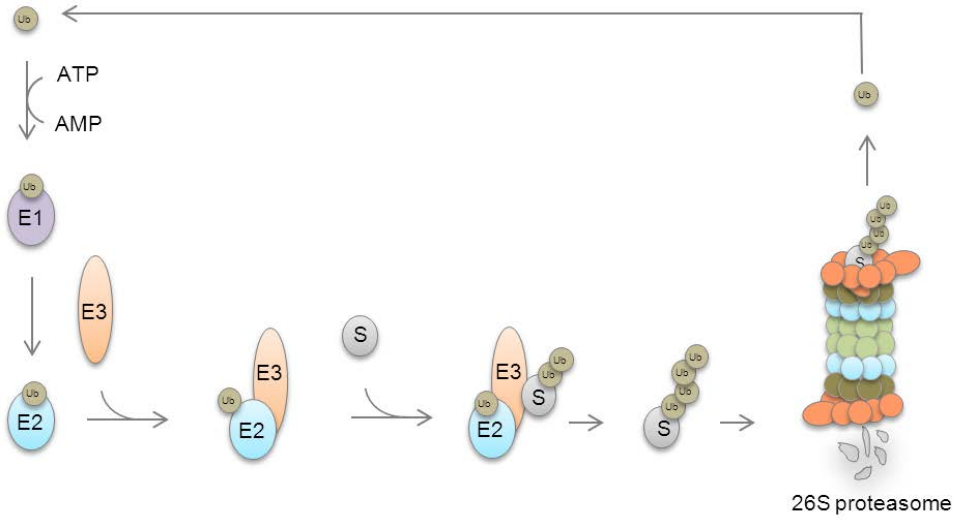

Fig. 1: Protein degradation by the UPS. Ub is activated by an E1 enzyme and transferred to an E2 enzyme, bound to an E3. Ub ligases mediate the transfer of Ub to its specific target protein. Proteins labeled with Ub chains bind to the 26S proteasome (Gummlich et al., 2016).

HECT ubiquitinate substrates in a two-step reaction (Wertz et al., 2011). Ub is transferred from the E2 to an active site cysteine in the E3 and further from the E3 to the substrate (Huibregtse et al., 1995; Spratt et al., 2014). Contrary, the E3 RING family catalyzes the transfer of Ub from E2 directly to the substrate (Deshaies and Joazeiro, 2009). Cullin-RING-Ub ligases (CRLs) comprise the major portion of Ub ligases and ~20% of the proteasome-dependent cellular protein degradation is mediated by these E3s (Lee et al., 2011a). Ub ligases themselves demand precise regulation. In case of CRLs two components of the UPS, the multimetric complex COP9 signalosome (CSN) and cullin-associated and neddylation-dissociated 1 (CAND1), regulate the prominent E3 and constitute the CSN-CRL pathway (Gummlich et al., 2013).

1.1.1 Cullin-RING-Ub Ligases (CRLs)

CRLs are multisubunit complexes comprising the largest family of E3 Ub ligases with more than 250 family members (Lee et al., 2011a). Each CRL is composed of a cullin scaffolding protein (CUL1-7), a C-terminal bound RING finger protein (Rbx1 or 2) and a N-terminal bound substrate recognition subunit (SRS) (Deshaies and Joazeiro, 2009; Sarikas et al., 2011). In most of the CRLs the SRS is linked via adapter protein to the cullin (Bosu and Kipreos, 2008). CRLs are activated via covalent modification of cullins by the Ub-like protein Nedd8 (Liakopoulos et al., 1998). Substrate specificity of CRLs is assured by a variety of SRSs. In case of CUL1 the SRSs are F-box proteins (FBPs) and complexes are called $CRL1^{FBP}$ (Petroski and Deshaies, 2005). The SRS von Hippel-Lindau (VHL) forms complexes with CUL2 ($CRL2^{VHL}$). CRL3 complexes are associated with BTB proteins as SRS ($CRL3^{BTB}$) (Deshaies and Joazeiro, 2009).

Different CRLs were found in distinct molecular pathways. CRL1 complexes are involved in cell cycle regulation (Petroski and Deshaies, 2005), whereas CRL3 complex are associated with control of cell differentiation (Dubiel et al., 2015a). Further, functional alterations of $CRL3^{BTB}$ have been linked to metabolic disorders, muscle and nerve degeneration as well as cancer (Genschik et al., 2013). CRL4 complexes act on chromatin and play crucial roles in DNA repair and chromatin remodeling. They can provoke drug resistance and counteract chemotherapy (Hannss and Dubiel, 2011).

Often substrate modification is required to mark substrates for recognition by CRLs and subsequent ubiquitination. Under normal conditions hydroxylation of HIF-1α by prolyl-hydroxylases directs the substrate to bind to $CRL2^{VHL}$ for ubiquitination and degradation.

Hypoxic conditions inactivate prolyl-hydroxylases and promote HIF-1α target genes inducing angiogenesis (Hoeller and Dikic, 2009). Moreover, phosphorylation of the prominent cell cycle regulator p27 on Thr187 stimulates the binding to $CRL1^{Skp2}$ leading to its ubiquitination and degradation (Skaar et al., 2013).

1.1.2 The $CRL1^{Skp2}$ substrate p27

The protein p27 (also known as KIP1 or $p27^{Kip1}$) is an atypical tumor suppressor and a potent inhibitor of various cyclin-dependent kinase (Cdks) complexes and a regulator of cell cycle G1-S phase transition (Besson et al., 2008). The Cdk inhibitor 1B (*CDKN1B*) gene is mapped on chromosome 12p13 and encodes for a 27kDa protein conserved in a variety of eukaryotes including yeast and *A. thaliana* (Suarez et al., 2000; Barberis et al., 2005; Chu et al., 2008; Guérinier et al., 2013; Roy and Banerjee, 2015). Two decades ago, Fero and co-workers created the first p27 null mice, which displayed an overall increased body size and multiple organ hyperplasia and suggested p27 involvement in growth limitation (Fero et al., 1996). Since then p27 emerged as one of the best characterized cell cycle regulators and is involved in numerous malignancies.

For an ordered cell cycle progression the interaction between cyclins and Cdks has to be tightly controlled (Fig. 2, green box). One of the key events in cell cycle regulation is transversion of the restriction point late in G1 phase. It is crucial to the cell's destiny towards division, differentiation, senescence or apoptosis. Cyclin-Cdk binding is controlled by several Cdk inhibitor proteins to ensure sufficient Cdk activity for each phase of the cell cycle, especially for the activation of gene transcription required for G1-S transition (Chu et al., 2008).

In G0 and early G1 phase, p27 translation and protein stability are at a maximum and enable binding to and inhibition of Cdks (Fig. 2, red box) (Chu et al., 2008). During that cell cycle phase p27 was found to preferentially inhibit cyclin A-Cdk2 or cyclin E-Cdk2 complexes (Fig. 3) (Blain et al., 1997) and to promote the assembly of cyclin D-Cdk 4/6 complexes in early G1 to mid-G1 phase (LaBaer et al., 1997). However, under adverse conditions, including contact inhibition (due to $p27^{Y88}$ or $p27^{Y89}$) or UV radiation, p27 mediates inhibition of D-type cyclin Cdks. Consequently, p27 coexists in both, cyclin bound inhibitory and non-inhibitory confirmations (James et al., 2008). These interesting findings launched the current development of specific pharmacological Cdk inhibitors, targeting cyclin-Cdk binding with observed anti-tumor effects (e.g. Flavopridol) (Cihalova et al., 2015; Roy and Banerjee, 2015) or anti-viral effects (Schang, 2005).

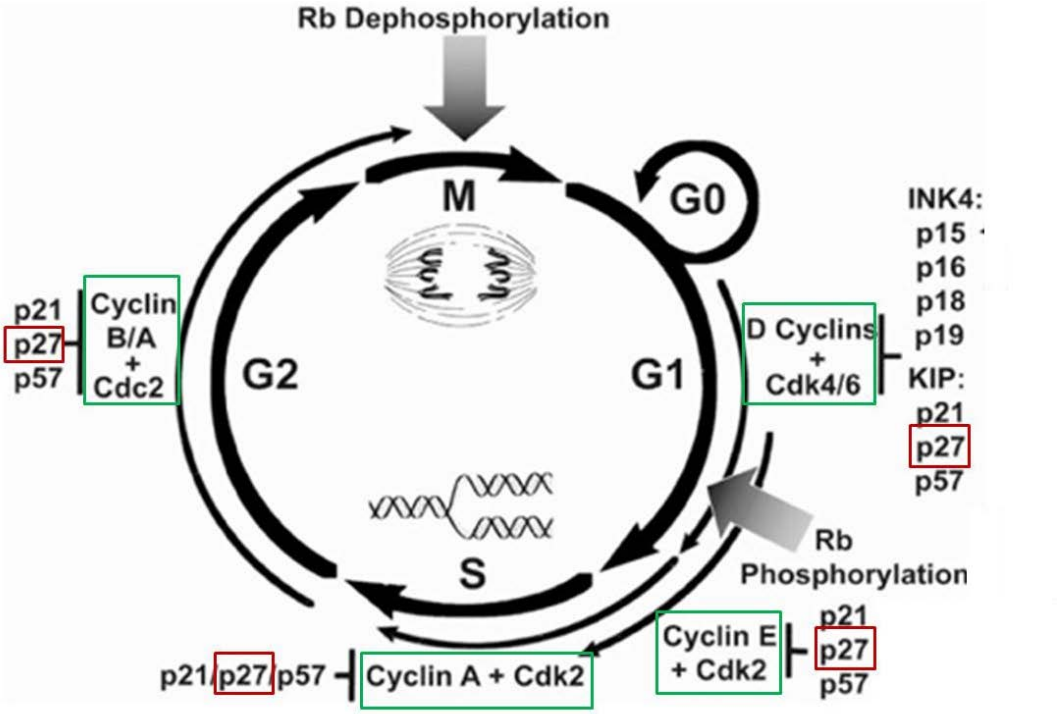

Fig. 2: Cdk inhibitor p27 during the cell cycle (G1-M phase). Cell cycle progression is mediated by cyclin-dependent kinases (Cdks) and their corresponding cyclins (Cyclin A-Cdk2, Cyclin E-Cdk2 and Cyclin D-Cdk 4/6) (green box). Their activities are regulated by phosphorylation and by Cdk inhibitors. Two inhibitor families are involved: inhibitors of the Cdk4 (INK4) family (p15, p16, p18 and p19) and the kinase inhibitor protein (KIP) family (p21, p27 and p57), including p27 (red box). Rb = retinoblastoma protein. (Donovan and Slingerland, 2000, modified).

Many signal transduction networks control p27 protein levels, contributing to the final decision between cell proliferation and cell-cycle exit. p27 homeostasis is fine regulated by multiple proteins on transcriptional as well as translational level (for review see (Chu et al., 2008)). Nevertheless, protein degradation has a major impact on p27 regulation (Fig. 3). Proteolysis of p27 rises dramatically during G1 phase and the p27 half-life falls five- to eightfold during G1-S phase (Nakayama and Nakayama, 2006). The activity of p27 is tightly controlled by protein concentration, subcellular localization and phosphorylation status. The latter is regulated by prominent kinases (Chu et al., 2008) and can also lead to change of cellular localization of p27 (Ishida et al., 2000). In early G1 phase, p27 break down is cytosolic and initiated by nuclear export following degradation (Fig. 3a). Phosphorylation of p27 on S10 by hKIS kinase promotes translocation via CRM1 from the cell nucleus to the cytoplasm. In the cytosol $p27^{S10}$ is recognized by the RING finger ligase KPC (Kip1 ubiquitination-promoting complex) inducing ubiquitination and subsequent proteasomal degradation. In addition,

phosphorylation of p27 at T157 and T198 by Akt kinase prevents the return to the cell nucleus (Roy and Banerjee, 2015) and promotes the assembly of Cyclin D-Cdk4/6 complexes (Fig. 3b).

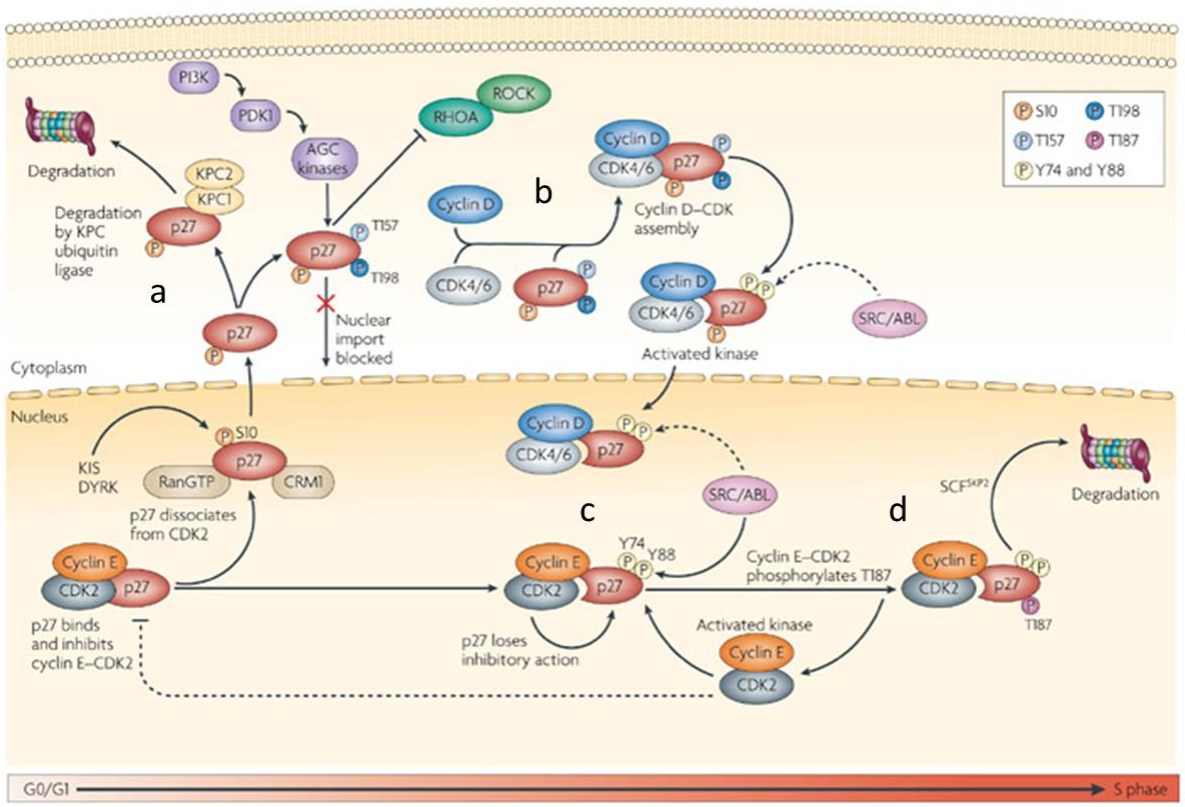

Fig. 3: Model of signaling pathways that regulate p27 during the cell cycle. (a) In early G1 phase $p27^{S10}$ is transferred from the nucleus to the cytoplasm and recognized by the KPC complex. (b) Phosphorylated $p27^{S10/Y187/Y198}$ promotes CyclinD-Cdk4/6 assembly. (c) $p27^{Y74/Y88}$ impairs Cdk inhibitory activity. (d) $p27^{T187}$ is recognized and ubiquitinated via $CRL1^{Skp2}$ and degraded by the UPS (Chu et al., 2008, modified).

In mid G1 phase the oncogenic kinases Src and Abl phosphorylate p27 at tyrosines Y74 and Y88 (Fig. 3c) and impair the ability of p27 to inhibit Cdks. Unphosphorylated Y88 is part of the 310-helix that normally inserts into the ATP-binding site of the Cdk (Grimmler et al., 2007; Roy and Banerjee, 2015). During S till mid G2 phase, phosphorylation on Thr187 by active cyclin E-Cdk2 leads to the ubiquitination of p27 via $CRL1^{Skp2}$ (feedback loop). Skp2 and its accessory protein Cks1 specifically recognize $p27^{Thr187}$ in a phosphorylation-dependent manner (Fig. 3d) that is characteristic for an FBP substrate interaction (Carrano et al., 1999).

Ubiquitinated p27 is recognized and degraded by the UPS. Skp2 overexpression was found in various cancers and correlates with reduced p27 levels. Consequently, small inhibitory molecule inhibitors are currently developed as a novel strategy to treat cancers dependent on the Skp2-p27 axis (Wu et al., 2012). Furthermore, the CSN also regulates p27 proteolysis during G1 phase as shown by our group (Huang et al., 2006).

1.1.3 The COP9 Signalosome (CSN)

The CSN complex was first identified in plants (*Arabidopsis thaliana*) as repressor of constitutive photomorphogenesis (Wei et al., 1994; Chamovitz et al., 1996; Wei and Deng, 1998) and was found conserved in all eukaryotes (Seeger et al., 1998; Wei and Deng, 2003). The human CSN consists of eight distinct subunits (CSN1-8) as displayed in Fig. 4 (Deng et al., 2000; Wei et al., 2008; Schmaler and Dubiel, 2010). The CSN shows similarity to the 26S proteasome LID complex and to the translation initiation complex 3 (eIF3) suggesting a common ancestor of all three complexes (Meister et al., 2015). All subunits are essential for cell survival and mutation in any of them is lethal in mice (Wei et al., 2008; Lingaraju et al., 2014). Six of the CSN subunits harbor a C-terminal *Proteasome-COP9 signalosome-Initiation factor eIF3* (PCI) domain (CSN1, CSN2, CSN3, CSN4, CSN7 and CSN8, labeled green in Fig. 4) (Hofmann and Bucher, 1998). The remaining two subunits exhibit N-terminal *MOV34-Pad1-N-terminal (MPN)* domains (CSN5 and CSN6) (Fig. 4, labeled pink) (Deng et al., 2000). Holding a MPN+/JAMM motif, the CSN functions as an isopeptidase by removing NEDD8 and is a member of the JAMM family of deubiquitinating enzymes (DUBs). The subunit CSN5 provides the catalytic centre for the CSN (Cope et al., 2002) and requires the whole CSN complex for its activity (Echalier et al., 2013).

CSN complex composition differs among different species and a number of CSN variants exist resulting from CSN subunit isoforms (for review see (Dubiel et al., 2015b)). In *A. thaliana* two CSN5 and CSN6 subunits were found encoded by homologous genes originating from gene duplicates; CSN5A/B and CSN6A/B (Kwok et al., 1996; Gusmaroli et al., 2007). Recently, Jin and co-workers revealed an important role of CSN^{CSN5B} complexes in seed development and suggest a model for further examination of CSN5 functions (Jin et al., 2014). CSN complex diversity was also found in mammals. The complexes CSN^{CSN7A} and CSN^{CSN7B} complexes were found coexisting in human red blood cells (Rozen et al., 2013) and other mammalian cells (Wei and Deng, 1998). Further, CSN variants possessing CSN8A and CSN8B isoform were described (Dubiel et al., 2015b).

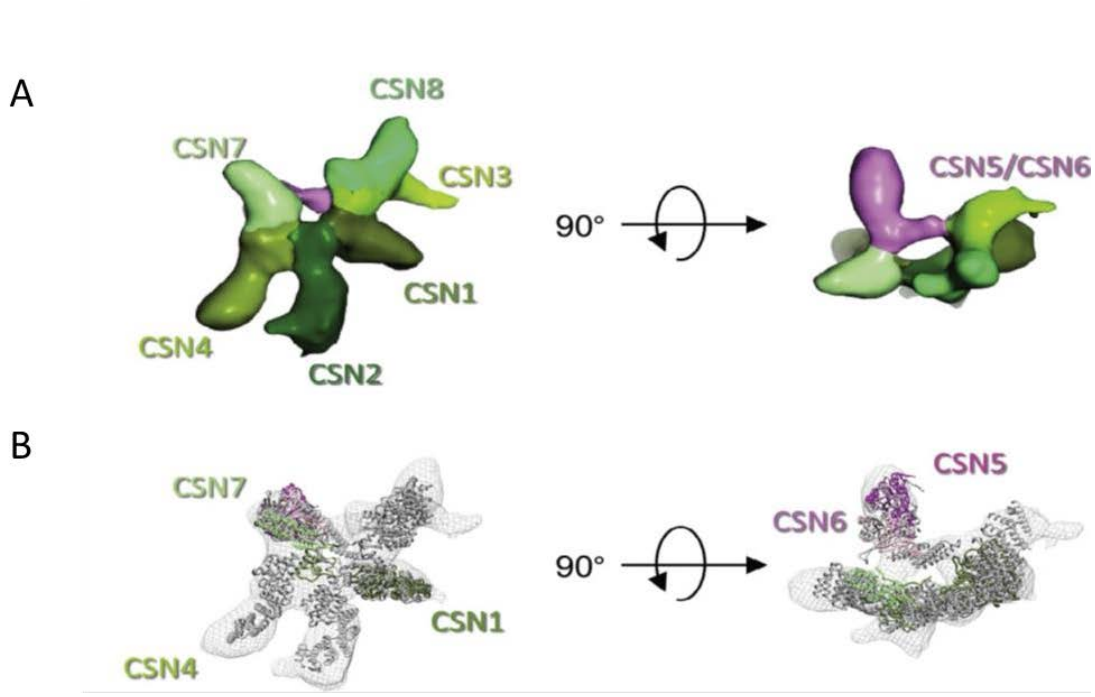

Fig. 4: Cryo-structure of native human CSN. (A) Segmented CSN surface-representation, PCI domains: green, MPN domain: pink. (B) Mesh-representation with ribbon structures of Lid and the CSN subunits, coordinates for CSN subunits are colored, the coordinates for Lid-Rpn9 are not shown (Rockel et al., 2014).

Unfortunately, the functions of $CSN^{CSN7A/B}$ and $CSN^{CSN8A/B}$ complexes have not yet been identified. Apart from varying CSN subunits post-translational modified CSN complexes were also found, e.g. modification by phosphorylation. For example, CSN1 was obtained to be phosphorylated (Fang et al., 2008; Beli et al., 2012). CSN complexes were also found associated with protein kinases (Akt, PKD and CK2), which phosphorylate the CSN subunits CSN2 (Uhle et al., 2003) and CSN7 (Uhle et al., 2003; Dessau et al., 2008). To date the functions of CSN variants and CSN modifications have not yet been identified.

Further, CSN associated kinases specifically modify and regulate stability of substrates of the UPS like p53, c-jun and p27 (Bech-Otschir et al., 2002). The kinase CK2 phosphorylates p27 at two regions. One is central to the protein (amino acids 101–113), and the other was mapped near to the C-terminus (amino acids 170–189) (Huang et al., 2006). Removal of the C-terminal phosphorylation sites stabilized p27 and prevented its proteasomal degradation. Moreover, inhibition of CSN-associated kinase activity by curcumin reduced loss of p27 upon cell cycle re-entry (Huang et al., 2006). Moreover, the CSN subunit CSN5 directly binds to p27 (amino acids 97-151) and the authors indicate cytoplasmic shuttling regulated by CSN5 and other

CSN components (Tomoda et al., 2002). Apart from kinases the CSN also binds DUBs. The Ub-specific protease UPS15 was found to protect components of the UPS (Hetfeld et al., 2005), whereas CSN-associated USP48 confers stability to nuclear NF-κB/RelA (Schweitzer and Naumann, 2015). The interaction between CSN and the deneddylating enzyme 1 (DEN1) promotes Den1 destabilization in human cells (Christmann et al., 2013).

The key function of CSN includes formation of super complexes with CRLs in the CSN-CRL pathway (Fig. 5) (Lyapina et al., 2001; Cope and Deshaies, 2003; Duda et al., 2011; Lingaraju et al., 2014). The pathway is a dynamic interplay of the CSN and CRLs and essential for maintaining protein homeostasis and assuring substrate selectivity (Gummlich et al., 2013; Jin et al., 2014; Dubiel et al., 2015b). Active CRLs modify substrates with Ub chains (Fig. 5a). Therefore, Nedd8 attachment to the highly-conserved lysine on the C-terminus of cullins induces conformational changes of CRLs. Subsequently, Ub molecules are efficiently transferred from E2 enzymes to the targeted substrate. Removal of NEDD8 is performed by the CSN. The CSN complex forms super complexes with CRLs and cleaves NEDD8 via CSN subunit CSN5 metalloprotease activity (Fig. 5b). CSN binding and NEDD8 removal induces

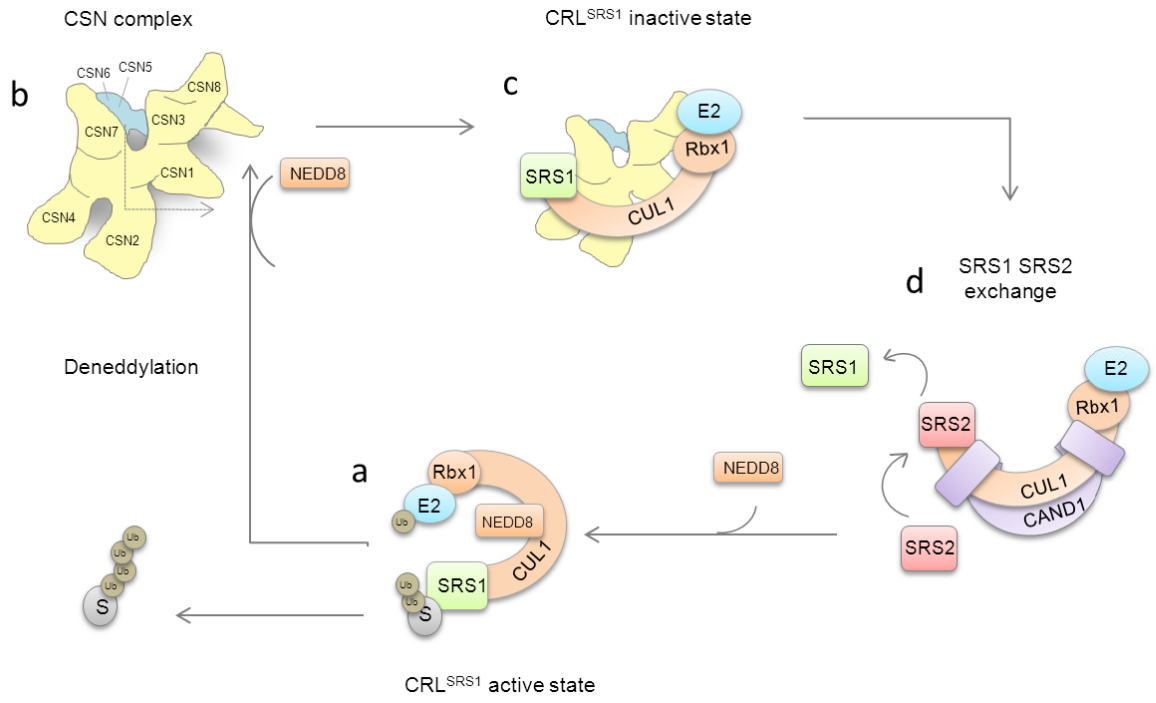

Fig. 5: The COP9 signalosome (CSN)-Cullin-RING Ub ligase (CRL) pathway. (a) Active CRL^{SRS1} ubiquitinates target proteins (S). (b) CSN binds to CRL complexes and removes NEDD8 via intrinsic deneddlyase activity via subunit CSN5. (c) Inactive CRL^{SRS1}-CSN supercomplex. (d) Exchange of SRS1 to SRS2 upon CRL^{SRS1} and CAND1 binding. Rbx = RING box protein (Gummlich et al., 2016).

conformational changes in CRLs and the complexes are maintained in a deactivated state (Fig. 5c). CSN was found to bind predominantly to the C-terminus of CUL1 via the CSN subunit CSN2 (Petroski and Deshaies, 2005; Enchev et al., 2012). Interestingly, structural analysis showed that neddylated CRL1 was bound tighter to CSN than deneddylated CRL1 (Enchev et al., 2012). The inactive deneddylated state prevents autocatalytic breakdown (Schmidt et al., 2009a) and enables new CRL assembly. SRS exchange is supported via subsequent CAND1 protein binding (Pierce et al., 2013) (Fig. 5d). CAND1 increases the dissociation of FBP-Skp1 modules by million-fold (Pierce et al., 2013) and new FBPs are recruited to CUL1. Moreover, exchange of BTB proteins in CRL3 complex initiated by CAND1 was shown recently by our group (Dubiel et al., 2015a). New SRS complexes can remove CAND1 and be reactivated by neddylation for specific substrate ubiquitination. Current studies show that silencing of CAND1 in various species severely alters the cellular repertoire of CRL1 complexes (Dubiel et al., 2013; Pierce et al., 2013). Taken together both, CSN variants and CAND1 control CRLs assembly enabling adjustment to sudden substrate changes.

1.2 Deregulation of the CSN-CRL pathway in cancer

The CSN-CRL pathway is critical for intracellular protein degradation and thereby cellular function (Gummlich et al., 2013). Deregulation of these fine-tuned processes might trigger diseases and cancer. Disturbances within the CSN-CRL pathway have an immense impact on cells. Various components of the pathway can be affected as shown in Tab. 1 (for review see (Gummlich et al., 2013)). Substrate recognition can be prevented by mutations in the substrate gene or additional modifications of the substrate. The expression and function of oncoproteins is often regulated by numerous posttranslational protein modifications including phosphorylation, acetylation and subsequent ubiquitination. Hence, targeting specific posttranslational protein modifications provides an attractive strategy for anticancer drug development (for review see (Ray et al., 2015)). The SRSs can be altered or mutated promoting accumulation of oncoproteins or augmented degradation of tumor suppressors leading to tumorigenesis. For example Skp2 overexpression reduces p27 levels in a subset of human tumors (Gstaiger et al., 2001). In addition, altered cullin, CSN subunit or CAND1 expression was found in various cancers and tumor viruses can manipulate Ub ligases to their advantage (Gummlich et al., 2013).

Tab. 1: Deregulation of selected CSN and CRL components in cancer.

Part	Group	Deregulation	Cancer	Reference
CAND1	Regulator of CRLs	CAND1 levels decreased	Prostate cancer	(Murata et al., 2010; Korzeniewski et al., 2012)
CUL1	Cullins	CUL1 levels decreased	Melanoma, breast cancer	(Chen and Li, 2010)
CUL3	Cullins	CUL3 strongly decreased	RCC	(Berthold et al., 2008)
CUL4	Cullins	CUL4 overexpression	Breast cancer	(Chen et al., 1998)
CUL5	Cullins	CUL5 levels decreased	Lung cancer	(Singhal et al., 2003)
CUL1-7	Cullins	Review of cullins in gastric cancer		(Chen and Yao, 2015)
CSN2	CSN	CSN2 overexpression	Multiple cancer	(Leal et al., 2008)
CSN3	CSN	CSN3 gene amplified	Osteosarcoma	(Yan et al., 2007)
CSN5	CSN	CSN5 overexpression	Multiple cancer	(Patil et al., 2005)
CSN6	CSN	CSN6 overexpression	Breast cancer, multiple cancer	(Lee et al., 2011b)
FBPs	FBP	Review of FBPs in cancer		(Heo et al., 2015),
		Review of FBPs in cancer		(Uddin et al., 2015)
Fbw4	FBP	No Fbw4 dimerization	Esophageal carcinoma	(Barbash et al., 2008)
Fbw7	FBP	Mutations in Fbw7 substrate binding regions, tumor suppressor	Lymphomas, multiple cancer	(Mao et al., 2004), (Welcker and Clurman, 2008)
Keap1	BTB	Mutations in *Keap1* gene, accumulation of Nfr2	Lung cancer	(Singh et al., 2006)
Skp2	FBP	Skp2 overexpression, oncoprotein	Multiple cancers	(Frescas and Pagano, 2008)
β-TrCP	FBP	Oncoprotein/tumor suppressor	Multiple cancers	(Kim et al., 2007)
p27	Substrate	p27 levels decreased	Multiple cancers	(Chu et al., 2008)

Although it has to be stressed that in case of CSN subunits not all the subunits were examined. Consequently, it cannot be ruled out that the whole CSN complex is upregulated rather than one single CSN subunit. Moreover, recent studies in our group revealed a CSN upregulation under conditions of DNA damage response (Feist et al., 2014). The interplay between CSN and CRLs is critical for maintaining genome stability (Hannss and Dubiel, 2011; Meir et al., 2015). Therefore, an increase of the CSN holo complex under cancer conditions and a role in developing drug resistance is very likely (Feist et al., 2014). Recently, inhibition of CSN deneddylating activity has been reported to block tumor growth of diffuse large B-cell lymphomas (Pulvino et al., 2015). Deregulation of CSN-CRL pathway substrate such as p27 and HIF1α have been detected in many tumors. HIF1α was found overexpressed in various tumors, triggering an upregulated expression of proteins that promote angiogenesis, anaerobic metabolism, and many other survival pathways for review see (Koh et al., 2010). These findings marked HIF1α as a potential target and induced the identification of new therapeutic

agents that inhibit HIF-1α (Koh et al., 2010). The tumor suppressor p27 is inactivated through impaired synthesis, accelerated degradation and by mislocalization. Moreover, studies in several tumour types indicate that p27 expression levels have both prognostic and therapeutic implications (for review see (Chu et al., 2008)). Mutations in the *CDKN1B* gene are rare. Germline mutations were found in patients presenting with breast cancer (Spirin et al., 1996) and endocrine carcinomas (Molatore et al., 2010). A current study recognized hairy cell leukemia (HCL) with the highest frequency of *CDKN1B* mutations among cancers and identified *CDNK1B* as the second most common mutated gene in HCL (Dietrich and Zenz, 2015). Although the mutations were not found to impact clinical characteristics or outcome in this cohort, the authors suggest a novel role for alterations in regulation of cell cycle in HCL with *CDKN1B* mutations (Dietrich and Zenz, 2015). Expression levels of the CSN-CRL pathway components CUL3, p27 and Skp2 were found altered in renal carcinomas. However, due to limited clinical data the concrete mechanisms behind these findings have not yet been revealed and are further investigated in the present thesis.

1.3 Renal cell carcinoma (RCC)

1.3.1 The kidney

The main functions of the kidneys include formation of urine, regulation of blood pressure, electrolyte balance as well as being involved in red blood cell and hormone production. The bean-shaped structure of the kidney possesses both a concave and a convex border. It is surrounded by the renal capsule, a tough fibrous tissue, and is embedded in perirenal fat (adipose capsule). A recessed area on the concave border is called renal hilum where the renal artery enters the kidney while the ureter and renal vein leave (Fig. 6). The parenchyma of the kidney is divided into major structures: the outer renal cortex and the inner renal medulla, the latter formed in 6-9 cone-shaped renal lobes (renal pyramids) (Boron, 2012). The renal nephron is the urine producing subunit of the kidney and spans the cortex and medulla (Fig. 7b). A human kidney harbors 1-1.2 million nephrons (Boron, 2012). The glomerulus - the initial filtering portion of the nephron - is the renal corpuscle which is located in the cortex, while the collecting ducts are located in the pyramids of the medulla (Fig. 7b,c). Modification of the primary urine occurs mainly in the proximal convoluted tubules; secretion of urea, uric acid, creatinine and amino acids into the tubules takes places as well as the reabsorption of electrolytes, glucose and proteins and water into the blood. Concentration of the urine occurs in the loop of Henle and collecting tubes. Salt concentration and pH is regulated within the distal convoluted tubule (Fig. 7c).

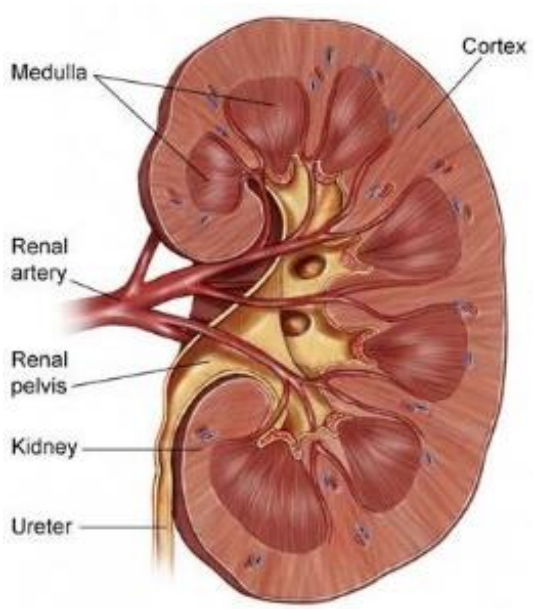

Fig. 6: Anatomy of kidney cross section. The kidney comprises two main structures: the cortex and the medulla, surrounded by the renal capsule. The renal artery enters at the renal hilum whilst the renal vein and ureter exit the kidney (Miller, 2015).

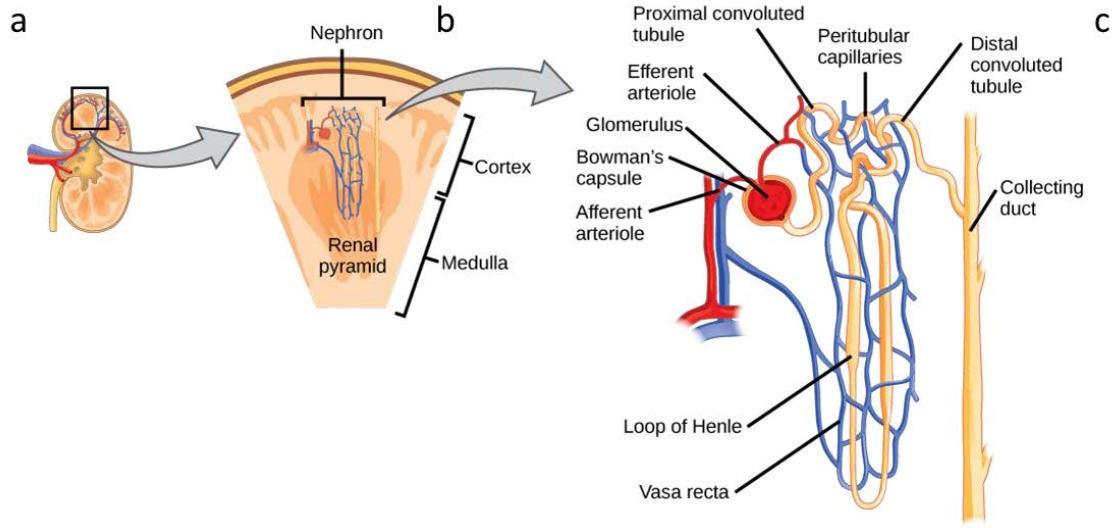

Fig. 7: Scheme of the kidney nephron unit and renal tube formation. (a) Kidney cross section. (b) Nephron unit embedded in renal medulla and cortex. (c) Renal tube formation (Admin, 2015).

1.3.2 Renal cancer etiology and pathobiology

Renal cancer accounts for 2-3% of all adult tumors and this figure is increasing worldwide (Patard et al., 2011). It causes significant morbidity and mortality with 115,200 new RCC cases registered in men and in woman in Europe in 2012. According to their prognosis 42% of RCC patients will die due to their tumors (49,000 cases) (Ferlay et al., 2015). Meanwhile in the United States, 62,700 new RCC cases in men and women were predicted for 2016. Most likely 14,240 will die as a result from their disease (Siegel et al., 2016). Renal tumors are twice as common in males as in females and are most prevalent between 60 and 70 years of age (Ljungberg et al., 2015). Large epidemiological studies have established risk factors for RCC including smoking cigarettes, obesity, end-stage renal failure, western-style diet, hypertension and a family history of renal cancer (Patard et al., 2011). Familial predisposition seems to be a risk only in relatively few RCC cases (Curti, 2014).

Contrary to initial assumption, kidney cancers are very heterogeneous. There are a number of distinct morphotypes with individual histological and prognostic features, each caused by mutations of different genes (Patard et al., 2011). The four main prominent subtypes are clear cell RCC (ccRCC, 80-90%), papillary RCC (pRCC, 10-15%), chromophobe RCC (cRCC 4-5%) and few oncocytomas (Lopez-Beltran et al., 2006). Most papillary and ccRCC were found to originate from the proximal renal tubular epithelium whereas chromophobe RCC and oncocytomas start frequently in the collecting duct.

1.3.3 Renal cancer diagnosis, prognosis and therapy

Primary RCCs show no early clinical symptoms. Only 10% of patients present with the classic triad of flank pain, hematuria, and flank mass (Curti, 2014). Fortunately the use of new techniques such as ultrasound, computerized tomography and magnetic resonance imaging has increased the detection rate of asymptomatic tumors (Abecasis et al., 2012). However, at the time of discovery, 20% of the RCC patients already present with distant metastases in lung, brain, bones and liver and another 30% of the patients would develop metastases after nephrectomy causing high morbidity and poor prognosis (De Mulder, 2007).

RCC progression is characterized by a TNM staging system (Greene and Sobin, 2002; Webber et al., 2014) and histological appearance (Fuhrman grade), which is used to estimate the patient's risk and possible therapy strategies (Delahunt et al., 2015). T abbreviates tumor and the current tumor size (T1-4) pathologically (p). N and M portray the metastasis process (M0 or

M1) including involvement of adjacent lymph nodes (N0 or N1). Stage 1 (pT1) tumors appear only in the kidney and are smaller than 7 cm (pT1a < 4 cm, pT1b > 4 cm) (Fig. 8). pT2 tumors are larger than 7 cm in width but are still restricted to the kidney. RCC tumors larger than 7 cm and that grow into a major vein or into tissue around the kidney, but into the adrenal gland (top of the kidney) or beyond Gerota's fascia (the fibrous layer surrounding the kidney and nearby fatty tissue) are categorized as pT3 tumors (pT3a-c). pT4 tumors spread beyond Gerota's fascia, may grow into the adrenal gland and nearby lymph nodes (Fig. 8).

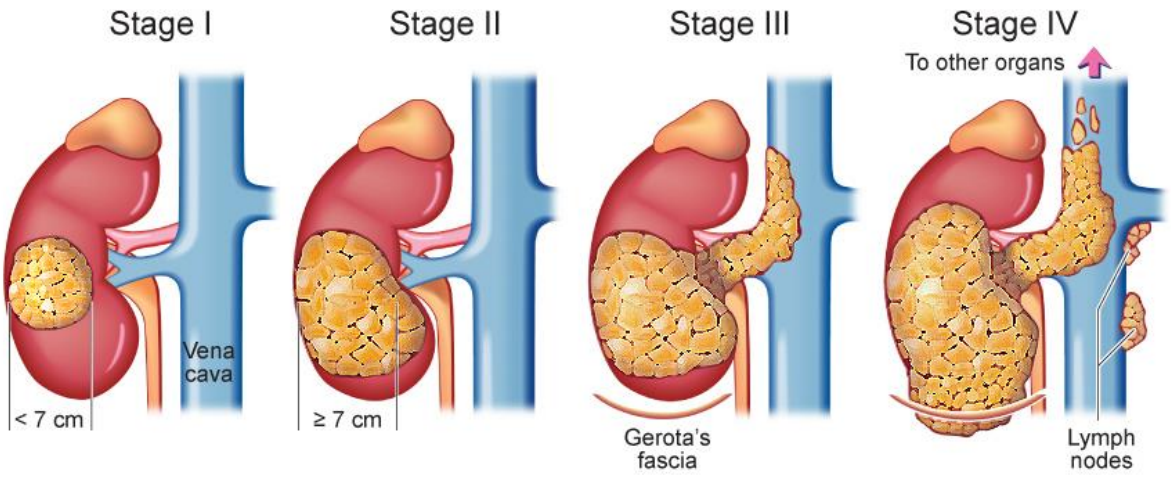

Fig. 8: Illustration of RCC tumor stages pT1-4 (New, 2015).

Furthermore, RCCs are categorized by Fuhrman grading as shown in Tab.2. A number of advances in the management of kidney cancers have been developed over the past decades, including surgery options, immunotherapy and targeted therapy. RCC morphological subtypes have different clinical courses and drug responses and therefore require individual therapy. Currently, standard treatment of localized tumors (pT1-2) involves partial nephrectomy (nephron-sparing surgery) rather than the radical tumor nephrectomy (Ljungberg et al., 2015). Almost 20-30 % of localized RCC patients experience relapses after surgery within the following 1-2 years (Patard et al., 2011) and are treated with adjuvant medication. Individualized targeted therapies including tyrosine kinase inhibitors and angiogenesis inhibitors as well as immunotherapy are available for RCC patient subgroups (Su et al., 2014; Ljungberg et al., 2015). Unfortunately, RCC are considered resistant to standard cytotoxic and DNA-damaging therapy, with response rates from 4-18% for single agents or combined therapy (Patard et al., 2011). One explanation could be high expression of the multiple-drug resistance protein P-glycoprotein (mdr-1-related gp-170) in the proximal tubule, an origin of RCCs

(Buczek et al., 2014). Furthermore, there is no general effective curative treatment for metastasized RCC to date. Novel prognostic biomarkers to evaluate RCC patient's risks and more targeted drugs are urgently needed to fight the poor RCC outcomes, especially for RCC that have already metastasized. In order to reveal potential molecular targets for RCC, various involved molecular pathways have been discovered over the past decades.

Tab. 2: Staging system and 5-year disease specific survival of RCC. TNM Staging system according to the American Joint Committee on Cancer (AJCC) and the International Union Against Cancer (UICC) (Patard et al., 2011). pT = tumor, pathologically, N = lymph node invasion, M = metastasis.

Patient group		TNM stage	Fuhrman Grade	5-year survival
Localized disease	Low risk	pT1	1-2	91.1 %
(N0, M0)	Intermediate risk	pT1	1-2	80.4%
		pT1	3-4	
		pT2	any	
		pT3	1	
	High	pT3	2-4	54.7%
		pT4	Any	
Metastatic disease	Low risk	N1M0	Any	32%
		N2, M0/M1	1-2	
	Intermediate risk	N2, M0/M1	1-2	19.5%

1.3.4 Molecular basis of renal cancer

Different genes mutations implicate different RCC histological subtype (Tab. 3). Mutations of the *VHL* gene were specifically detected in ccRCC tumors but not in papillary or chromophobe renal cancer. In hereditary ccRCC the most prominent molecular factor involved is the non-functioning tumor suppressor VHL. Along with these findings almost 90% of sporadic ccRCC were found to harbor an inactive VHL protein (Moore et al., 2011). Germline mutation or deletion in the *VHL* gene leads to a non-functioning protein, affecting the HIF-pathway (Latif et al., 1993; Linehan, 2012; Su et al., 2015). Inactive VHL protein induces impaired proteasomal

degradation of HIF proteins, triggering angiogenic pathways and results in strongly vascularized renal tumors. The transcription factor HIF-1α accumulates and leads to an increase of downstream targets such as VEGF, VEGF receptor and PDGF. The growth factors and their receptors are already targeted by various kinase inhibitors approved by the Food and Drug Administration (FDA) (Choueiri, 2011; Czarnecka et al., 2015), but with limited success due to resistance mechanisms.

Tab. 3: Genetic mutations detected in different RCC morphotypes and their gene loci.

Histological subtype	Gene implicated	Gene locus
Clear cell RCC	*VHL* (Von Hippel-Lindau)	3p25
	*LCSTGR1, 2 (*Lung cancer tumor suppressor 1,2)	3p21, 3p12
	FHIT (Fragile histidine triad)	3p14
	RAS association domain family 1A	3p21
	PBRM1 (Polybromo1)	3p52
	SETD2	3p47
	BAP1 (deubiquitinase BRCA1-associated protein-1)	3p21
Papillary RCC type 1	*MET* (c-MET)	7q31
Papillary RCC type 2	*FH* (fumarate hydratase)	1q42
Papillary RCC	*NFEL2 (*Nuclear factor (erythroid-derived-2)-like 2)	2q31
Chromophobe RCC	*BHD* (Birt-Hogg-Dubé)	17p11
RCC (no subtype defined)	*CUL3 (*Cullin 3)	2q36

Recently, Polybromo1 (PBRM1), SETD2 and BRCA1-associated protein-1 (BAP1) were observed as novel targets for renal cell carcinoma (Brugarolas, 2013). The chromatin-remodeling genes *PBRM1* and *SETD2* were found to be mutated in sporadic ccRCC, revealing deregulation of the chromatin modulation machinery (Linehan, 2012). Truncation mutations in the *PBRM1* gene leading to protein loss were identified in 41% of the ccRCC tumors (Varela et al., 2011) whilst the *SETD2* gene was somatically mutated in 11.5% of ccRCC cases (Network, 2013).

In addition, the deubiquitinase BAP1 was recently found to be altered in ccRCC but not in other RCC subtypes (Network, 2013; Wang et al., 2014). The encoded enzyme binds to the breast cancer type 1 susceptibility protein (BRCA1) via the RING finger domain to form a multiprotein complex and is involved in the regulation of DNA repair, the cell cycle and cell differentiation (Carbone et al., 2013). Mutations in the *BAP1* gene were associated with higher Fuhrman grade and metastasis suggesting BAP1 as a powerful marker in predicting poor oncological

outcomes and adverse clinicopathological features in patients with non-metastatic ccRCC (Joseph et al., 2014; Kapur et al., 2014). BAP1 protein belongs to the Ub C-terminal hydrolase subfamily of DUBs that is involved in the removal of Ub from proteins and acts as a tumor suppressor in various cancers (Carbone et al., 2013). Inactivation or loss of BAP1 protein leads to an accumulation of its target ubiquitinated proteins.

Interestingly, gene mutations found in ccRCC are in the 50-Mb region on the short arm of chromosome 3p that also encompasses the *VHL* gene (Tab. 3). Brugarolas and co-workers discovered *PBRM1* mutations anti-correlating with *BAP1* mutations in ccRCC. Furthermore, *PBRM1*- and *BAP1*-mutated tumors exhibit different biology and are associated with different outcomes. These finding established the foundation for the first molecular genetic classification of sporadic ccRCC (Brugarolas, 2013). The exact role of BAP1, PBRM1 and SETD2 alterations and their interplay with important factors in ccRCC like VHL still remains to be discovered.

The molecular patterns involved in pRCC type 1 and type 2 tumorigenesis are not yet as well understood as for ccRCC. Potential proto-oncogenes mutations within the *MET* gene were discovered whilst screening patient families with hereditary pRCC type 1 (Schmidt et al., 1997). The *MET* gene encodes for the transmembrane receptor tyrosine kinase Met triggering the hepatocyte growth factor (HGF)/MET pathway. Mutations found along with pRCC affect the tyrosine kinase domain suggesting its potential as therapy target (Fay et al., 2014). The dual MET/VEGF inhibitor Foretinib has already been used in a phase II clinical trial that induced a response in 13.5% of the pRCC (Choueiri et al., 2013). Moreover, the small molecule MET inhibitor, INC280, showed a positive response in ovarian cancers and is currently also being tested in a phase II clinical trial in patients with advanced pRCC (Moran-Jones et al., 2015).

Cancer tissues from patients with pRCC type 2 were associated with a defect in the Krebs cycle enzyme, fumarate hydratase (FH), an enzyme that catalyzes the transformation from fumarate to malate (Tomlinson et al., 2002). *FH* gene germline mutations were found in all analyzed samples (Wei et al., 2006). Non-functioning FH protein leads to an accumulation of fumarate and induces metabolic changes providing anaerobic glycolysis as an energy supply in these tumors (Warburg effect). Based on these findings, novel approaches to target tumor vasculature and glucose transport evolved (Linehan, 2012). Furthermore, fumarate leads to an increase of oxidative stress response and activation of the transcription factor nuclear factor (erythroid-derived-2)-like 2 (Nrf2) (Su et al., 2015). In pRCC intracellular levels of Nrf2 are regulated by the $CRL3^{Keap1}$ complex (Ooi et al., 2013). Accumulated fumarate triggers posttranslational modification Keap1 and impairs the recognition of Nrf2 resulting in an increase of Nrf2 target proteins (Adam et al., 2011). On the other hand, mutations in the *NFE2L2* gene causing altered Nrf2 protein can lead to reduced Nrf2 protein degradation (Ooi

et al., 2013). Furthermore, CUL3 was found to be deregulated in RCC. CUL3 protein levels were reduced in RCC patient samples suggesting an accumulation of $CRL3^{SRS}$ substrates, which are involved in fundamental cellular pathways (Berthold et al., 2008). Interestingly, CUL3 is involved in cell differentiation processes (Dubiel et al., 2015a) and loss of CUL3 protein might explain the strong dedifferentiated phenotype of RCC. Despite extensive research and development of targeted agents, a large group of RCC is still therapy resistant and accelerates the urgent need for novel therapy targets. Other pathways aside from those described above might be involved in renal tumorigenesis. The examples summarized above show that the literature is giving hints to deregulation of some CSN-CRL pathway components in RCC. Therefore the investigation of the CSN-CRL pathway deregulation and its substrate p27 is the major focus of the present thesis.

1.4 Aim of this study

RCC remains a largely incurable disease and is the most lethal among common urological cancers. Despite advances in understanding the molecular basis of RCC and treatment options, surgery remains the key curative treatment modality. Considering the limitations of known molecular changes causing individual variants of urological neoplasia and of existing treatment methods, intensified research into novel targetable pathways is necessary. In recent years, on the search for new targets the UPS moved into the focus of interest. It has been hypothesized that cancer cells have an increased burden of unfolded proteins, due to numerous mutations in protein coding sequences. Therefore, inhibition of the UPS in particular the 26S proteasome, which is responsible for the degradation of unfolded proteins, seemed to be a promising approach for tumor therapy. However, unspecific blockage of the proteasome also induced a more explicit targeting of UPS subcomponents/regulators like the CSN or CRLs are recommended. So far CSN-CRL pathway deregulation in RCC had been inadequately described. Apart from clinical data revealing alteration of CUL3, Skp2 and CAND1 expression in urological cancers the exact mechanism of their deregulation and possible involvement in tumorigenesis remains unclear.

1.) A major aim of this study was a systematic immunohistochemical and Western blot analysis of selected CSN-CRL pathway components and their substrates in RCC tissue and RCC cell lines.

2.) In one RCC cell line two p27 mutants were identified as substrates of the CSN-CRL pathway. They are most likely responsible for accelerated proliferation of the particular tumor cell line. The association of the p27 mutants with CSN-CRL pathway deregulation in RCC cancers and other urological neoplasia were addressed in detail in the present thesis.

2. Materials and methods

2.1 Materials

2.1.1 Reagents and chemicals

Product	Company
Agarose	Carl Roth®, Karlsruhe, Germany
Albumin bovine, fraction V	Carl Roth®, Karlsruhe, Germany
ANTI-FLAG® M2 Affinity Gel Freezer Safe	Invitrogen, Darmstadt, Germany
Ammonium persulfate	AppliChem GmbH, Darmstadt, Germany
Antibody Diluent	Invitrogen, Darmstadt, Germany
Aprotinin	Sigma-Aldrich®, Munich, Germany
Aquatex®	MERCK Millipore, Darmstadt, Germany
Bovine serum albumine	Carl Roth®, Karlsruhe, Germany
Cycloheximid	AppliChem GmbH, Darmstadt, Germany
Dimethylsulfoxide	AppliChem GmbH, Darmstadt, Germany
EDTA	AppliChem GmbH, Darmstadt, Germany
Eosin solution (1%)	Waldeck GmbH, Münster, Germany
Ethanol (70%, 90%)	AppliChem GmbH, Darmstadt, Germany
Ethidiumbromid	Sigma-Aldrich®, Munich, Germany
Fast^{TM}FastRed Tr/Naphtol AsMX Tablets	Sigma-Aldrich®, Munich, Germany
Fetal Calf Serum	Biochrom, Berlin, Germany
Glucose	Sigma-Aldrich®, Munich, Germany
Glycerol	AppliChem GmbH, Darmstadt, Germany
Glycine	AppliChem GmbH, Darmstadt, Germany
HEPES	Sigma-Aldrich®, Munich, Germany
Isopropanol	AppliChem GmbH, Darmstadt, Germany
LightCycler®FastStart DNA Master HyProbe	Roche Diagnostics, Mannheim, Germany
Lipofectamin®2000 Transfection Reagent	Invitrogen, Darmstadt, Germany
Mayer's hemalaun solution	Hollborn und Söhne, Leipzig, Germany
Methanol	AppliChem GmbH, Darmstadt, Germany
MG132	Calbiochem, Darmstadt,Gerrmany
Non-essential amino acids (NEAA)	Sigma-Aldrich®, Munich, Germany
Nonfat powdered milk	Carl Roth®, Karlsruhe, Germany
NonidentP40 (NP-40)	AppliChem GmbH, Darmstadt, Germany
OPTI-MEM©+Glutamax	Invitrogen, Darmstadt, Germany

Product	Company
PBS (steril)	PAA Laboratories, Pasching, Austria
Penicillin	Biochrom, Berlin, Germany
Paraformaldehyde	AppliChem GmbH, Darmstadt, Germany
PERTEX®	MEDITE, Burgdorf, Germany
PMSF	AppliChem GmbH, Darmstadt, Germany
Polyoxyethylsorbitanmonolaurat (Tween20)	AppliChem GmbH, Darmstadt, Germany
Ponceau S solution	Sigma-Aldrich®, Munich, Germany
Protein block	DAKO, Hamburg, Germany
Roti®load 1	AppliChem GmbH, Darmstadt, Germany
Protein A - Sepharose® 4B	Thermo Scientific, Dreieich, Germany
Sodium lauryl sulphate	SERVA electrophoresis
Sodium azide	AppliChem GmbH, Darmstadt, Germany
Sodium chloride	AppliChem GmbH, Darmstadt, Germany
Sodiumhydrogenphosphate	Carl Roth®, Karlsruhe, Germany
Sodium pyruvate	Biochrom, Berlin, Germany
Streptomycin	Biochrom, Berlin, Germany
Tetramethylethylenediamine (TEMED)	AppliChem GmbH, Darmstadt, Germany
Trichloroacetic acid (TCA)	Sigma-Aldrich®, Munich, Germany
Tris-(hydroxylmethyl)-aminomethane	AppliChem GmbH, Darmstadt, Germany
Xylol	Sigma-Aldrich®, Munich, Germany
β-Mercaptoethanol	SERVA, Heidelberg, Germany

2.1.2 Kits

Kit	Company
Bio-Rad D_c Protein Assay	BIO-RAD Laboratories, München, Germany
Cell Proliferation Kit II (XTT)	Sigma-Aldrich®, München, Germany
GeneMATRIX Agarose-OUT DNA Purification Kit	Roboklon GmbH, Berlin, Germany
GeneMATRIX PCR/DNA Clean-Up Purification Kit	Roboklon GmbH, Berlin, Germany
Insorb®Spin Plasmid Mini Two Kit	STRACTEC Molecular GmbH
LightSNiP® Assay	TIB MolBiol, Berlin, Germany
NucleoBond®Xtra Midi Kit	MACHERY-NAGEL GmbH, Düren, Germany
QIAamp DNA Mini Kit	Qiagen, Hilden, Germany
RNeasy Mini Kit	Qiagen, Hilden, Germany
TA Cloning® Kit	Invitrogen, Darmstadt, Germany
Transcriptor First Strand Synthesis	Roche, Mannheim, Germany

2.1.3 Buffers and solutions

All buffers and solutions were prepared with double deionized H_2O.

Buffer or solution	Components
Aprotinin solution	10 mg/ml aprotinin
APS solution	10% Ammonium persulfate
Blocking solution	5% milk in 1x PBS-T or 5% BSA in 1x PBS-T
Blotting buffer	25 mM TRIS, 192 mM Glycine, 10% Methanol (pH 8.3)
Citrate buffer (10x)	19.6 mM citric acid, 81.9 mM Trisodium citrate dehydrate (pH 6)
Glycine Buffer	0.1 M (pH 3.5)
Glycerol gradient buffer	20 mM Tris, pH 7.2, 1mM ß-Mercaptoethanol, 50 mM KCl
SDS electrophoresis buffer	25 mM TRIS, 192 mM Glycine, 0.1% SDS
PBS (10x)	1.37 M NaCl, 120 mM Phosphate, 27 mM KCL (pH 7.4)
PBS-T	0.1% Tween20 in PBS
Ponceau S solution	1 g Ponceau, 50 ml acetic acid, 50 ml ddH_2O
Tripple lysis buffer	50 mM TRIS (pH 8.0), 150 mM NaCl, 0.5% sodiumdeoxylcholat, 0.1% SDS, 1% NP-40, 0.02% sodium acid (add fresh: 10 µg/µl aprotinin, 1 mM PMSF)
Mono lysis buffer	50 mM TRIS (pH 8.0), 150 mM NaCl, 1 mM EDTA, 1% Triton X-100
TAE (50x)	2 M TRIS, 2 M acetic acid, 50 mM EDTA
TBS (10x)	190 mM TRIS-HCl, 1.36 M NaCl (pH7.5)
TE	10 mM TRIS-HCl, pH 7.5, 1 mM EDTA

2.1.4 Primary antibodies

Antibodies were diluted as indicated in 5% milk/PBS for Western blotting (WB) and in Antibody Diluent (Invitrogen) for immunohistochemistry (IHC). IP = immunoprecipitation

Antibody	Host species	Company	Method	Dilution
Anti-CSN1	Rabbit IgG	ENZO, Lörrach, Germany	WB, IHC	1:1000, 1:25
Anti-CSN3	Mouse IgG	BETHYL, Montgomery, USA	WB, IHC	1:1000, 1:25
Anti-CSN5	Mouse IgG	GenTex, Inc., USA	WB, IHC	1:500, 1:25
Anti-CSN8	Rabbit IgG	ENZO, Lörrach, Germany	WB, IHC	1:4000, 1:100
Anti-CUL1	Rabbit IgG	Santa Cruz, Heidelberg, Germany	WB, IHC	1:10000, 1:50
Anti-CUL2	Rabbit IgG	Invitrogen, Darmstadt, Germany	WB	1:2000, 1:100
Anti-CUL3	Mouse IgG	BD Transduction laboratories	WB, IHC	1:1000, 1:50

Anti-CAND1	Goat IgG	Santa Cruz, Heidelberg, Germany	WB, IHC	1:1000, 1:50
Anti-Skp2	Rabbit IgG	Santa Cruz, Heidelberg, Germany	WB	1:500
Anti-β-TrCP	Rabbit IgG	Santa Cruz, Heidelberg, Germany	WB	1:1000
Anti-Cdk5	Mouse IgG	Cell Signaling, Danvers, MA, USA	WB	1:250
Anti-Cylin E	Mouse IgG	Santa Cruz, Heidelberg, Germany	WB	1:1000
Anti-p27	Rabbit IgG	Santa Cruz, Heidelberg, Germany	WB	1:500
Anti-p27	Mouse IgG	Santa Cruz, Heidelberg, Germany	WB, IP	1:200, 1:50
Anti-γ-tubulin	Mouse IgG	Santa Cruz, Heidelberg, Germany	WB	1:1000
Anti-Xpress	Mouse IgG	Invitrogen, Darmstadt, Germany	WB	1:1000

2.1.5 Secondary antibodies

Antibodies were diluted as indicated in 5% milk/PBS for Western blotting (WB) or in Antibody Diluent (Invitrogen) for immunohistochemistry (IHC).

Antigen	**Host**	**Company**	**Method**	**Dilution**
Anti-goat-IgG-HRP	Rabbit IgG	SERAMUN, Heidesee, Germany	WB	1:2000
Anti-mouse-IgG-HRP	Sheep IgG	SERAMUN, Heidesee, Germany	WB	1:2000
Anti-rabbit-IgG-HRP	Sheep IgG	SERAMUN, Heidesee, Germany	WB	1:2000
Anti-rabbit-IgG-AP	Donkey IgG	DAKO, Hamburg, Germany	IHC	1:500
Anti-mouse-IgG-AP	Donkey IgG	DAKO, Hamburg, Germany	IHC	1:500

2.1.6 Expendable materials

Consumable	**Company**
15 ml, 50 ml tubes	Greiner bio-one GmbH, Frickenhausen, Germany
6 well, 96 well plates	Greiner Bio-one GmbH, Frickenhausen, Germany
6cm, 10cm, 15cm dishes	Greiner Bio-one GmbH, Frickenhausen, Germany
Concentration filters	Amplicon, UK
Pipet tips	SARSTEDT AG&Co, Nümbrecht, Germany
Disposable Columns (1 ml)	Qiagen, Hilden, Germany
Pasteur pipets	Carl Roth®, Karlsruhe, Germany
1.5 ml, 2 ml reaction tubes	SARSTEDT AG&Co, Nümbrecht, Germany
Safe seal 1.5 ml reaction tubes	SARSTEDT AG&Co, Nümbrecht, Germany
Scaple	Carl Roth®, Karlsruhe, Germany
X-Omat UV films	Kodak GmbH, Stuttgart, Germany

Nitrocellulose membrane	Carl Roth®, Karlsruhe, Germany
Whatman 3 mm chromatography paper	VWR International GmbH, Darmstadt, Germany

2.1.7 Centrifuges and devices

Device	Company
ELISA plate reader	Anthos Labtec Instruments HT 3, Krefeld, Germany
Freezer (-80°C)	FORMA SCIENTIFIC ltd., UK
Freezers, refrigerators	Robert Bosch Hausgeräte GmbH, Germany
Gased incubator	Hera Cell, Germany
Laminar work bench	Hera Safe, Germany
Lightcycler®480 Instruments	Roche, Mannheim, Germany
Ice machine	SCOTSMan ICE SYSTEMS, Italy
Microscope	Leica DM 2000, Wetzlar, Germany
Microwave	Robert Bosch Hausgeräte GmbH, Germany
pH meter	WTW GmbH, Weilheim, Germany
Pipetus®	Hirschman Laborgeräte GmbH, Germany
Power supply	BIO-RAD Laboratories, Munich, Germany
Scanner	EPSON EUROPE ELECTRONICS GmBH, Germany
Thermomixer	Eppendorf, Hamburg, Germany
Thermoblock	Biometra/ Eppendorf, Hamburg, Germany
UV gel documentation	UV system Intas GmbH, Göttingen, Germany
Varioklav® steam sterilizer	H+P Labortechnik, Oberschleißheim, Germany
Shaker ST5 CAT, Centromat®	Neolab, Heidelberg, Germany
Ultra sound stick	BANDELIN SONOPLUS, Berlin, Germany
SDS-PAGE Chamber	BIO-RAD Laboratories, Munich, Germany
Hemocytometer, Neubauer	VWR International GmbH, Darmstadt, Germany
Biofuge fresco	HERAUS, UK
Biofuge pico	HERAUS, UK
Centrikon T-124	Kontron Instruments GmbH, Neufarn, Germany
Megafufe 1.0R	HERAUS, UK
Western Blot system	BIO-RAD Laboratories, Munich, Germany

2.1.8 Eukaryotic cells

Cell line	Characteristics	Company
ACHN	renal cell adenocarcinoma, derived from metastatic site; pleural effusion, adherent	ATCC®
A498	renal carcinoma, primary tumor, adherent	ATCC®

Caki-1	renal clear cell carcinoma, derived from metastatic site; skin, adherent	ATCC®
786-O	renal carcinoma, primary tumor, adherent	ATCC®

2.1.9 Media and supplements for eukaryotic cells

Media	Company	Cell line	supplements
Eagle's salt MEM	Biochrom	ACHN, A498	10% FCS, 100 µg/ml Penicillin /Streptomycin, 1 mM NEAA, 1 mM sodium pyruvate
McCoy's 5A	Invitrogen	Caki-1	10% FCS, 100 µg/ml Penicillin /Streptomycin
RPMI 1640	Biochrom	786-O	10% FCS, 100 µg/ml Penicillin /Streptomycin, 4.5 g/l Glucose, 10 mM HEPES, 1 mM Sodium pyruvate

2.1.10 Bacterial cells

Bacterial Strain	Company
DH5α	Life Technologies GmbH, Darmstadt, Germany
TOP10	Life Technologies GmbH, Darmstadt, Germany
XL2 Blue	Agilent Technologies, Böblingen, Germany

2.1.11 Media and supplements for bacterial cells

All solutions were prepared with double deionized H_2O. (LB = lysogeny broth)

Solution	Concentration in LB	Company
LB broth	10 g/l tryptone , 5 g/l yeast extract, 10 g/l sodium chloride, pH 7.0	Carl Roth®, Karlsruhe, Germany
LB agar	LB broth recipe, 15 g/l agar	Carl Roth®, Karlsruhe, Germany
Ampicillin	100 µg/ml	Sigma-Aldrich®, München, Germany
Kanamycin	50 µg/ml	Sigma-Aldrich®, München, Germany
X-Gal	40 µg/ml	Agilent Technologies GmbH, Germany

2.1.12 Vectors

Vector	Application and Company
pcDNA™3.1	Eukaryotic expression vector, N-terminal HIS-Tag (Invitrogen)
pCMV-Tag3A	Eukaryotic expression vector, N-terminal 3x FLAG-tag (Stratagene)
pCR®2.1 (3.9 kb)	TA cloning vector (Invitrogen)

2.1.13 DNA primers

Primers were provides by BioTeZ Berlin-Buch GmbH and diluted in ddH_2O to a final concentration of 50 µM.

Primer name	Sequence
p27wtBam_for	TCG GAT CCA TGT CAA ACG TGC GAG TGT CT
p27wtEco_rev	GCA AAT TCT TAC GTT TGA CGT CTT CTG AG
p27mut_1	CAG GAG AGC CAG GAT GGC AGC GGG AGG CGC CCG CCG GC
p27mut_2	GCC GGG CGG CTC CCG CTG CCA TCC TGG CTC TCC TG

2.1.14 DNA and protein markers

Marker	Company
GeneRuler 1 kb DNA ladder	Fermentas GmbH, Darmstadt, Germany
GeneRuler 100 bp DNA ladder	Fermentas GmbH, Darmstadt, Germany
X2 PAGE Ruler™Prestained protein ladder	Fisher Scientific, Schwerte, Germany

2.1.15 Enzymes

Enzyme	Activity	Company
BamHI	Restriction enzyme	Fermentas GmbH, Darmstadt, Germany
EcoRV	Restriction enzyme	Fermentas GmbH, Darmstadt, Germany
KpnI	Restriction enzyme	Fermentas GmbH, Darmstadt, Germany
SmaI	Restriction enzyme	Fermentas GmbH, Darmstadt, Germany
T4	DNA ligase	Fermentas GmbH, Darmstadt, Germany
Pfu	DNA polymerase	Promega, Mannheim, Germany
OptiTaq	DNA polymerase	Roboklon GmbH, Berlin, Germany

2.1.16 Software

Program	Application
IBM SPSS Statistics 17.0	Statistical analysis
LightCycler®480SW1.5	Software for LightCycler®480
MikroWin2000	Software for XTT test
ApE-A plasmid editor v2.0.47	Analysis of sequences
MedCalc	Statistical analysis
ImageJ	Densitrometrical analysis
GraphPad Prism 5.04	graphical and statistical analysis

2.2 Methods

2.2.1 Cell culture methods

2.2.1.1 Cultivation of renal carcinoma cells

A laminar air flow work bench (Hera Safe) was used for all cell culture experiments. The four human kidney cancer cell lines were cultivated in a cell culture dish in a humidified 5% CO_2 incubator (Hera Cell) at 37°C. Cell line type specific media was used as described in 2.1.9. Every 2-3 days ACHN and A498 cells were split 1:3, Caki-1 cells 1:4 and 786-O cells 1:4-6. Cryostocks were generated using full growth media with 5% DMSO and were stored in liquid nitrogen.

2.2.1.2 Transient cell transfection with vector DNA and siRNA

Upon transfection A498 cells and 786-O cells were seeded into 6 well plates (1x 10^6 cells) or 15 cm cell dishes (8-10x 10^6 cells) and grown to 90-95% confluency overnight. The next day, transfection approaches were prepared in 2 ml OPTI-MEM©+Glutamax media. DNA approach (5-10 µg/µl DNA plasmid), siRNA approach (50 nM) and Lipofectamine®2000 approach (20 µl) were incubated separately for 5 min at room temperature (RT).

The Lipofectamine®2000 approach was then added drop-wise to the DNA/siRNA approach and incubated for another 10 min at RT. In the meantime, the cells were washed 2 times with

PBS to remove old medium containing FCS traces. The transfection medium was incubated on cells for 5-6 hours before it was replaced with cell line specific medium and incubated overnight. After 16h transfected cells were harvested and lysed for Western blotting or FLAG pull down analysis.

2.2.1.3 Proliferation Assay

XTT proliferation assay (*Cell Proliferation Kit II*) was performed according to manufacturer's protocol. A498 and 786-O cells were grown in 96 well microplates (tissue culture grade, flat bottom) in cell specific media in a humidified atmosphere (5% CO_2, 37°C). 4x 10^3 cells per well were seeded in triplicates in a final volume of 100 µl culture medium and incubated overnight. After the respective incubation time, 50 µl of the *XTT labeling mixture* was prepared according to manufacturer's protocol and added to each well (final XTT concentration 0.3 mg/ml). The formed formazan dye is quantified by using a scanning multi-well spectrophotometer (Anthos HT III). The measured absorbance recorded at 570 nm directly correlates with the number of viable cells.

To quantify and compare cell proliferation of cell lines 786-O and A498, a XTT-proliferation assay was performed in both cell lines 0 h, 24 h, 48 h and 72 h after seeding. The experiments were performed in triplicates independently and statistics were calculated using GraphPad Prism version 5.01 (GraphPadPrism Software Inc., USA). An unpaired Student's t-test was applied for statistical analysis.

2.2.2 DNA and RNA methods

2.2.2.1 Transformation of competent *E.coli*

For bacterial transformation 50 µl of chemocompetent *E.coli* bacteria were thawed on ice for 10 min. Vector (1-30 ng) or ligation mixture (5-10 µl) were added, mixed gently and incubated on ice for another 10 min. Heat shock method was applied to incorporate the DNA. The suspension was heated at 42°C for exactly 90 sec and placed directly on ice for 2 min. The DNA/bacteria mixture was either plated directly on agar plates or cultured in 1 ml of LB medium on a shaker at 37°C for 45 min before being transferred on agar plates. Appropriate antibiotics in the media (Ampicillin, Kanamycin) enabled to select bacterial clones harboring the plasmid of interest.

2.2.2.2 Preparation of plasmid DNA from bacterial cells

For small scale preparation of plasmid DNA a single transformed bacterial clone (agar plate) was inoculated in 3 ml LB medium with an appropriate antibiotic and incubated shaking at 37°C overnight. The *Insorb®Spin Plasmid Mini Two Kit* was used as described in the manufacturer's protocol. DNA pellet was dissolved in 30 µl sterile PBS. Concentration and purity was determined using NanoDrop technology. For preparation of plasmid DNA from large scale bacterial batch, 3 ml LB medium 250 ml LB medium bacterial culture was incubated overnight and *EndoFree Plasmid Maxi Kit* and manufacturer's protocol was used. DNA pellet was dissolved in 90 µl sterile PBS per 2 ml tube and incubated shaking at 37°C for 3 min. DNA concentration and purity was determined using NanoDrop technology.

2.2.2.3 Preparation of RNA from eukaryotic cells

RNeasy Mini Kit was used for RNA preparation from mammalian cells. 0.4x 10^6 786-O and A498 cells were seeded in 6 well plates and incubated in appropriate cell medium overnight before being lysed in QIAzol Lysis Reagent. The kit was applied according to manufacturer's protocol. RNA concentration and purity was determined using NanoDrop Technology.

2.2.2.4 Preparation of DNA from human tissue samples

QIA amp DNA Mini Kit was used for DNA preparation from cancer tissue samples according to manufacturer's protocol. 25 mg of frozen RCC patient tissue sample (consisting of tumor tissue plus adjuvant normal tissue) was used per approach. DNA concentration and purity was determined using NanoDrop Technology (NanoDrop2000 and Software, Nano Drop Instruments).

2.2.2.5 Synthesis of cDNA

For cDNA synthesis *Transcriptor First Strand Synthesis Kit* was used. First a Template Primer Mix was prepared (1 reaction: 1µg total RNA, 2.5 µM Anchored-oligo$(dT)_{18}$ Primer (50pmol/µl), 60 µM Random Hexamer Primer (600 pmol/µl), the final volume was adjusted to 13 µl with

nuclease-free ddH_2O). The samples were incubated in a thermo block cycler at 65°C for 10 min (Biometra Cycler) and thereafter, immediately chilled on ice. In the meantime a *Master Mix* was prepared (1 reaction: 1x *Transcriptor Reverse Transcriptase Reaction Buffer* (5x), 20 u Protector RNase Inhibitor (40 U/µl), 1 mM dNTP Mix (10 mM), 10 U transcriptor reverse transcriptase (20 U), final volume was adjusted to 7 µl with nuclease-free ddH_2O). Per reaction 7 µl *Master Mix* were added to 13 µl *Template Primer Mix* and incubated in a thermo block cycler (Biometra) for 60 min (10min at 25°C, 60 min at 55°C, 5 min at 85°C). The transcriptase was inactivated by the last incubation step. The reaction mixture was immediately chilled on ice until further usage or stored at -20°C.

2.2.2.6 Polymerase chain reaction (PCR)

PCR was used to amplify DNA fragments from templates (vectors, cDNA). For all PCR reactions OptiTaq DNA polymerase was used due to its 3' → 5' proof reading activity. For DNA amplification *Reaction Mix* was prepared (1 reaction: 1-200 ng DNA, 5 µl of Buffer C (10x), 2.5 µl DMSO, 1 µl dNTPs (5 mM), 0.1 µl forward primer (50 µM), 0.1 µl reverse primer (50 µM), add ddH_2O to 50 µl). The general PCR temperature protocol used is displayed in Tab. 4. The duration of the extension step (cycles) was depended on the length of DNA to be amplified (expecting synthesis speed of 1 kb per minute).

Primers and double stranded DNA were removed from PCR products using *GeneMatrix PCR/DNA Clean-Up Purification Kit* according to manufacturer's protocol.

Tab. 4: General PCR temperature protocol.

Temperature	Step	Cycles	Time
95°C	Initial denaturation		2-3 min
95°C	Denaturation		30 sec
primer specific	Annealing	30-35 cycles	30 sec
72°C	Extension		30 sec
72°C	Terminal extension		7 min
4°C	hold		4 min

2.2.2.7 Digestion of DNA with restriction enzymes

For molecular cloning experiments plasmids or DNA fragments were cut using restriction enzymes. 10 U of enzyme per 1 µg DNA were used in an appropriate enzyme buffer provided by the manufacturer. 1-5 µg DNA were digested in a final volume of 20 µl and incubated at an enzyme appropriate temperature (30-37°C) for 1 h.

2.2.2.8 DNA agarose gel electrophoresis

DNA fragments can be separated according to their fragment size by agarose gels. Depending on the DNA fragment size, argarose gels with different concentrations were prepared (0.8-2%). Agarose was boiled in 1x TAE buffer in a microwave till the powder was completely dissolved and the suspension cooled down to 50-60°C. In the meantime chambers with combs were prepared. Ethidium bromide (1 µl/ml) was added to the agarose solution, poured into the chamber and left to polymerize at RT for 15-20 min. Afterwards, the combs were removed and 10 µl DNA samples diluted in 10x DNA sample loading buffer/ddH_2O were transferred into the comb chambers. One lane was filled with an appropriate 100 or 1000 bp DNA marker. The DNA fragments were separated electrophoretically in 1x TAE buffer on constant voltage (25-100 V, depending on agarose concentration).

2.2.2.9 Isolation of DNA from agarose gel

A UV light transilluminator was utilized to visualize DNA. A scalpel was used to cut out preferred bands. To isolate the DNA from TAE-agarose gel *GeneMATRIX Agarose-Out DNA Purification Kit* was used according to manufacturer's protocol.

2.2.2.10 Ligation of DNA fragments

T4 DNA ligase was used for cloning of sticky end DNA fragments generated by restriction enzymes. Reaction mixtures were prepared in a final volume of 20 µl (20-100 ng of linear vector DNA, insert DNA fragment (3:1 ratio over vector), 2 µl 10x T4 DNA Ligase Buffer, 1 U T4 ligase, nuclease-free ddH_2O) and incubated at 14°C overnight. T4 DNA ligase was heat inactivated at 65°C for 10 min. 5 µl of the mixture were used for transformation of 50 µl

chemically competent cells. Grown bacteria clones were screened for the desired vector and isolated plasmid DNA was sequenced by Eurofins MWG GmbH (Berlin, Germany).

2.2.2.11 Sequencing of p27 cDNA from 786-O and A498 cells

The isolation and sequencing strategy is shown in Fig. 9. First 0.5x 10^6 786-O and A498 cells were grown in 6 well plates overnight. The next day RNA was isolated using *RNeasy Mini Kit* according to manufacturer's protocol. cDNA was synthesized using *Transcriptor First Strand Synthesis Kit*. Concentrations of 437 ng/µl total RNA from 786-O cells and of 537 ng/µl total RNA from A498 cells were used in a 20 µl approach. 2 µl cDNA served as template for amplification of p27 PCR product using 0.1 µl of primers p27-Bamfor (50 mM) and p27-Ecorev (50 mM). Purified p27 PCR product was further cloned in a TA vector using *TA Cloning® Kit* as described in manufacturer's protocol. TA-p27 vector was transformed by heat-shock into INVαF bacterial cells (Invitrogen) and screened for desired clones by Blue-White screening. X-gal (40 mg/ml) was added to the agar plate. Non-recombinant clones appeared in blue while the recombinant ones appeared in white. White bacterial clone potentially harboring the desired p27-TA vector were cultivated in 3 ml LB medium and vector DNA was isolated using *Insorb®Spin Plasmid Mini Two Kit* according to manufacturer's protocol. Purified vector DNA was sent for sequencing to Eurofin, MWG GmbH.

2.2.2.12 Genotyping assay

In order to detect p27V109G and p27I119T in DNA isolated from RCC tissues, two LightSNiP-SimpleProbe-Assays (TIBMolBiol, Berlin Germany) based on melt curve genotyping were established. *Assay 1* was used to detect point mutation p27V109G (rs2066827) and *Assay 2* was used to detect point mutation p27I119T (rs142833529). Simple probes, specific primers carrying a fluorescent dye and quencher, were designed by TIBMolBiol for both assays. Primer samples/probes were dissolved in 100 µl PCR grade water and stored at -20°C. LightCycler®FastStart DNA Master HybProbe and LightCycler 480 Instruments were used in all experiments. Master Mix was prepared as displayed in Tab. 5. A small cohort of 20 RCCs with known p27 gel migration pattern was selected to determine appropriate master mix volume and specific melting temperatures (T_m) peaks (Tab. 6).

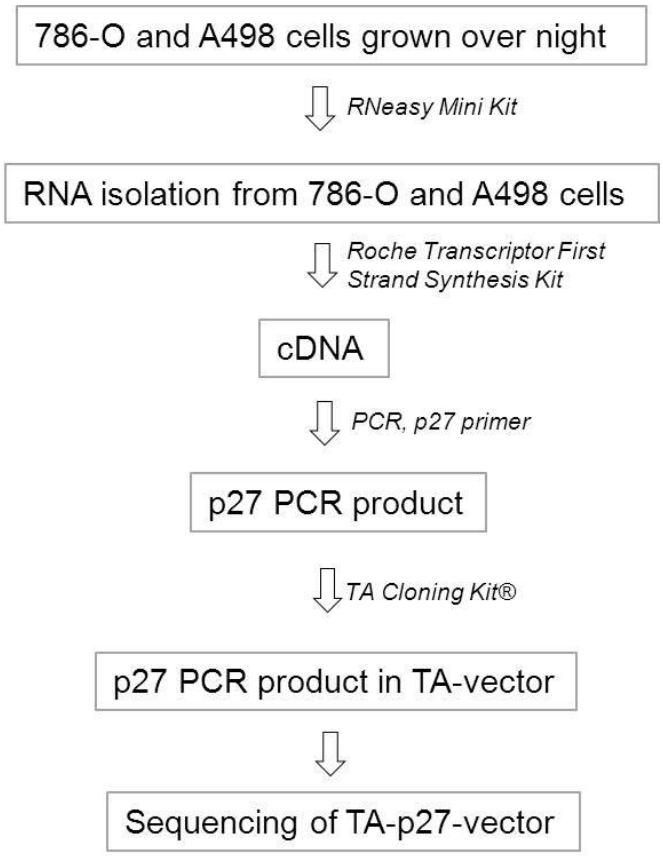

Fig. 9: Scheme of the isolation and sequencing of p27 cDNA from 786-O and A498 cells.

Tab. 5: General Genotyping assay pipetting scheme.

Component	Volume
ddH_2O	6.7 µl
Reagent Mix (TIB MOLBIOL primer/probe)	0.5 µl
10x FastStart DNA Master	1 µl
$MgCl_2$	0.8 µl
DNA (50 ng)	1 µl
	10 µl

Tab. 6: Genotyping assay specific melting temperatures.

Assay	Melting Temperature	bp position	Allele	Protein
Assay 1	T_{m1} = 61.01°C	bp 326	[G]	p27wt
Assay 1	T_{m2} = 67.75°C	bp 326	[T]	**p7V109G**
Assay 2	T_{m3} = 58.46°C	bp 356	[C]	**p27I119T**
Assay 2	T_{m4} = 65.41°C	bp 356	[T]	p27wt

Both assays were further applied on a larger cohort of 71 RCC patients. DNA was isolated from RCC patient tissues using *QIA amp DNA Mini Kit*. Per sample amounts of 10-200 ng DNA were tested in 96 well triplicates. After the run, patients were grouped according to melting temperature in patient harboring p27wt, p27V109G and p27I119T. *Assay 1* and *Assay 2* were statistically analyzed using Chi square test. The generated FLAG-p27 mutant constructs served as controls to validate the function of the two assays. The optimized PCR and Melting Curve temperature protocol is shown in Tab. 7 using 50 ng DNA per approach.

Tab. 7: Genotyping assay temperature protocol.

	Temperature	Step	Cycles	Time
Quantification	95°C	Initial denaturation		10 min
	95°C	Denaturation	45 cycles	10 sec
	60°C	Annealing		10 sec
	72°C	Extension		15 sec
Melting Curves	95°C	Denaturation	1 cycle	30 sec
	40°C	Annealing		2 min
	72°C	Terminal extension		3 min
	40°C	Cooling		30 sec

2.2.3 Protein methods

2.2.3.1 Preparation of protein extracts from RCC cell lines

For protein extraction media was removed and cells washed twice with ice-cold PBS. The cells were immediately placed on ice and lysed using ice-cold triple lysis buffer with freshly added PMSF (0.1 mM) and Aprotinin (10 ng/ml). 100-120 µl modified triple lysis buffer was used for 1x 10^6 cells. Detached cells were transferred into a reaction tube followed by a centrifuging step at 10.000x g at 4°C for 10 min to separate cell debris from protein lysate. Supernatants were transferred into a fresh reaction tube and protein concentration was measured.

2.2.3.2 Preparation of protein extracts from frozen RCC tissues

Proteins were extracted from frozen RCC tissues (stored at -80°C). 30-45 mg of tissue were cut into smaller pieces with a scalpel and transferred in 2x 500 µl ice-cold PBS in a *Protein LowBind Eppendorf* Tube. Tissue samples were centrifuged at 4°C and 500x g for 5 min and supernatants were discarded. For lysis of the tissues ice-cold triple lysis buffer with freshly added PMSF (0.1 mM) and Aprotinin (10 ng/ml) was used. Additional ultra sound application (15 intervals, 5 cycles each) helped to homogenize the samples. Further incubation on ice for 30 min was used to complete cell lysis, followed by another centrifugation step (20,000x g, 4°C for 10 min) to separate cellular debris from protein lysate. Finally, the protein containing supernatants were stored at -80°C until further usage.

2.2.3.3 Protein concentration determination

For protein concentration determination, Bio-Rad D_C Protein Assay was utilized according to manufacturer's protocol. A BSA/PBS standard curve was prepared (0, 0.21, 0.51, 0.73, 0.94, 1.24, 1.46 mg/ml). After concentration determination final protein concentrations of 2 µg/µl protein were adjusted using triple lysis buffer. Protein extracts were either stored at -80°C or immediately mixed with Roti®Load1 (1:4) and denatured at 95°C for 5 min for SDS electrophoresis analysis.

2.2.3.4 SDS polyacrylamide gel electrophoresis (SDS)

SDS PAGE is used to separate proteins according to their size in polyacrylamide (PAA) gels containing SDS. The PAA gels consist of two parts; a stacking gel with low PAA concentration and pH (5%, pH 6.8) to concentrate the proteins in one band and a separation gel with high PAA content. A high PAA concentration and pH (8-15%, pH 8.8) were used to separate the proteins according to their size. First PAA containing separation gel was prepared and polymerized at RT for 15 min. On top a PAA stacking gel was poured and polymerized at RT for 15-20 min. The *SDS-PAGE BioRad System* was assembled and the chambers filled with electrophoresis buffer. Protein samples were denatured in 1x *Roti®Load1*, containing SDS and ß-Mercaptoethanol, prior transfer into the gel pockets. The proteins were separated electrophoretically on constant voltage (90 V for 15 min and 120 V for 90 min).

Separation gel (10% gel, 5ml):	
ddH2O	0.688 ml
1.5 M TRIS (pH 8.8)	1.25 ml
PAA (30%)	1.67 ml
SDS (10% [w/v])	50 µl
APS (10% [w/v])	50 µl
TEMED	5 µl

Stacking gel (1ml):	
ddH_2O	0.688 ml
0.5 M TRIS (pH 6.8)	0.3 ml
PAA (30%)	0.2 ml
SDS (10% [w/v])	12 µl
APS (10% [w/v])	6 µl
TEMED	2.4 µl

2.2.3.5 Western blotting

For further protein experiments separated proteins were transferred and immobilized on a nitrocellulose membrane in an electric field using wet-blotting technique. The wet gel was placed directly and air-free on a nitrocellulose membrane covered with 2 filter paper layers and installed in the *BioRad Western Blot System*. The device chambers were filled with blotting buffer and blotted at constant amperage of 240 mA at RT for 2-3 h or at 120 mA at 4°C overnight. After the membrane was immediately rinsed in ddH_2O and directly stained with Ponceau S solution (0.02% [w/v]) for 5-10 min to visualize the transferred proteins. The visualization helped to control the blotting process and to mark protein areas for further immobilization experiments. In order to block protein-free areas of the membrane, it was incubated in 5% milk/PBS-T or 5% BSA/PBS-T (referring to antibody protocol) solution at RT for 1 h. Further the membrane was incubated in an appropriate primary antibody in 5% milk or primary antibody/5% BSA solution preferably at 4°C overnight or at RT for 2 h followed by incubation in a suitable secondary antibody/PBS-T solution at RT for 1h. Additional washing

steps (3x PBS-T for 10 min) in between the incubation steps removed diluted proteins and excessive antibody. To visualize desired protein, antibody interaction the membrane was incubated in fresh mixed *PIERCE® ECL Western Blotting Substrate* solution according to manufacturer's protocol. Used *X-Omat UV* films were chemically developed and dried films scanned for documentation (*EPSON PERFECTION 1240U*).

2.2.3.6 Immunoprecipitation

Immunoprecipitation (IP) was used to isolate specific proteins. All steps were performed on ice to prevent protein degradation by active proteases. Protein extracts were prepared from A498 and 786-O cells using mono lysis buffer. 50 µl of the protein supernatant were immediately stored at -80°C as input control for Western blotting and the remaining supernatant used for IP. To rule out unspecific binding of the target protein or other proteins the protein solution was incubated in 50 µl sepharose beads/PBS solution *(Protein A - Sepharose® 4B beads*) rotating on a wheel rotor at 4°C for 1 h. The beads were separated in an additional centrifugation step at RT and 5.000x g for 2-3 min. Afterwards the supernatant was split into experimental approaches and a control approach. 300 µl lysate per approach were diluted 1:2 in lysis buffer to increase the sample volume. Antibodies against the desired proteins were added and incubated rotating at 4°C for 1 h (p27 (1:200), CSN7 (1:500)). Antibody species matching serum was used in the control samples. Subsequently, 100 µl beads/PBS solution per approach was added and incubated rotating at 4°C for 2-4 h or overnight. Beads binding desired proteins were washed 4x in lysis buffer rotating at RT for 5 min followed by a centrifugation step (5.000x g). After the last centrifugation step the supernatant was discarded. Per approach the beads solution was mixed with 60 µl 2x *Roti®Load1*, then boiled at 95°C for 5 min followed by electrophoretically separation by SDS-PAGE and analysis by Western blotting.

2.2.3.7 Generation of FLAG-p27 constructs

Three FLAG-p27 constructs harboring the p27 variants and p27wt were designed to investigate the properties of p27 mutants in RCC (Fig. 10). First, p27wt and p27 mutant DNA were excised from pcDNA3.1-TA-p27 vectors using BamHI and EcoRI restriction enzymes. Subsequently they were incorporated into 3x FLAG-pcDNA vectors and transformed in TOP10

bacterial cells. FLAG-p27 plasmid DNA was isolated from bacterial clones using *Insorb®Spin Plasmid Mini Two Kit* according to manufacturer's protocol. Correct sequences of FLAG-p27wt, FLAG-p27V109G and FLAG-p27I119T were verified by Eurofin MWG GmbH.

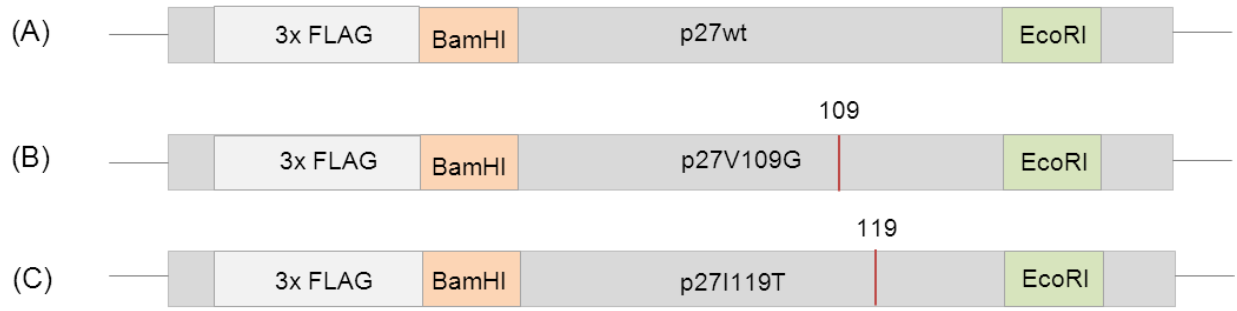

Fig. 10: Scheme for generation of FLAG-p27wt and FLAG-p27 mutant constructs. (A) FLAG-p27wt is shown. The amino acid changes at position 109 in FLAG-p27V109G (B) and position 119 in FLAG-p27I119T (C) are marked in red. BamHI and EcoRI = restriction sites.

2.2.3.8 FLAG pull down

FLAG pull down (PD) was used to examine specific protein binding partners. Therefore, 8-10x 10^6 cells were seeded in a 15 cm cell culture dish and transfected with desired FLAG constructs FLAG-p27wt, FLAG-p27V109G and FLAG-p27I119T (40-50 µg vector DNA per approach). After 16 h cells were harvested and protein extracts were prepared using 1.25 ml triple lysis buffer per approach. 80 µl of the protein supernatant were immediately stored at -80°C as input control. All steps were performed on ice to prevent protein degradation by active proteases. First, 1 ml disposable columns were equilibrated 2x in 2 ml ddH_2O. 0.25 ml of anti-FLAG beads (ANTI-FLAG® M2 Affinity Gel Freezer Safe) were added to each prepared column and drained at RT for 5 min. The columns were washed 1x with TBS at 4°C. Subsequently, anti-FLAG beads were activated by application of 2x 2-3 ml of ice-cold glycine buffer (pH 3.5) within 20 min. Subsequently, the column was washed 1x in 2-3 ml TBS at 4°C. Fresh prepared cell protein lysate was added and non-attached lysate was washed from the column 2x with TBS. FLAG bead bound proteins were eluted using FLAG peptid/TBS (0.1 mg/ml) at 4°C. Protein eluates were either concentrated using TCA precipitation or concentration filters (cut off 30 kDa). Subsequently concentrated eluates were analyzed by SDS-PAGE and Western blotting.

2.2.3.9 Cycloheximid chase and MG132 application

Protein stability of p27wt and p27 variants was determined by applying cycloheximid (CHX) and proteasome inhibitor MG132. Overnight 5x 10^5 of 786-O and A498 cells were grown in a 6 well plate. The cells were treated with CHX (35.4 µM) for 0, 2, 3 and 4 hours and with MG132 (10 µM) for 2 and 4 hours. Subsequently cells were harvested and protein cell lysates prepared with triple lysis buffer. Lysates were checked for Ubiquitin and p27expression levels by Western blotting.

2.2.3.10 Glycerol density gradient centrifugation

Glycerol density gradient centrifugation was used to examine protein to protein complex binding. First, gradient buffer solution was prepared and mixed thoroughly. Five gradient fractions (5%, 10%, 20%, 30% and 40%) were prepared diluting glycerol in gradient buffer solution and stored at 4°C until further usage. Per protein lysate one glycerol gradient was prepared on ice. Therefore, 400µl of each gradient fraction was cautiously filled in layers starting with the 40% fraction. 100 µl of freshly prepared protein lysates were carefully coated on top of the gradient. Proteins were separated by centrifugation at 150,650x g for 1 h or 93,000x g for 4 h, 4°C using a TLA.103 Rotor. The glycerol density gradient was separated in 13 x 123.3 µl fractions. The fractions were immediately analyzed by Western blotting or frozen at -80°C until further use. The glycerol density gradients were calibrated using purified CSN and CRL complexes. In the present thesis anti-CSN5 and anti-CUL1 antibody mark the positions of both complexes. The CRL component CUL1 was found in fractions with lower density (F3-5, 8.8-12.76% glycerol), whereas the CSN5 was observed in more dense fractions (F6-8, 14.7-18.5% glycerol).

2.2.3.11 p27 variant isolation and mass spectrometry analysis

Mass spectrometry (MS) analysis was used to identify p27 mutants. MS analysis requires preferably unmixed p27 protein. Endogenous p27 protein of 786-O and A498 cells was isolated using IP and visualized by Commassie stained SDS-PAGE gels (Fig. 11, 786-O data shown only). In gels, the 27 kDa protein migrates close to the light chain of p27 antibody (25 kDa). Thus acidic elution was applied in order to concentrate the IP eluate. The upper and lower band of p27 were cut out from the gel separately (red box) and analyzed by mass spectrometry.

MS analysis was performed by AG Naumann (Otto-von-Guericke University, Magdeburg, Germany). The experimental approach was repeated 2 times.

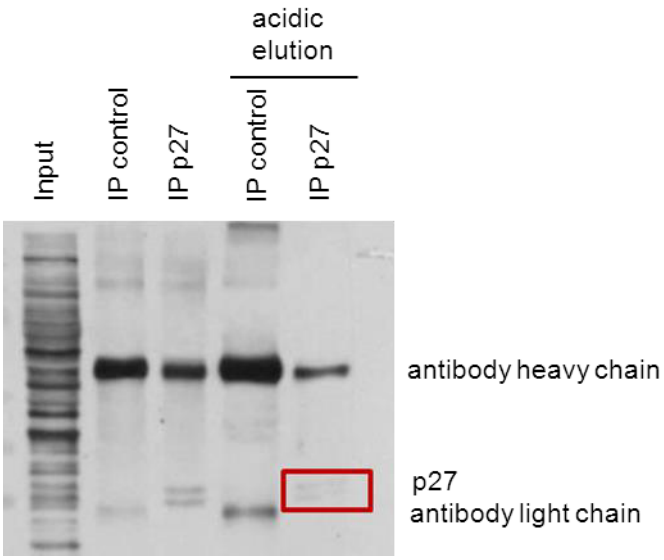

Fig. 11: Isolation of p27 variants from 786-O cells. Immunoprecipitation (IP) of the p27 variants from 786-O cells using the anti-p27 antibody with and without subsequent application of acidic elution was performed. Subsequently, p27 protein bands were cut out (red box) separately for mass spectrometry analysis. Input = 786-O lysate, IP control = rabbit anti-serum, ab = antibody.

2.2.4 Immunohistochemistry

2.2.4.1 Preparation of formalin-fixed paraffin-embedded (FFPE) tissues

RCC tissue was fixed in 4% PFA in a volume of 5-10x of the tissue volume. The fixed tissue was cut into suitable portions and placed in an embedding cassette (Electron Microscopy Sciences). Tissue samples had to be dehydrated before paraffin application using an ascending ethanol row (2x 70% ethanol for 1 h, 2x 80% ethanol for 1 h, 2x 95% ethanol for 1 h, 3x 100% ethanol for 1 h, 3x xylene for 1 h). The samples were incubated in paraffin wax (58°C) twice for 1.5 h for the final embedding in paraffin blocks. For large block slices 3-4 µm slices were cut from the paraffin blocks by microtome (Leica RM 2125RT), transferred immediately in a water bath (50°C) and further onto a microscopic slide (SuperFrost®Plus, VWR Leuven). For tissue microarray (TMA) 1.0 mm spots were punched from the paraffin blocks by Stanze (Beecher Instruments) into a fresh paraffin block, which was cut as described above. All objective slides were dried at 60°C in a heater for 4 h and were stored at RT until further analysis.

2.2.4.2 Immunohistochemical staining of FFPE tissue

For immunohistochemical analysis tissue sections had to be deparaffinized (rehydrated) using a descending ethanol row (2x 10min xylene, 2x 100% ethanol, 1x 95% ethanol, 1x 80% ethanol, 1x 70% ethanol, ddH_2O), each step for 3-5 min. Rehydrated tissue sections were stored in ddH_2O until further use.

Hematoxylin/Eosin staining

For nucleus staining tissue section slides were incubated in Mayer's Hemalaun solution for 5-10 min, developed under warm running tap water and rinsed with ddH_2O. Afterwards, slides were stained with Eosin for cytoplasmic staining for 1-2 min, than rinsed with ddH_2O. An ascending ethanol row was performed (each step for 30 sec.) to embed tissue sections in xylol-based mounting medium *PERTEX*® (MEDITE). Covered slides were stored at RT.

Immunohistochemical staining

Tissue sample proteins were demasked using citric buffer (pH = 6.0) in a pressure cooker for 5 min and washed in 1x TBS. Further samples were blocked in a protein-blocking solution (*Protein block*, DAKO) for 10 min before incubation in an appropriate primary antibody at RT for 1 h. The slides were washed (1x ddH2O, 1x TBS/Tween and 1x ddH_2O) and incubated in streptavidin-conjugated secondary antibodies for 30 min and *Fast™ Fast Red* (Sigma-Aldrich, 1 tablet dissolved in 1 ml TBS). The staining was monitored under a microscope (Leica DM 2000) until the desired staining intensity was reached. For additional nucleus counter staining Mayer's Hemalaun solution was applied. The slides were embedded in water-based *Aquatex*® and stored at RT. Six large block RCC tissues were used to examine components of the CSN-CRL in renal cancers. RCC FFPE sections were stained with antibodies against four CSN subunits and three cullins as well as CAND1. Antibody specificities were validated by Western blotting.

2.2.4.3 TMA analysis of CAND1 expression

A renal TMA from the Department of Urology (Charité-Universitätsmedizin Berlin, Germany) was used to examine CAND1 expression in RCC subtypes. 357 RCC matched patients (cases from 1992 - 2005) embedded in 13 paraffin blocks were examined, each patient represented by 3 cylindrical core RCC biopsies. 3-4 µm width TMA FFPE slices were stained with CAND1

antibody (1:50) overnight. 337 TMA biopsies were examined and evaluated in cooperation with a pathologist (Dr. Kilic, Department of Pathology, Charité-Universitätsmedizin Berlin, Germany). 20 Biopsies could not be evaluated due to tissue removal during the staining process or lack of RCC patient data. CAND1 was found in the cell nuclei (N) and cytoplasm (C) of all patients. The staining intensities of cytosolic CAND1 protein expression were subdivided into four different classes ranging from 0 to 3 (C0-C3). Each tumor spot was categorized due to expression of no (C0), weak (C1), intermediate (C2) or strong (C3) CAND1 staining. Furthermore, nuclear CAND1 expression was grouped in 3 categories; no (N0), weak (N1) and strong (N2) expression of nuclear CAND1. All biopsies from 337 RCCs were categorized due to their CAND1 expression levels (N1-2, C0-3). Per patient all three biopsies were evaluated and averaged for statistical analysis. Pearson-Chi square analysis was performed using selected clinicaopathological data of RCC patients and the localization of CAND1 expression. The data obtained from the assessment of the staining intensity of CAND1 expression were analyzed with regard to tumor stage (pT1-4), Fuhrman Grade (G1-4), metastasis (M0,1), age at nephrectomy and histological subtype.

2.2.5 Statistical methods

Statistical analysis were performed using SPSS version 17.0 (SPSS Inc., USA) and GraphPad Prism version 5.01 (GraphPad Software Inc., USA). Parametric tests (Student's t-Test, ANOVA) as well as non-parametric tests (Pearson’s chi-square test) for paired and non-paired data was used as described in the text. For disease progression analysis, the Kaplan-Meier approach (Log Rank test) and Cox proportional hazard regression analysis was used (event = death of patient).

3. Results

3.1 Characterization of components of the CSN-CRL pathway in RCC

The expression of several components of the CSN-CRL pathway, spatially that of selected CSN subunits and cullins as well as of CAND1, at protein levels were investigated in six ccRCCs and adjacent renal normal tissues by immunohistochemical analysis (Fig. 12).

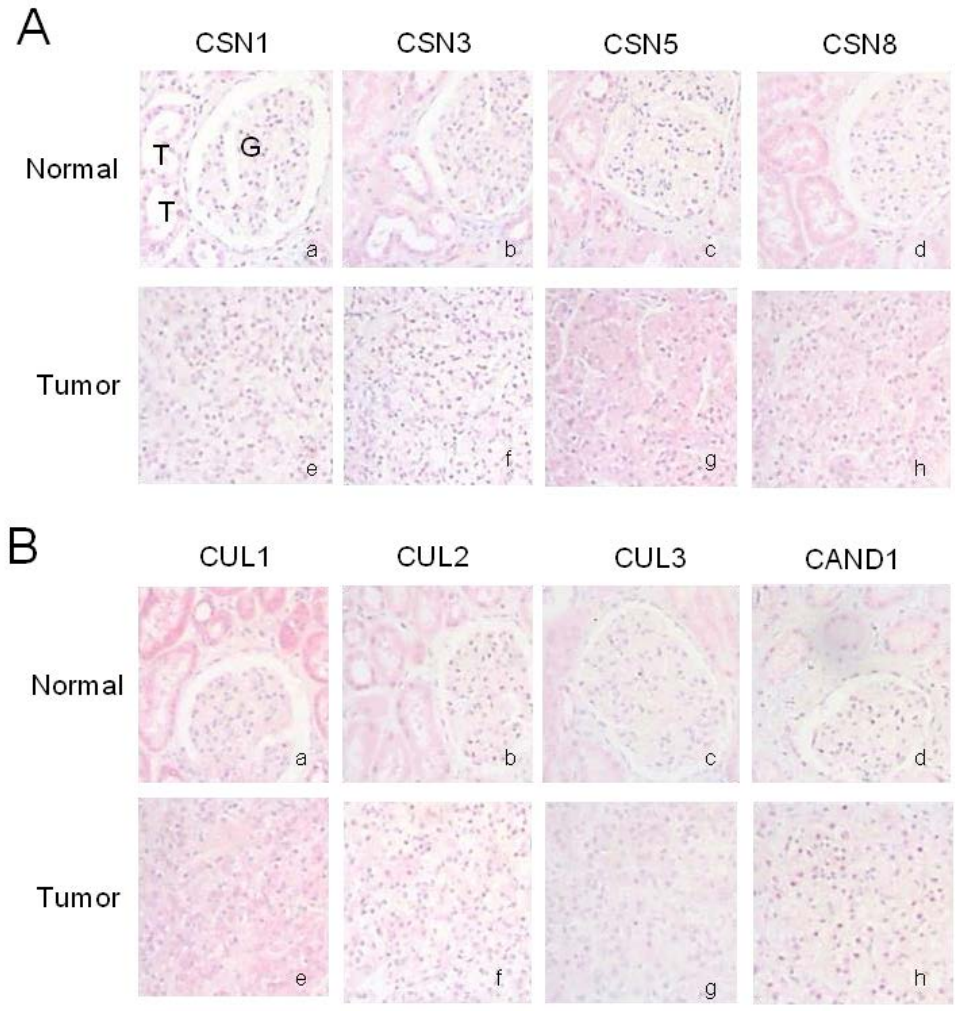

Fig. 12: Expression levels of selected CSN-CRL pathway components in ccRCC. Representative micrographs show matched FFPE non-neoplastic and RCC tissues stained with antibodies against CSN subunits (CSN1, CSN3, CSN5 and CSN8) (A), cullins (CUL1, CUL2 and CUL3) as well as CAND1 (B). Meyer's Hemalaun counter stained the nuclei (blue). T = renal tubule, G = renal glomerulum. Magnification: 400x.

In non-neoplastic renal tissues CSN1, CSN3, CSN5 and CSN8 were expressed highly in the cytosol of epithelial cells of the renal tubules, but they were only weakly expressed in the cytosol of glomerular cells (Fig. 12Aa-d). The nuclei of both renal normal tissue compartments showed only slight CSN subunits expression. In ccRCC tissue, CSN1, CSN3 and CSN8 were weakly expressed in the cytosol and intermediate in the nuclei (Fig. 12Ae-h). The ccRCCs and corresponding normal tissues showed strong nuclear and cytosolic CSN5 expression.

CUL1, CUL2 and CUL3 are moderately expressed in the nuclei of renal normal tissue as well as ccRCC (Fig. 12B). In renal normal tissues CUL1 was strongly expressed in the cytosol of tubules, but not in that of the glomeruli, whereas CUL2 and CUL3 showed intermediate cytosolic staining in both compartments (Fig. 12Ba-c). Strong CUL1 expression was also found in the cytosol of ccRCCs (Fig. 12Be). The expression levels of CSN subunits and cullins in renal normal and RCC tissues are summarized in Tab. 8.

Tab. 8: Expression levels of components of the CSN-CRL pathway in renal normal and ccRCC tissue. C = cytosol, N = nuclei. Expression levels: weak (+), moderate (++) and high (+++).

Component of CSN-CRL pathway	Renal normal tissue				RCC tissue	
	Renal tubules		Glomeruli			
	C	N	C	N	C	N
CSN1	+++	++	+	+	+	++
CSN3	+++	++	+	+	+	++
CSN5	+++	+++	+	+	+++	+++
CSN8	+++	++	+	+	+	++
CUL1	+++	++	+	++	+++	+
CUL2	++	++	+	++	+	+
CUL3	++	++	+	+	+	+
CAND1	varies	varies	+	varies	varies	varies

CAND1 expression varies in the nuclei and the cytoplasm within the tissue of six ccRCC patients. The displayed example in Fig. 12 represents tissue with strong nuclear and intermediate cytosolic CAND1 staining. Consequently, tissue microarray technique was used to examine CAND1 expression in a larger cohort of RCCs comprising four histological subtypes of RCC.

3.1.1 Expression of CAND1 in RCCs

The clinicopathological parameters of the examined 337 patients and tumors are summarized in Tab. 9. The patient cohort represented a common RCC subtype distribution within the European population and a common male to female ratio (2:1).

Tab. 9: Patient and tumor characteristics. Clinicopathological parameters of 337 RCC patients.

		n	%	mean	range
Sex	male	219	65.0		
	female	118	35.0		
Age	age at nephrectomy [years]			60.41	30 – 86
Overall Survival	survival after nephrectomy [month]			104.26	0 – 194
Status	alive	133	39.5		
	dead	204	60.5		
Histological subtype	clear cell	273	81.0		
	papillary	34	10.1		
	chromophobe	13	3.9		
	sarcomatoid	17	5.0		
Tumor stage	pT1	190	56.4		
	pT2	26	7.7		
	pT3	117	34.7		
	pT4	4	1.2		
Fuhrman grade	G1	37	10.7		
	G2	249	73.9		
	G3	48	14.2		
	G4	3	0.9		
Metastasis	M0	305	90.5		
	M1	32	9.5		

The relation of the pathological tumor stage (pT), Fuhrman grade (G) and histological subtypes of the RCC cohort is shown in Tab. 10, representing a common RCC cohort. The distribution of tumor stages and grades varied significantly within the different subtypes ($p < 0.0001$ and $p = 0.002$). The majorities of clear cell and papillary RCCs were pT1 tumors (56.2% and 76.4%), whilst chromophobe RCCs and sarcomatoids are mainly pT3 tumors. The majority of RCCs in the cohort are G2 tumors.

Tab. 10: Pathological tumor stage (pT) and Fuhrman grade (G) in relation to histological subtypes of the RCC cohort (n = 337).

Stage/ Grade	Clear cell n = 273		Papillary n = 34		Chromophobe n = 13		Sarcomatoid n = 17		Pearson Chi-Square test
	n	%	n	%	n	%	n	%	
pT1	**156**	**57.2**	25	**73.6**	4	30.8	5	29.4	p < 0.0001
pT2	18	6.5	2	5.8	3	23.0	3	17.6	
pT3	97	35.5	7	20.6	6	**46.2**	7	**41.2**	
pT4	2	0.8	0	0	0	0	2	11.8	
G1	33	12.0	3	8.8	0	0	1	5.8	p = 0.002
G2	**202**	**73.9**	29	**85.2**	10	**76.9**	8	**47.0**	
G3	37	13.5	2	5.8	2	15.3	7	41.1	
G4	1	0.3	0	0	1	7.6	1	5.8	

CAND1 was found in the cell nuclei (N) and cytosol (C) of all patients and staining intensities were subdivided in different classes (see 2.2.4.3). Representative tumor tissue sections for the categories C1-3 combined with N1-2 are shown in Fig. 13.

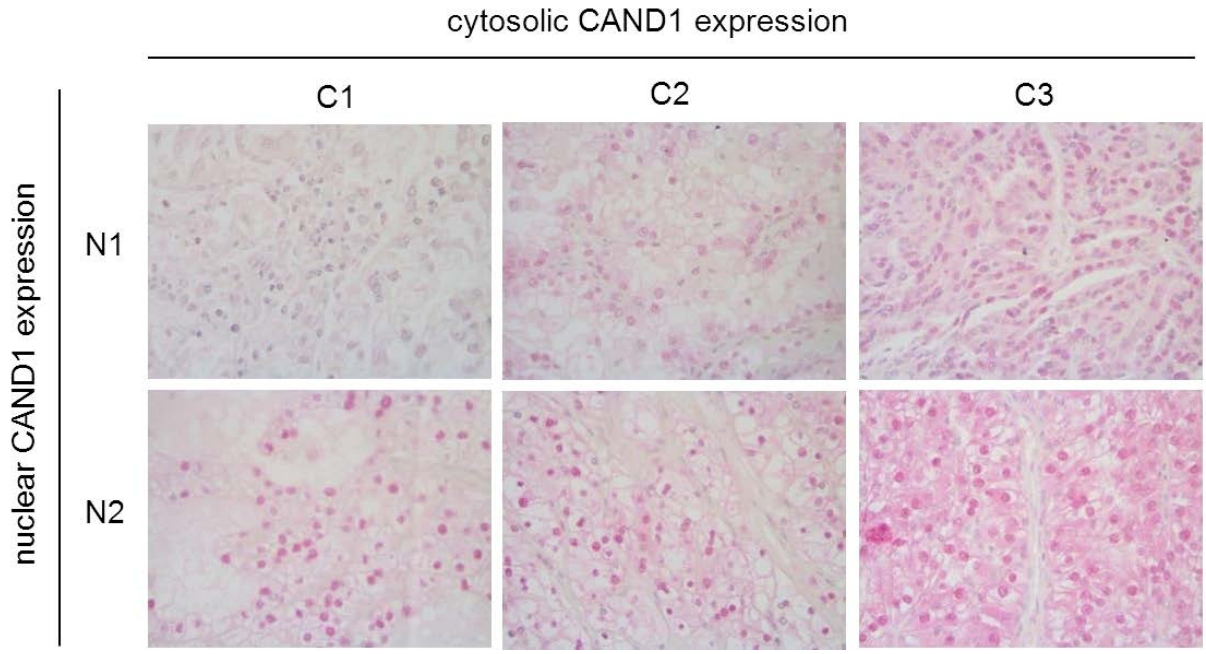

Fig. 13: CAND1 expression in RCCs. Nuclear CAND1 expression in RCC tissue was categorized in weak (N1) and strong (N2) expression in the nuclei. Cytosolic CAND1 staining intensities were categorized as weak (C1), intermediate (C2) and strong (C3) CAND1 expression. Meyer's Hemalaun solution counterstained the nuclei (blue). Magnification: 400x.

RCC patients categorized as CAND1 N1/C1 showed only a weak CAND1 expression in the cell nuclei, cytosol and vessels (Fig. 13a). In RCC patients labeled N2/C1, CAND1 was highly expressed in the nuclei, but only slightly in the cytosol and vessels (Fig. 13d). Cytosolic CAND1 expression was found moderate in categories N1/C2 and N2/C2 (Fig. 13b,e). The strongest CAND1 expression in the nuclei and in the cytosol was observed in N2/C3 RCCs (Fig. 13f). Moderate CAND1 staining intensities in the nuclei and cytosol (N1/C2 and N2/C2) were found in the majority of renal tumors (Tab. 11).

Tab. 11: Localization and intensity of nuclear (N) and cytosolic (C) CAND1 expression in a RCC cohort (n = 337). Expression level: weak (N0, C0), moderate (N1, C1, C2) and strong (N2, C3).

	n	**%**
N0/C0	2	0.6
N0/C1	2	0.6
N1/C0	3	0.9
N1/C1	68	20.2
N1/C2	**116**	34.4
N1/C3	13	3.9
N2/C0	0	0
N2/C1	31	9.2
N2/C2	**78**	23.1
N2/C3	24	7.1

Kaplan-Meier analysis revealed a negative tendency between strong cytosolic CAND1 expression and overall survival (Fig. 14A, $p = 0.241$). RCC patients showing strong cytosolic CAND1 expression (C3) died earlier than patients with lower CAND1 staining intensity (C0-C2). Nuclear CAND1 expression level alone was not associated with overall survival in RCC patients. However, patients with low nuclear and high cytosolic CAND1 expression (N1/C3) were observed with the lowest survival rate in RCCs (Fig. 14B). In contrast, high expression of nuclear and low levels of cytosolic CAND1 (N2/C1) increased the probability of survival in RCC patients. Association between age at the time of nephrectomy, sex, Fuhrman grade, metastasis status and localization of CAND1 expression was not found to be significant (Tab. 12). However, nuclear and cytosolic CAND1 staining significantly correlated with the RCC histological subtypes ($p < 0.0001$). Furthermore, tumor stage (pT1–4) was found to be significantly associated with cytosolic CAND1 ($p = 0.035$). Nuclear CAND1 expression differed within the

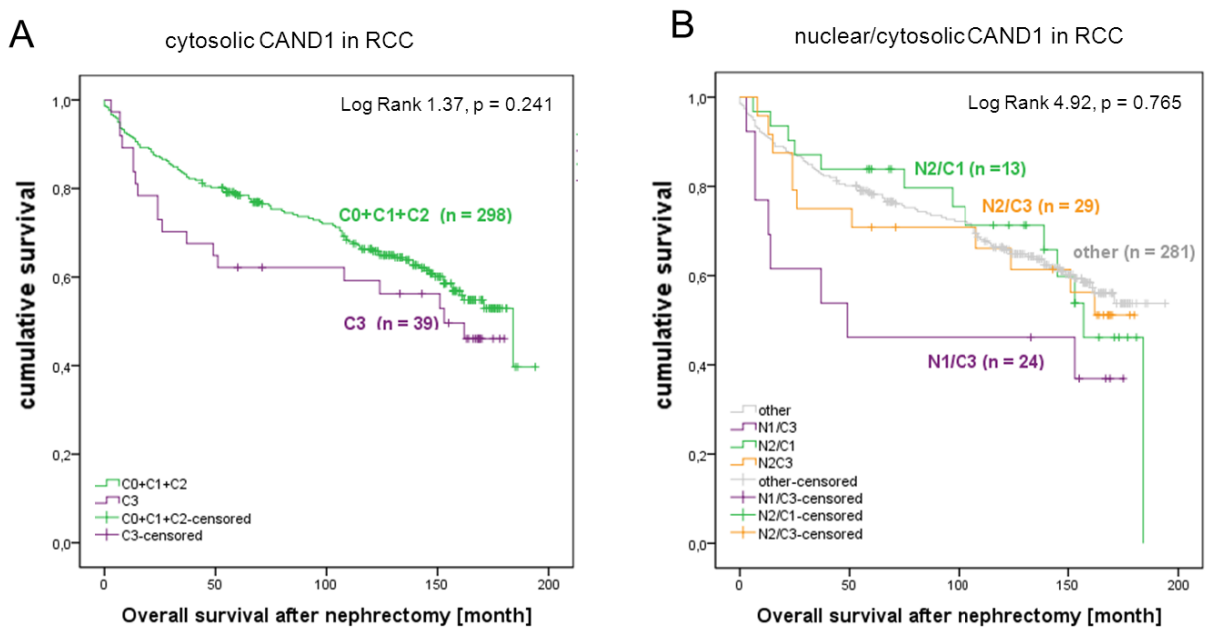

Fig. 14: High cytosolic CAND1 expression is negatively associated with overall survival in RCC. Kaplan-Meier analyses of 337 RCC patients are displayed. (A) Patients with strong cytosolic CAND1 expression (C3) show a worse outcome than patients with less CAND1 expression (C0-2 grouped). (B) Low levels of nuclear accompanied with high levels of cytosolic CAND1 reduced the survival rate in RCC patients.

Tab. 12: Clinicopathological data with regard to localization of CAND1 expression in RCC cohort (n = 337). Pearson's chi-square test (2-tailed). *p< 0.05, **p< 0.001, *** p<0.0001

		Nuclear CAND1 (N0-N2)	Cytosolic CAND1 (C0-C3)	Nuclear/Cytosolic CAND1 (N0-2)x(C0-3)
Sex	male, female	p = 0.450	p = 0.741	p = 0.349
Age at nephrectomy	< median > median	p = 0.213	p = 0.258	p = 0.220
Histological subtype	clear cell RCC, papillary RCC, chromphobe RCC, sarcomatoid	**p < 0.0001*** **	**p = 0.001** **	**p < 0.0001*** **
Tumor stage	pT1-4	p = 0.591	**p = 0.035***	p = 0.220
Fuhrman grade	G1-4	p = 0.501	p = 0.301	p = 0.243
Metastasis status	M0, M1	p = 0.806	p = 0.417	p = 0.833

RCC histological subtypes ($p > 0.0001$). Low expression of CAND1 (N1) was observed in 85.2% of the papillary renal tumors, whereas only 55.6% of the ccRCC tissues showed N1 staining intensities. Strong nuclear CAND1 expression (N2) was found in 44% of the clear cell RCC patients, compared to 17.1% of papillary RCCs. Cytosolic CAND1 expression levels varied significantly among the RCC subtypes ($p = 0.001$). Kaplan-Meier analysis of the ccRCC patient group only did show an even stronger negative tendency of high cytosolic CAND1 expression and overall survival (Fig. 15).

Tab. 13: Expression and localization of CAND1 in RCC subtypes. Nuclear (N) and cytosolic (C) CAND1 protein expression level related to histological subtypes of RCCs.

		all RCC		**Clear cell**		**Papillary**		**Chromophobe**		**Sarcomatoid**		**Pearson's chi-square test**
		n = 337		n = 273		n = 34		n = 13		n = 17		
		n	%	n	%	n	%	n	%	n	%	
nucleus	**N0**	4	1.2	2	0.84	0	0	2	15.3	0	0	**p < 0.0001**
	N1	200	**59.1**	152	**55.6**	29	**85.2**	9	**69.2**	10	**58.8**	
	N2	133	42.5	119	**43.5**	5	14.7	2	15.3	7	41.2	
cytosol	**C0**	5	1.4	1	0.13	3	8.8	1	7.6	0	0	**p = 0.001**
	C1	104	29.5	85	31.3	8	23.5	2	15.3	6	**35.3**	
	C2	204	**57.9**	158	**57.8**	21	**61.7**	9	**69.5**	6	35.3	
	C3	39	11.0	29	10.3	2	5.8	1	7.6	5	29.4	

3.1.2 Expression of selected components the CSN-CRL pathway in RCC cell lines

The expression intensity of selected components of the CSN-CRL pathway were investigated in four human renal cancer cell lines by Western blotting (Fig. 16). Two cell lines derived from primary tumors (A498 and 786-O) and two from metastatic site (ACHN and Caki1). CSN subunits (CSN1, CSN5 and CSN8), cullins (CUL1, CUL3), ß-TrCP, cyclin E and Cdk5 expression levels were found equal. CAND1 expression level was found slightly reduced in 786-O and A498 cells. Among all cell lines Skp2 was found highly expressed in 786-O cells. The same cell line presented a p27 double band, triggering investigation of the CAND1-Skp2-p27 axis in 786-O cells (Fig. 16, red boxes).

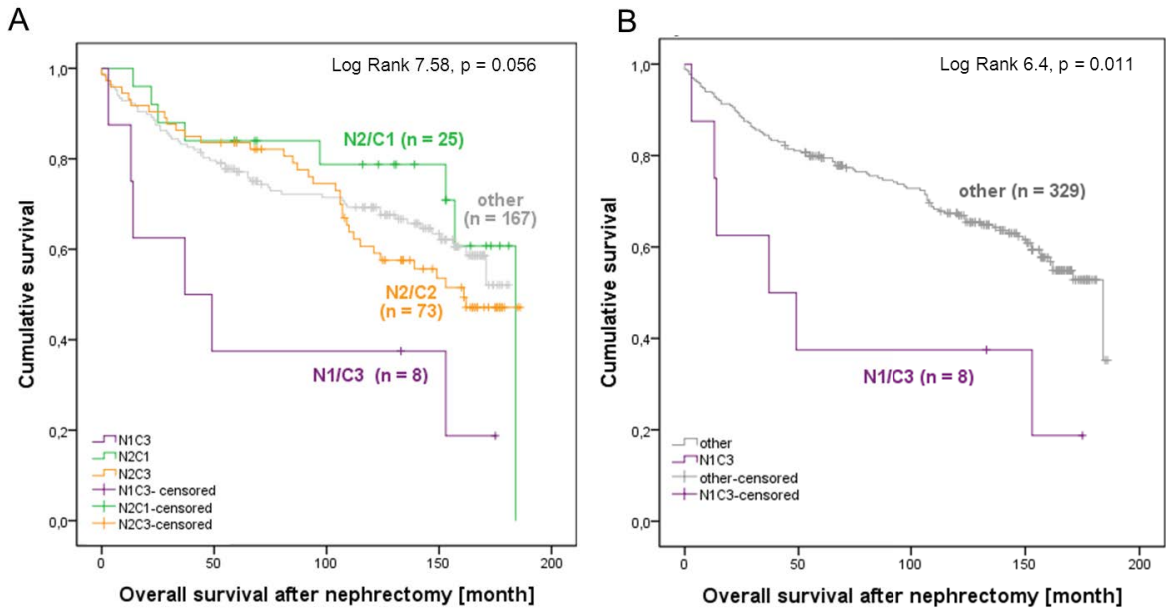

Fig. 15: High cytosolic and low nuclear CAND1 expression reduced the survival rate in ccRCCs. Kaplan-Meier analyses of 273 ccRCC patients are displayed. (A) Patients with strong cytosolic CAND1 expression (C3) show a worse outcome than patients with less CAND1 expression (C1, C2). (B) a significant reduction of the survival rate in ccRCC patients with low levels of nuclear CAND1 and high levels of cytosolic CAND1 (N1/C3) compared to other RCC patients was found.

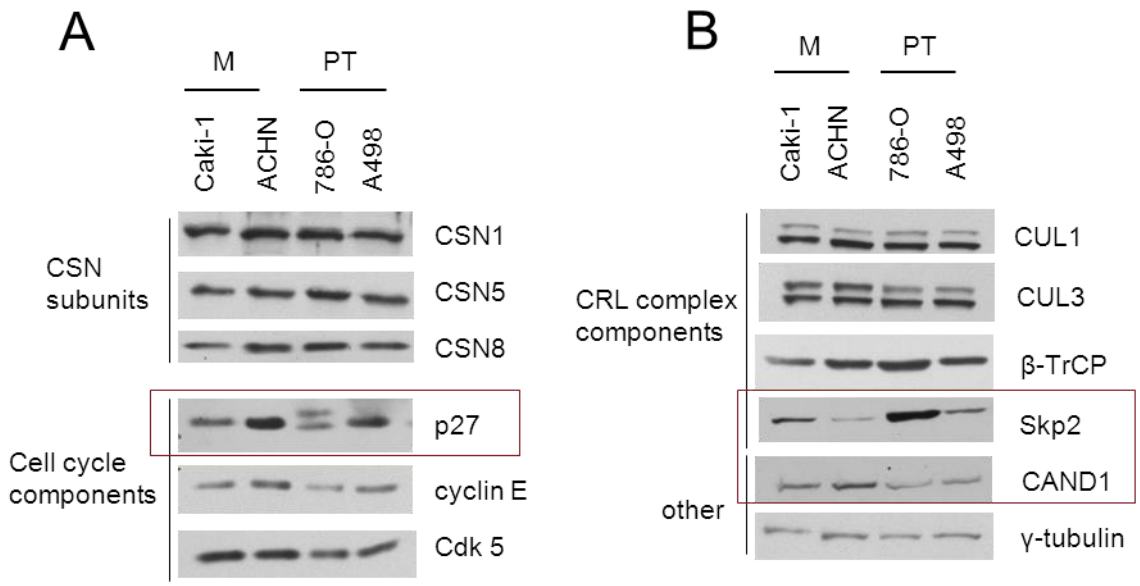

Fig. 16: Expression of selected CSN and CRL components in RCC cell lines. 4 RCC cell lines (Caki-1, ACHN, 786-O, A498) originating from metastasis (M) or primary tumor (PT) were investigated by Western blot analysis. Expression levels of selected CSN subunits and cell cycle regulators (A) as well as CRL component and CAND1 (B) were analyzed. Levels of γ-tubulin were used as loading control.

The composition of the CSN and CRL complexes was investigated by glycerol density gradient centrifugation (Fig. 17). The complex assembly did not significantly differ among the 4 RCC cell lines. Fbw7, Skp2 and CAND1 were found in CRL and CSN containing fractions (F3-5, F6-8) indicating their binding to these protein complexes. A slight fraction shift for the $CRL1^{Skp2}$ substrate p27 among the four RCC cell lines was observed. In lysates of ACHN and A498 cells p27wt was presented in the peak fractions F4-7. Whereas p27 protein from 786-O cell lysates was found in F3-5 and in two parallel not shifted bands.

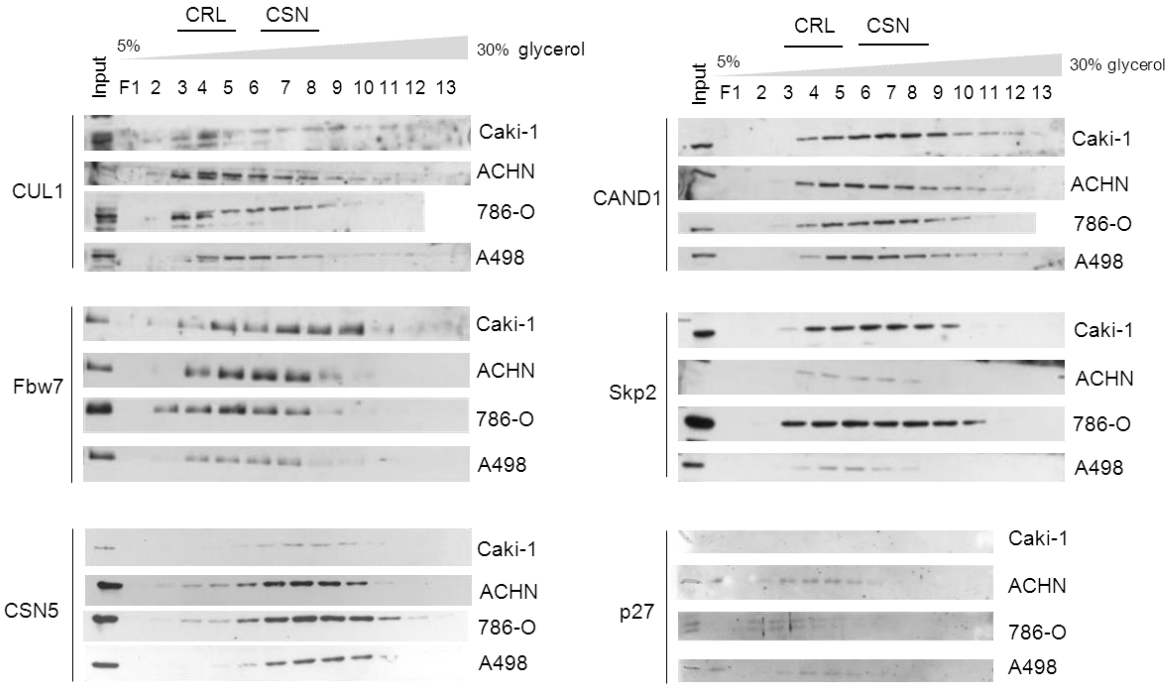

Fig. 17: Composition of CSN-CRL pathway complexes in four RCC cell line lysates focusing on selected CSN-CRL pathway components. Protein complexes of RCC cell line lysates were separated by glycerol density gradient centrifugation. Fractionations (F) were investigated using antibodies against CUL1, Fbw7, CSN5, CAND1, Skp2 and p27. Peak fractions containing CRL complex (F3-5) and CSN complex (F6-8) are marked.

3.2 Identification of two p27 mutants in 786-O cells

The observed p27 double band in 786-O cells consist of a higher and a lower molecular weight band when compared to p27wt. Differences in molecular weights might results from posttranslational modification or gene mutation. First, the modification of p27wt by 786-O cells was investigated. Therefore, Xpress-p27wt was transiently transfected in 786-O cells. Cell lysates harvested after 16h were analyzed by using Xpress antibody (Fig. 18B

A). Only one band was detected indicating that the recombinant Xpress-p27wt protein was not partly modified by these cells. In addition, endogenous p27 from 786-O cells was isolated by immunoprecipitation (IP) and subsequently treated with λ-phosphatase for 30 min and analyzed by Western blotting (Fig. 18B). The upper p27 band did not show any reduction after phosphatase treatment. Protein phosphorylation or other protein modifications cannot be ruled out completely, but are very unlikely.

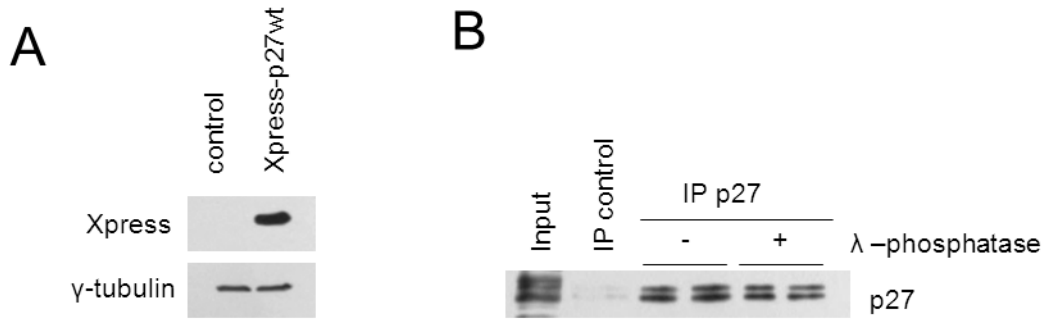

Fig. 18: No modification of p27 found in 786-O cells. (A) Recombinant Xpress-p27wt was exogenously expressed as a single band in 786-O cells. (B) Immunoprecipitates (IP) of the p27 variants from 786-O cells were treated with λ-phosphatase before Western blotting analysis and showed no reduction of the upper band. IP control = rabbit anti-serum.

Further, mass spectrometry experiments were performed to identify mutations of the amino acid sequence causing the appearance of two p27 protein bands (see 2.2.3.11). Endogenous p27 from A498 cells was identified as p27wt (Fig. 19A), whereas p27 isolated from 786-O cells revealed two amino acid changes, on position 109 (lower protein band) (Fig. 19B) and position 119 (upper protein band) (Fig. 19C). The mass spectrometry did not show any additional protein modifications on the isolated p27 protein bands and thereby confirmed the findings described above.

The p27 cDNA of 786-O and A498 cells was also sequenced (see 2.2.2.11). The sequencing data confirmed the results obtained from the mass spectrometry analysis. Cell line A498 harbored p27wt and cell line 786-O possessed two p27 point mutations at position bp 326 (p27V109G) and bp 356 (p27I119T) leading to an amino acid exchange (Fig. 20).

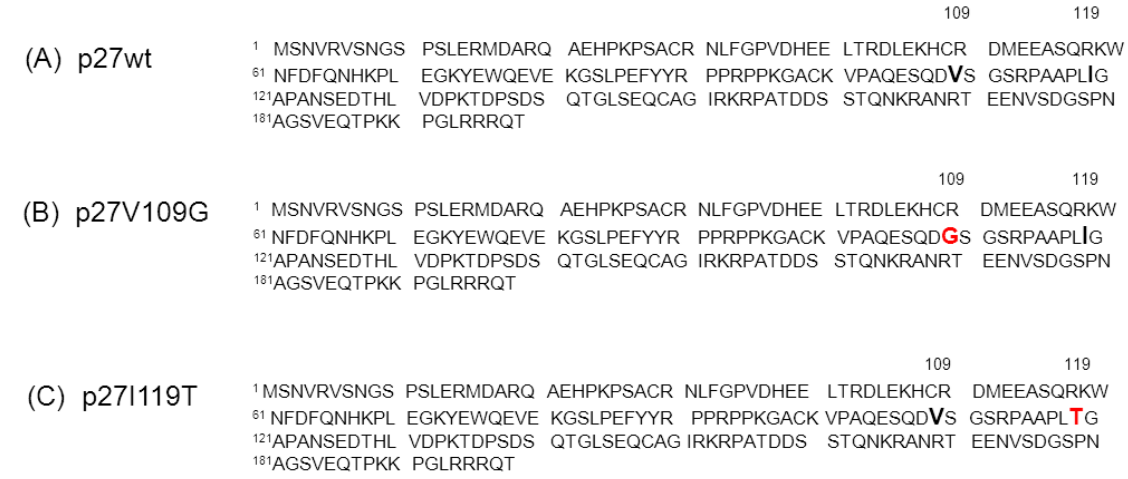

Fig. 19: Amino acid sequences (aa 1-198) of p27wt (A) and p27 variants (B,C). In A498 cells mass spectrometry analysis revealed p27wt (A). An amino acid exchange at position 109 (p27V109G) (B) and positon 119 (p27I119T)(C) was found in 786-O cells.

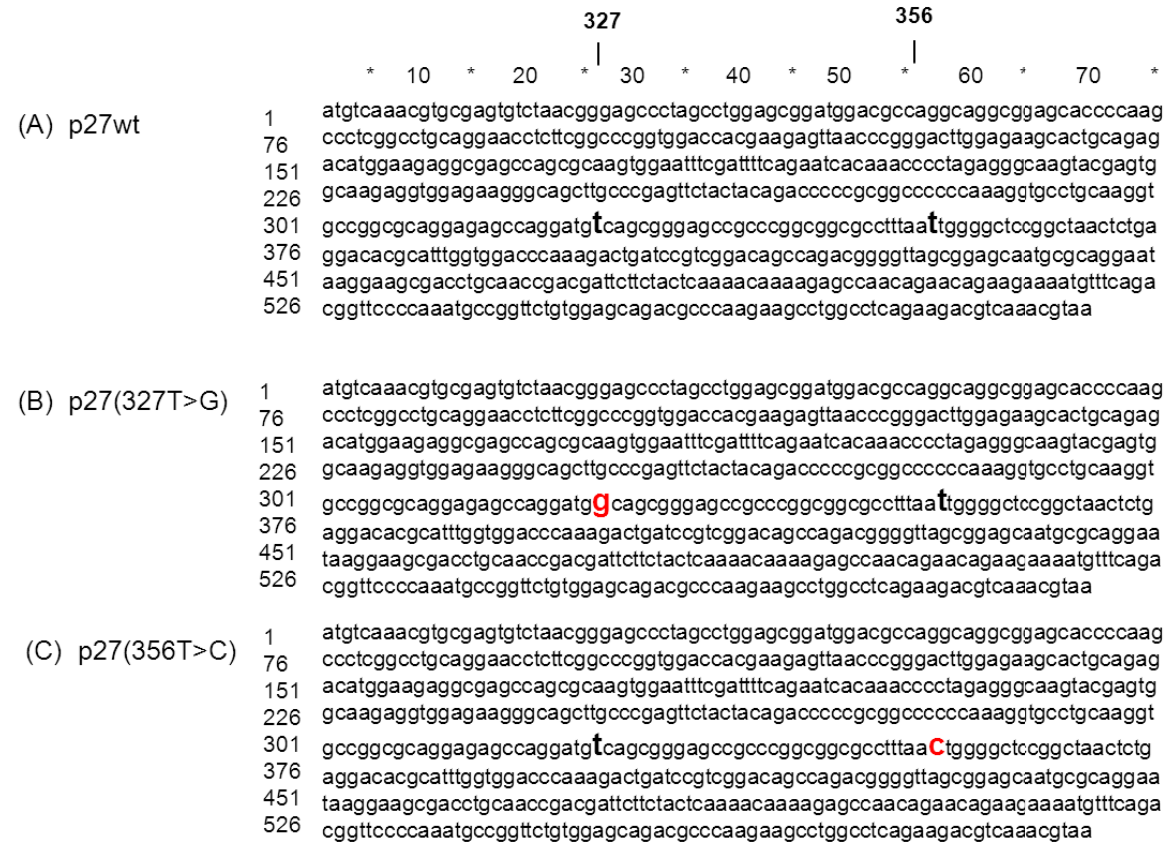

Fig. 20: DNA sequence (bp 1-594) of p27wt (A) and two p27 variant (B,C). Sequencing of p27 cDNA from A498 cells revealed p27wt (A). Nucleotide exchange at position 109 (p27327T>G) and position 119 (356T>C) was found in 786-O cells (B,C).

3.3 Characterization of p27 mutants in 786-O cells

3.3.1 p27wt and p27 mutants are degraded via UPS

The two p27 mutants (p27mut) found in 786-O cells were further characterized in order to understand their impact on renal tumorigenesis. Biosynthesis inhibitor cycloheximide (CHX) and proteasome inhibitor MG132 were used to investigate p27 with regard to degradation by the UPS (Fig. 21). CHX chase experiments showed reduced levels of p27wt and p27mut as well as of other ubiquitinated proteins in a time-dependent manner. Application of MG132 inhibited protein degradation and expression levels of all forms of p27 variants and other ubiquitinated proteins were increased indicating p27wt and p27 mutant degradation by the UPS. Both p27 mutants were equally degraded. The protein mutants seemed to be degraded slightly faster than the p27wt. However, it has to be stressed that the amount of p27wt in A498 cell lysates was higher compared to the amount of one p27 mutants in 786-O cell lysates at equalized γ-tubulin levels. The half-life of both, p27wt and variants amounted to about 0.75 -1 hours.

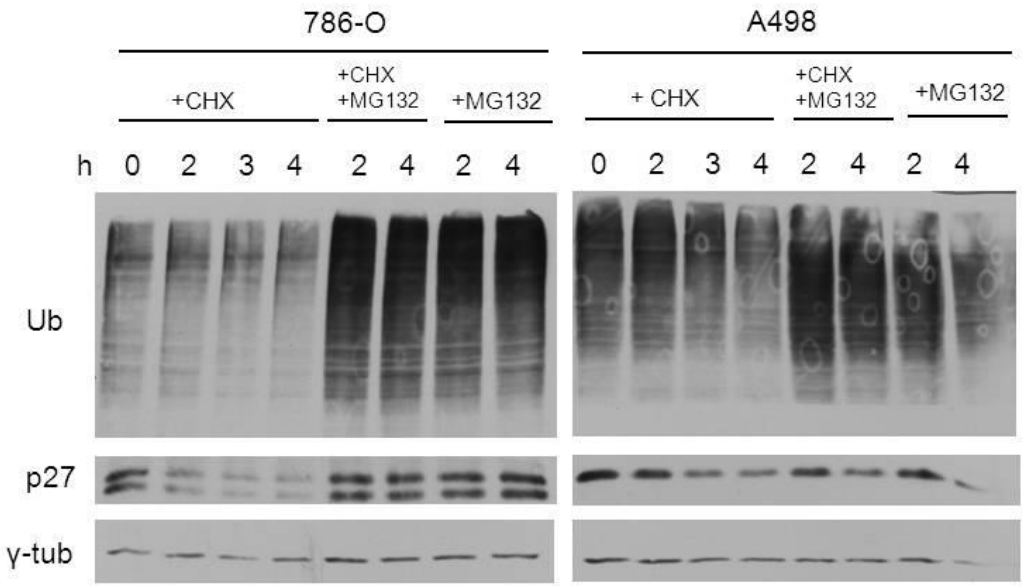

Fig. 21: Endogenous p27wt and p27 mutants are degraded via UPS. 786-O and A498 cell were treated with cycloheximide (CHX) for 0-4 hours (h), with proteasome inhibitor (MG132) or with both for 2 and 4 h before Ubiquitin and p27 protein levels were analyzed by Western blotting.

CAND1 was found to regulate both Skp2 integration into CRL1s and p27 degradation (Dubiel et al., 2013). To study the recognition of p27 by $CRL1^{Skp2}$ complexes, knockdown of CRL regulator CAND1 was performed. 786-O and A498 cells were transiently transfected with siCAND1 and siGFP and harvested after 16 h. Cell lysates were checked for CAND1-Skp2-

p27 axis protein levels by Western blotting (Fig. 22). CAND1 and p27wt and p27mut expression was found to be reduced in siCAND1 cells compared to siGFP control cells. As a consequence of CAND1 knockdown the Skp2 level is significantly increased in 786-O and A498 cells. Especially in siCAND1 786-O cells, Skp2 was found to be upregulated concurrent with reduced p27mut levels. Both p27mut protein bands were reduced equally indicating equal efficiency of degradation as deduced from CHX chase results.

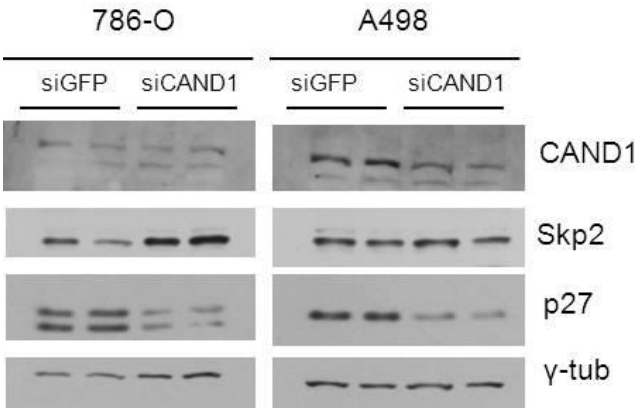

Fig. 22: Down regulation of CAND1 increased Skp2 and reduced p27 levels in 786-O and A498 cells. 786-O and A498 cells were transfected with siCAND1 and siGFP for 5 h. After 16 h cell lysates were analyzed for components of the CAND-Skp2-p27 axis by Western blotting using indicated antibodies.

3.3.2 Interactions of p27 mutants with other proteins

The amino acid exchanges of the two p27 mutants are located within the CSN5 binding region of p27 and may interfere with the interaction of p27 and the CSN complex. IPs were performed to precipitate p27 and the CSN complex plus their binding proteins and revealed a slight binding of p27 and CSN7 (Fig. 23A).

FLAG-p27 constructs harboring the p27 variants and p27wt were designed to further investigate the properties of p27 mutants in RCC (see 2.2.3.7). A498 cells were transiently transfected with FLAG-p27wt, FLAG-p27V109G and FLAG-p27I119T and cells lysates harvested after 16 h. FLAG-PDs were performed and followed by Western blot analysis. Ectopically expressed FLAG-p27mut did show a similar migration pattern as seen in Western blot analysis of endogenous p27mut (Fig. 23B). Binding of p27wt and p27 variants to CUL1, CUL3, CSN5, CSN8, cyclin E and Skp2 was confirmed. All three forms of p27 did bind equally to their binding partners when compared to FLAG-p27 protein levels.

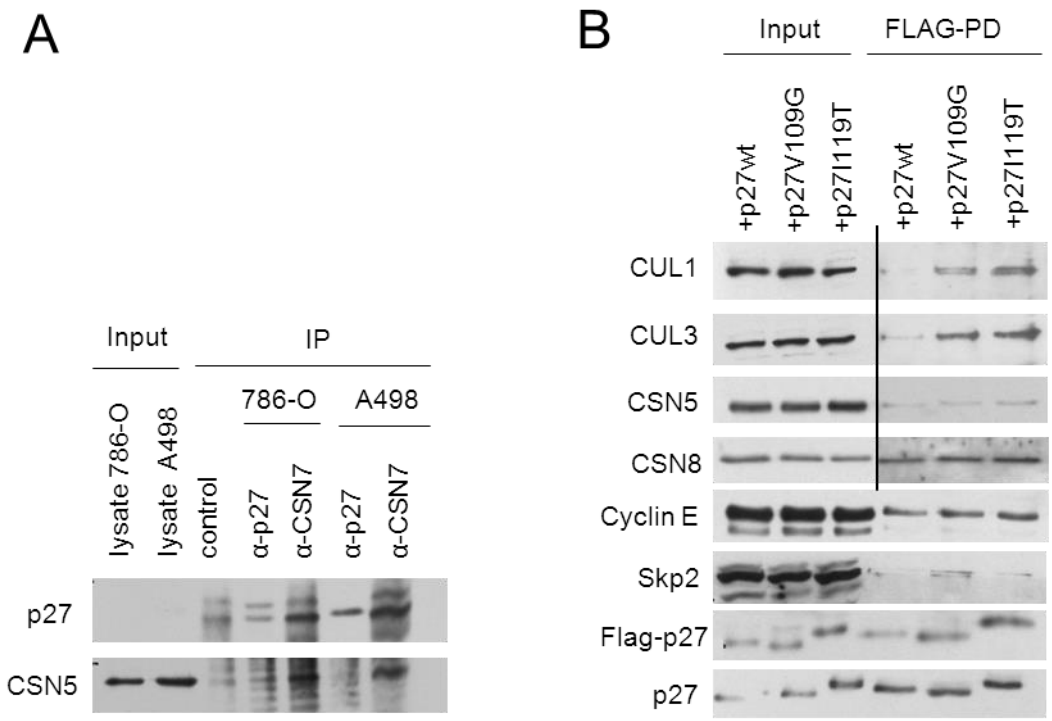

Fig. 23: Both p27 variants and p27wt bind to the CSN complex, CRL1Skp2 complex and cyclin E. (A) Immunoprecipitation (IP) of p27 from 786-O and A498 cells using anti-p27 and anti-CSN7 antibodies. P27 and CSN5 levels were determined by Western blotting. IP control = rabbit anti-serum. (B) FLAG-pull down (FLAG-PD) of p27wt and p27 variants. A498 cells were transfected with FLAG-p27wt, FLAG-p27V109G, and FLAG-p27I119T constructs for 16 h. Cell lysates were used for FLAG-PD and eluates were analyzed for selected CSN-CRL pathway components (CUL1, CUL3, CSN5, CSN8, Cyclin E, Skp2, p27) by Western blotting.

PD eluates were further analyzed by mass spectrometry for CSN-CRL components (see 2.2.3.8). The p27 binding partners Cdks and cyclins were found to bind differentially to p27wt and p27mut (Tab. 14). Cdk1, Cdk2 and cyclin A were found to bind to all three p27 proteins. Whereas Cdk5 was identified to bind to p27wt and p27I119T, but not to p27V109G. Moreover, Cdk6 was observed to bind to p27wt and p27V109G, but not to the other p27 mutant. Cyclin D3 was found to be associated with p27V109G only.

Tab. 14: Binding of Cdks, and cyclins with p27wt and p27 mutants. Mass spectrometry analysis of FLAG-p27 pull downs. A selection of Cdks and cyclins is displayed. X = binding.

	p27wt	p27V109G	p27I119T
Cdk1	X	X	X
Cdk2	X	X	X
Cdk5	X		X
Cdk6	X	X	
Cyclin A	X	X	X
Cyclin D3		X	

3.3.3 786-O cells proliferate faster than A498 cells

The Cdk inhibitor p27 is an important player in cell cycle regulation. During cell culture experiments 786-O and A498 cells were found to proliferate differently. To quantify these observations an XTT-proliferation assay was performed in both cell lines 0 h, 24 h, 48 h and 72 h after seeding. 786-O cells were found to significantly grow 2-3-fold faster than A498 cells ($p < 0.01$) (Fig. 24).

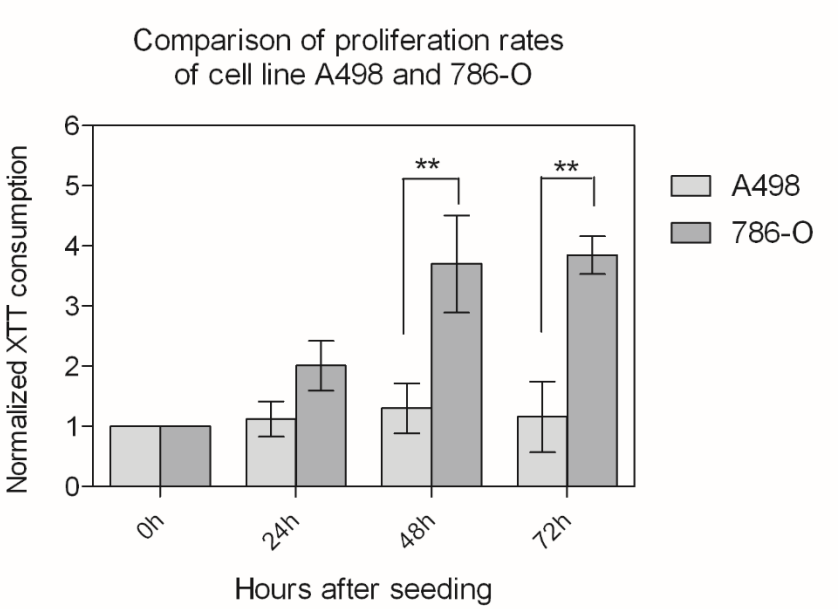

Fig. 24: 786-O cells grow significantly faster than A498 cells. Proliferation assay in 2 RCC cell lines An XTT-proliferation assay was performed in 786-O and A498 cells 0h, 24h, 48h and 72h after seeding. Error bars are standard error of the mean (SEM) **p<0.01.

3.4 The CAND1-Skp2-p27 axis in RCC tissue

To investigate the CAND1-Skp2-p27 axis also in patient tissues, a small cohort of 20 RCC tissues was examined. Each frozen RCC tissue consisted of a tumor tissue and corresponding normal tissue. Cell lysates were prepared from the tissue pairs and analyzed for CAND1, Skp2 and p27 expression levels by Western blotting (Fig. 25). The clinicopathological data of the six RCC tissue pairs is displayed in Tab. 15, also representing the variety of the 20 RCC cohort.

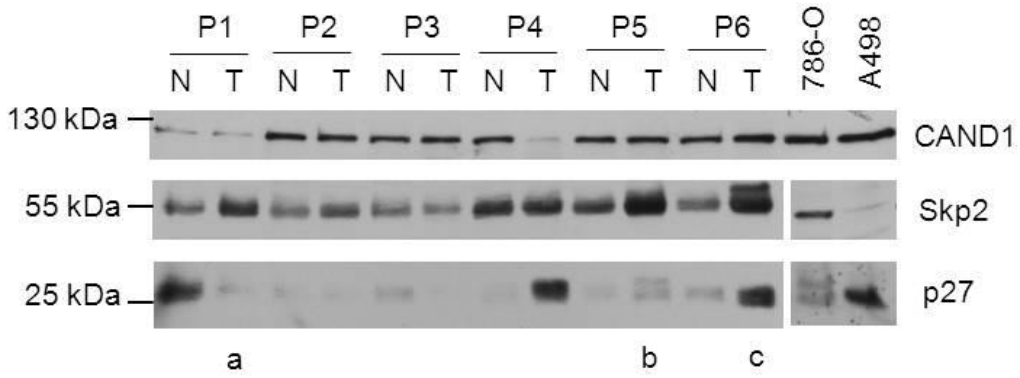

Fig. 25: The CAND1-Skp2-p27 axis in RCCs. RCC lysates were examined by Western blot analysis using anti-CAND1, -Skp2 and -p27 antibodies. Three p27 SDS PAGE migration patterns were observed; (a) p27 upper band, (b) p27 double band and (c) p27 lower band. P = patient number. N = normal tissue, T = tumor tissues. 786-O and A498 cell lysate served as controls.

Tab. 15: Clinic pathological characteristics of six RCCs. RCC subtypes, pathological tumor stage (pT) and Fuhrman grade (G). P = patient number.

Patient number	RCC subtype	Tumor stage	Fuhrman grade
P1	Clear cell RCC	pT1a	G2
P2	Clear cell RCC + Chromophobe RCC (Ø4mm)	pT1a	G2
P3	Chromophobe RCC	pT1b	G1
P4	RCC metastasis	n.d.	n.d.
P5	Clear cell RCC	pT3b	G2
P6	pRCC type 2	pT3b	G2

p27 SDS PAGE migration pattern in lysates from RCC tissue and from 786-O and A498 cells were compared in Western blot analysis. In two out of 20 patients tissue lysates a similar p27 double band migration pattern as seen in 786-O cells lysates was observed. In Fig. 25b the p27 double band is shown in the tumor tissue lysate from Patient 5 (P5), whereas normal tissue lysate P5 displays a single p27 band. In lysates from P1 and P4 the migration pattern of the p27 upper band was observed (Fig. 25a). P6 harbors p27 migrating as a lower protein band (Fig. 25c). Further, increased Skp2 protein expression levels were found in P1, P4 and P6. A high Skp2 expression was observed in P5, accompanied with the p27 double band pattern. CAND1 protein levels were found to be decreased in P1 normal and tumor tissue as well as in P4 tumor tissue lysates.

3.5 p27V109G in RCC tissue

3.5.1 Developing two genotyping assays to detect both p27 mutants in RCC tissues

In a small cohort of selected RCCs similar SDS-PAGE migration patterns of p27 variants as observed in 786-O cell lysates were found. To systematically investigate the p27 mutants in a larger cohort on p27 DNA level, a genotyping assay was developed (see 2.2.2.12). Both mutants are registered as SNPs in the literature (p27V109G: rs2066827 and p27I119T: rs142833529). Therefore, a LightSNiP-SimpleProbe-Assay (TIBMolBiol) based on melting curve genotyping was established using LightCycler®480 Instruments. LightCycler®FastStart DNA Master HybProbe was used in all experiments. Specifically designed primers carrying a fluorescent dye and quencher (simple probes) and the generated FLAG-p27 mutant constructs served as templates and controls to establish two assays. Assay 1 detects p27V109G (further called *Assay 1*) and assay 2 recognizes p27I119T (further called *Assay 2*). For each assay SNP specific melting temperature (T_m) peaks were observed using FLAG-27wt and FLAG-p27V109G control constructs for *Assay 1* and FLAG-p27 and FLAG-p27I119T control constructs for *Assay 2*. For *Assay 1* two peaks at T_{m1} = 61.01°C and T_{m2} = 67.75°C were measured. T_{m1} represents the melting temperature for bp326G (p27wt), whereas T_{m2} shows the melting temperature for bp326T (p27V109G). For *Assay 2* two peaks were measured, T_{m3} = 58.46°C and T_{m4} = 65.41°C. T_{m3} represents the melting temperature for bp356C (p27I119T), whereas T_{m4} shows the melting temperature for bp356T (p27wt). The first genotyping assay run was performed with cDNAs from seven selected RCCs tissue pairs (with known p27 proteins migrating pattern) out of the 20 RCC cohort. The runs confirmed the presence of

p27V109G in cDNAs from patient tissues and verified the functionality of *Assay 1* and *Assay 2*. The genotyping assay results for all seven RCC tissue pairs are displayed in Tab. 16. p27wt protein on position 109 was found in patients P4, P6, P8, P10 and P11. The p27V109G mutant was found in cDNAs from P15 tissue. P5 displayed a p27 double band in Western blot analysis (Fig. 25b). The p27 protein lower band was identified as p27V109G by applying cDNA from P5 tissue in *Assay 1*. p27I119T was not identified in P5 tissue cDNA after application of *Assay 2*.

Tab. 16: *Assay 1* and *Assay 2* test run results in cDNAs of seven RCCs. P = patient number. N = normal tissue. T = tumor tissue.

Patient	RCC subtype	Tissue	Genotyping assay
P4	RCC metastasis	N	p27wt
		T	p27wt
P5	clear cell RCC	N	**p27V109G**
		T	**p27V109G**
P6	papillary RCC	N	p27wt
		T	p27wt
P8	angiomyolipoma	N	p27wt
		T	p27wt
P10	papillary RCC	N	p27wt
		T	p27wt
P11	clear cell RCC	N	p27wt
		T	p27wt
P15	clear cell RCC	N	**p27V109G**
		T	**p27V109G**

3.5.2 p27V109G found in a RCC cohort

To systematically screen RCC tissues for p27 mutants a larger patient group was used. The cohort included 71 RCC patients displaying a common histological subtype distribution within the European population and a common female: male ratio (1:2). The clinicopathological characteristics of the RCC patients are shown in Tab. 17.

First, cDNA of the 71 RCC cases, each comprising a tumor tissue plus a normal tissue, was isolated. An optimized genotyping protocol of *Assay 1* and *Assay 2* was used for all 142 cDNA probes in duplicates. All patient melting curves for *Assay 1* are displayed in Fig. 26. The results exposed 40 RCC patients possessing the p27wt (blue line) on position 109 and 30 RCC patients harboring the p27 mutant heterozygously (p27V109G/wt) (red line). In 1 RCC patient

the p27V109G is present homozygously. The two constructs FLAG-p27wt (green line) and FLAG-p27V109G (pink line) served as controls to confirm the function of *Assay 1* (Fig. 26).

Tab. 17: Clinicopathological data of 71 RCCs used for genotyping assay.

		n	%	mean
Sex	male	49	62	
	female	22	38	
Age	age at nephrectomy [years]			61.4
Histological subtype	clear cell	55	77.4	
	papillary	8	11.2	
	chromophobe	4	5.6	
	onkocytoma	4	5.6	
Tumor stage	pT1	32	45	
	pT2	11	15.4	
	pT3	21	29.5	
	pT4	7	9.8	
Fuhrman grade	G1	6	8.5	
	G2	41	57.7	
	G3	16	22.5	
	G4	8	11.2	

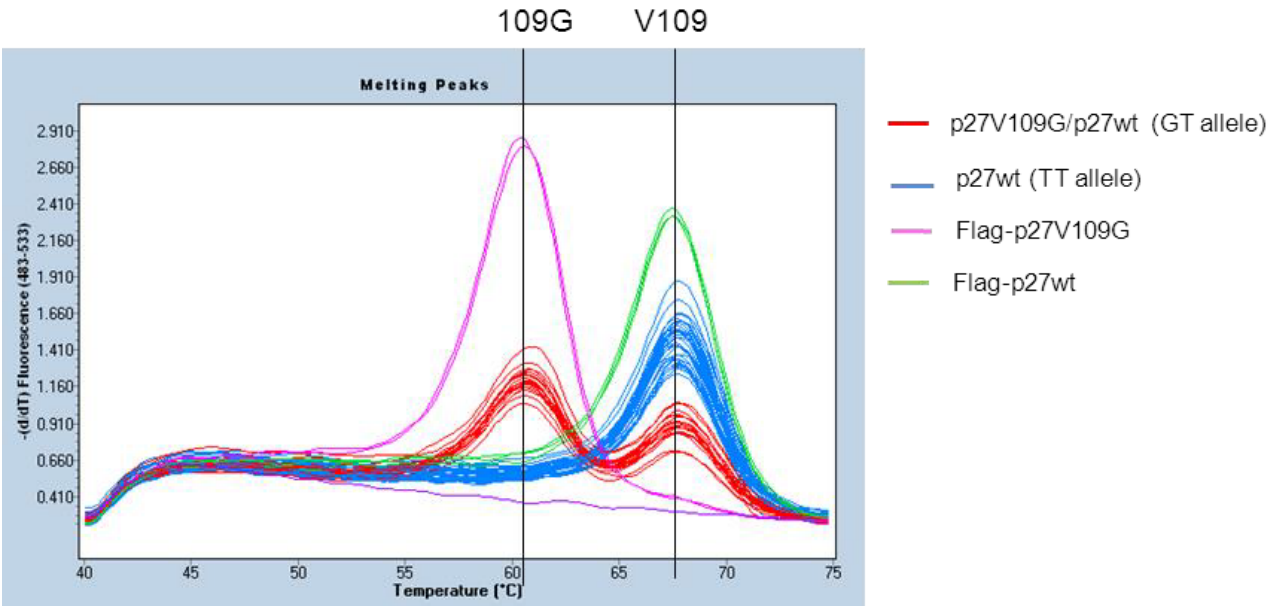

Fig. 26: *Assay1* applied on a cohort of 71 RCC patients. RCC patients harboring p27V109G/p27wt are shown in red and RCC patients harboring p27wt in blue. Constructs FLAG-p27wt (green) and FLAG-p27V109G (pink) served as controls. Tm1 (p27V109G) = 60.5°C and Tm2 (p27wt) = 67.5°C.

The results of *Assay1* including all 71 RCC patients are summarized in Tab. 18 (left panel). Almost half of the patients possessed heterozygous p27V109G (GT allele). As a non-tumor patient control group served the European population of the *1000 genome project* (Abecasis et al., 2012) comprising 503 people (Tab. 18, right panel). In 120 controls the p27 variant was present heterozygous, whereas none harbored the homozygous mutant. RCC patients harboring GT allele (42.5%) were almost doubled compared to the control group with GT allele (24%). Chi Square test analysis revealed a significant association of p27V109G in tumor versus normal tissue (p = 0.002).

Tab. 18: Summarized *Assay 1* results. Results of RCC patient (left panel) and results of control group (right panel). * European population of *1000 genome project*, **chi-square test (p = 0.002)

71 RCC patients			**503 Controls***		
Alleles on position 109	**Count (n)**	**[%]**	**Alleles on position 109**	**Count (n)**	**[%]**
GG	01/71	1.4	GG	0/503	0
GT	30/71	**42.5****	GT	120/503	**24****
TT	40/71	56	TT	383/503	76

Tab. 19: Summarized *Assay 1* results according to RCC subtype.

Alleles	**All RCC subtypes**		**ccRCC**		**pRCC**		**cRCC**	
	n	**%**	**n**	**%**	**n**	**%**	**n**	**%**
GG	01/71	1.4	0/55	0	0/8	0	1/4	25
GT	30/71	**42.5**	26/55	**47.2**	1/8	12.5	1/4	**25**
TT	40/71	56	29/55	52.7	7/8	**87.5**	2/4	50

Further, itemization of *Assay 1* results according to RCC subtypes are shown in Tab. 19. Heterozygous GT allele was found in almost half of the ccRCC (47.2%) but only in 25% of cRCC patients and in 12.5% of pRCC patients. The majority of pRCC possessed p27wt

(87.5%). All RCC melting curves for *Assay 2* are displayed in Fig. 27 and exposed all RCC patients harboring the p27wt (blue). None of the RCC patients was found possessing the p27I119T mutant. cDNA from 786-O cells (pink), FLAG-p27wt (green) and FLAG-p27V109G (orange) constructs served as control to validate the function of *Assay 2*. A larger cohort is needed to investigate the presence of p27I119T in patients with RCC.

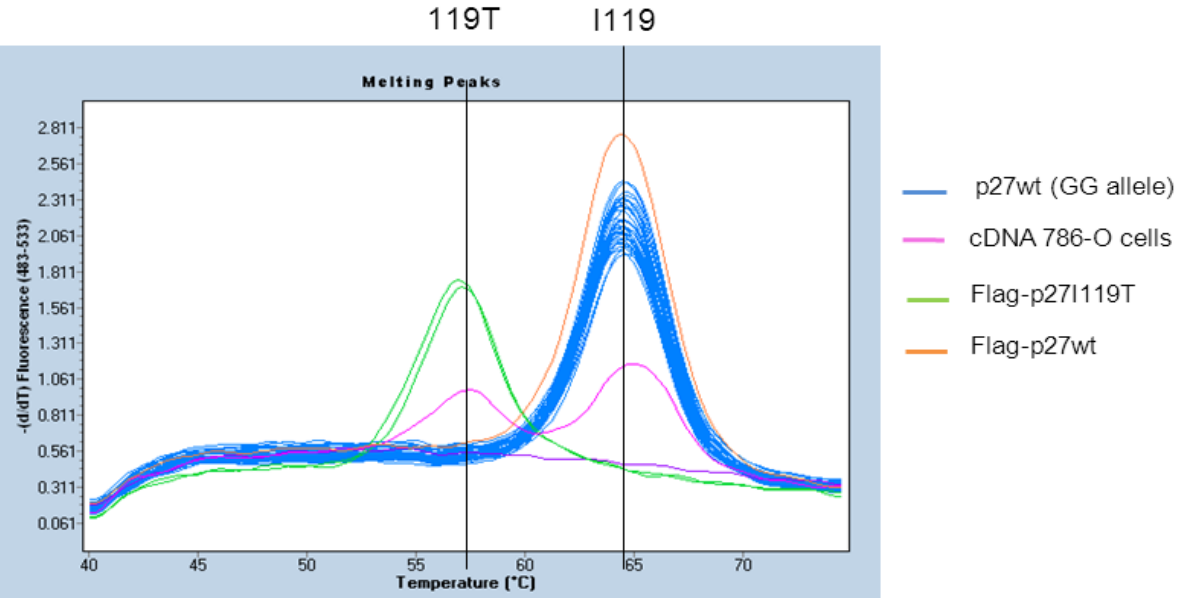

Fig. 27: *Assay 2* applied on a cohort of 71 RCC patients. Patients harboring p27wt are shown in blue and cDNA of 786-O cells in pink. FLAG-p27wt (green) and FLAG-p27I119T (orange) served as controls. Tm3 (p27I119T) = 57°C and Tm4 (p27wt) = 64.5°C.

4. Discussion

4.1 Characterization of components of the CSN-CRL pathway in RCCs

RCCs are very heterogeneous and often show drug-resistance, resulting in challenging difficulties regarding therapy selection for these tumors. In the past decades, several RCC tumorigenesis promoting oncoproteins, involved pathways and lack of tumor supressors in these tumors have been revealed. However, the complete mechanisms leading to RCC tumorigenesis are not yet understood, especially the establishment of therapy-resistant tumors. The literature hints at deregulation of some CSN-CRL pathway components in RCCs. CUL3, p27 and Skp2 were found with altered expression pattern in RCC and correlated with its clinicopathological data (Langner et al 2004). In the present thesis, the six immunohistochemical ccRCCs tissues revealed no deregulation of a single CSN subunit. Further, the stainings showed only slightly varying expression of cullins CUL1-3 in non-neoplastic and tumor tissues. In line with the immunohistochemical data, no single CSN subunit or cullin was found to be disproportionally upregulated within the four RCC cell lines used in this study. CSN subunit CSN5 was found higher expressed in RCC tissues than other CSN subunits (CSN1, CSN3 and CSN8) in both tumor and adjacent tissue. These findings might result from antibody quality. Antibody concentrations were adjusted in FFPE ccRCC test sections and do not allow quantification by comparing staining intensities between the antibodies used. Analysis of expression levels of additional CSN subunits (CSN2, CSN6 and CSN7) in ccRCC tissues (data not shown here) suggests the upregulation of the CSN holo complex rather than of one single CSN subunit, as described in the literature for other tumor types. For example an increased expression of CSN5 and CSN6 in various cancers was described in a recent review (Lee et al., 2011b). However, the authors studied the expression levels of these particular CSN subunits only, without comparing them to the expression levels of the remaining CSN subunits. Hence, the overexpression of the whole CSN complex has to be considered in these studies as well. Furthermore, an upstream regulatory mechanism of the CSN complex supports the assumption of an overexpression of whole CSN in RCC cells. CSN subunit mRNAs are targets of miRNAs of the *let-7* family, which suppress CSN subunit expression in human cells. CSN expression was restored by application of factors that reduce or block *let-7* miRNAs (Leppert et al., 2011). Interestingly, *let-7* was found downregulated in RCCs (Heinzelmann et al., 2011). A total of 30 human ccRCC tissues were screened for miRNA deregulation using microarray technique. The authors identified a group of 12 miRNAs,

including the *let-7* family, which are decreased in highly aggressive primary metastatic tumors, correlating with progression-free survival and overall survival (Heinzelmann et al., 2011). Therefore, down regulation of *let-7* might lead to CSN overexpression in RCC, with the consequence of involvement in cell transformation and tumorigenesis. In renal tissue sections presented here, CSN subunits, three cullins and CAND1 were found mainly expressed in the epithelial cells of renal tubules of non-neoplastic tissue. Renal tubules are the active parts of the kidney. They hold numerous functions concerning the reabsorption and secretion of various solutes, which might explain the accumulation of many regulatory proteins including CSN-CRL pathway components in these compartments. In contrast, in ccRCC tissues only faint cytosol staining intensities of CSN components and cullins were observed. ccRCCs are named after the disintegration of the cells' high lipid content in the cytoplasm. Lipids and other proteins are often removed during the immunostaining procedure and therefore the expression levels of CSN-CRL pathway compontents might be lower in tumor than in non-neoplastic tissues. Converse to initial prospects, CUL1 was found strongly expressed in the cytosol but decreased in the nuclei of renal tubules in the adjacent tissue of all 6 ccRCCs. For comparison, little data from *The Human Protein Atlas Project* exist (Uhlen et al., 2015). Two non-neoplastic tissues showed high nuclear and cytosolic CUL1 expression in the renal tubule (Uhlen et al., 2015). In the present thesis CUL3 expression was observed lower in ccRCCs compared to CUL2 and CUL1 protein levels. And is consistent with Berthold and co-workers results of reduced CUL3 protein expression in renal cancers (Berthold et al., 2008). CUL3 is involved in the regulation of cell differentiation processes (Dubiel et al., 2015a) and loss of CUL3 protein might explain the strong dedifferentiated phenotype of RCCs. Nevertheless, a larger cohort of RCCs including all RCC subtypes has to be examined for cullin expression to confirm these findings and to allow further investigation.

In the present study, localization and expression levels of CAND1 were found altered within six ccRCC FFPE tissues and 20 RCC lysates. Its expression was further studied in a TMA comprising 352 RCCs. This is the first study to analyze CAND1 expression levels in a large cohort of renal cancers with matched normal and tumor tissues. CAND1 showed differing staining intensities in both the nuclei and cytoplasm of non-neoplastic and tumor tissue in all patients. A small cohort of 18 RCCs and 3 non-neoplastic tissues obtained from *The Human Protein Atlas Project* data revealed cytosolic and nuclear CAND1 protein expression as well (Uhlen et al., 2015). Expression levels found in the TMA were categorized in staining intensity groups and analyzed with respect to clinicopathological data and patient prognosis. However, no significant correlation could be established regarding metastasis status, age at nephrectomy and Fuhrman grade of RCCs. Nevertheless, overall survival analysis revealed

increased cytosolic CAND1 to be associated with poor outcome. Moreover, nuclear and grouped cytosolic CAND1 were associated with histological subtypes of RCCs. In the majority of pRCCs and cRCC nuclear CAND1 expression was decreased, whereas half of the ccRCCs were found with high nuclear CAND1 staining intensity. In conjunction with established parameters these novel findings could help to discriminate between RCC subtypes and determine patient prognosis. Only a few studies include information about CAND1 function-associated localization (Yogosawa et al., 1999; Chua et al., 2011). Retinoic acid (RA) treated P19 cells differentiate as neural cells and were examined for CAND1 expression levels and localization. Immunohistological staining analysis revealed that the CAND1 localization pattern in the nucleus was altered by RA treatment from sharp to large speckles. Further, CAND1 protein was increased in RA-treated P19 cells indicating a role in differentiation in these cells (Yogosawa et al., 1999; Chua et al., 2011). In contrast, Chua and co-workers revealed FLAG-tagged CAND1 protein predominantly as cytoplasmic expressed in HEK293 cells, a human embryonic kidney cell line (Chua et al., 2011). They found a three-fold lower concentration of CAND1 in the nucleus compared to that in the cytoplasm. The predominant presence of CAND1 in the cytoplasm suggests that the protein may regulate CRLs differentially dependent on their localization. However, the different experimental settings have to be considered as well as tissue specific location and functions of CAND1. In RCCs cytosolic CAND1 might be involved in different pathways, which possibly contribute to renal tumorigenesis. However, these findings were only observed using immunohistochemical analysis and need to be further investigated using additional CAND1 expression level quantifying methods.

The SRS exchange factor CAND1 is an important regulator of CRLs and required for their function *in vivo* (Schmidt et al., 2009b; Flick and Kaiser, 2013; Pierce et al., 2013; Dubiel et al., 2015a). CAND1 was found to differently influence the integration of FBPs into CRL1 complexes and is involved in differentiation processes (Yogosawa et al., 1999; Dubiel et al., 2013). Recent studies show that CAND1 is involved in disassociation of Skp2 from $CRL1^{Skp2}$ complexes to promote incorporation of other FBPs (Schmidt et al., 2009b; Dubiel et al., 2013). Here, CAND1 knock down experiments displayed higher levels of Skp2 underlining the regulatory functions of CAND1 towards Skp2 in 786-O cells. In addition, four RCC cell lines were investigated regarding CSN-CRL pathway components expression. CSN subunits, CRLs, the CRL substrate cyclin E and FBP β-TrCP were not found disproportionally expressed in the tested cell lines. Interestingly, Skp2 expression appeared to be upregulated in cell line 786-O along with an unusual p27 double band and slightly reduced CAND1 levels. High levels of Skp2 in these cells might result from potential overexpression of CSN complexes. The CSN was observed to regulate Skp2 levels and the assembly of functional $CRL1^{Skp2}$ complexes (Denti

et al., 2006). Further, Roe *et al.* revealed another interesting Skp2 regulation by VHL in RCC cells (Roe et al., 2011). The β-domain of VHL protein interacts with Skp2, stimulating proteasome-dependent Skp2 degradation upon DNA damage. Expression of VHL into VHL-null RCC cells decreased Skp2 levels and restored DNA damage-dependent Skp2 degradation. 786-O cells harbor non-functioning VHL (Maynard et al., 2007). Inactive VHL accompanied by upregulation of CSN complexes would consequently lead to an overexpression of Skp2 in renal cancer cells. Due to reduced amounts of CAND1 in these cells an increased number of $CRL1^{Skp2}$ complexes and down regulation of target proteins expression of Skp2 have to be expected (Fig. 28)

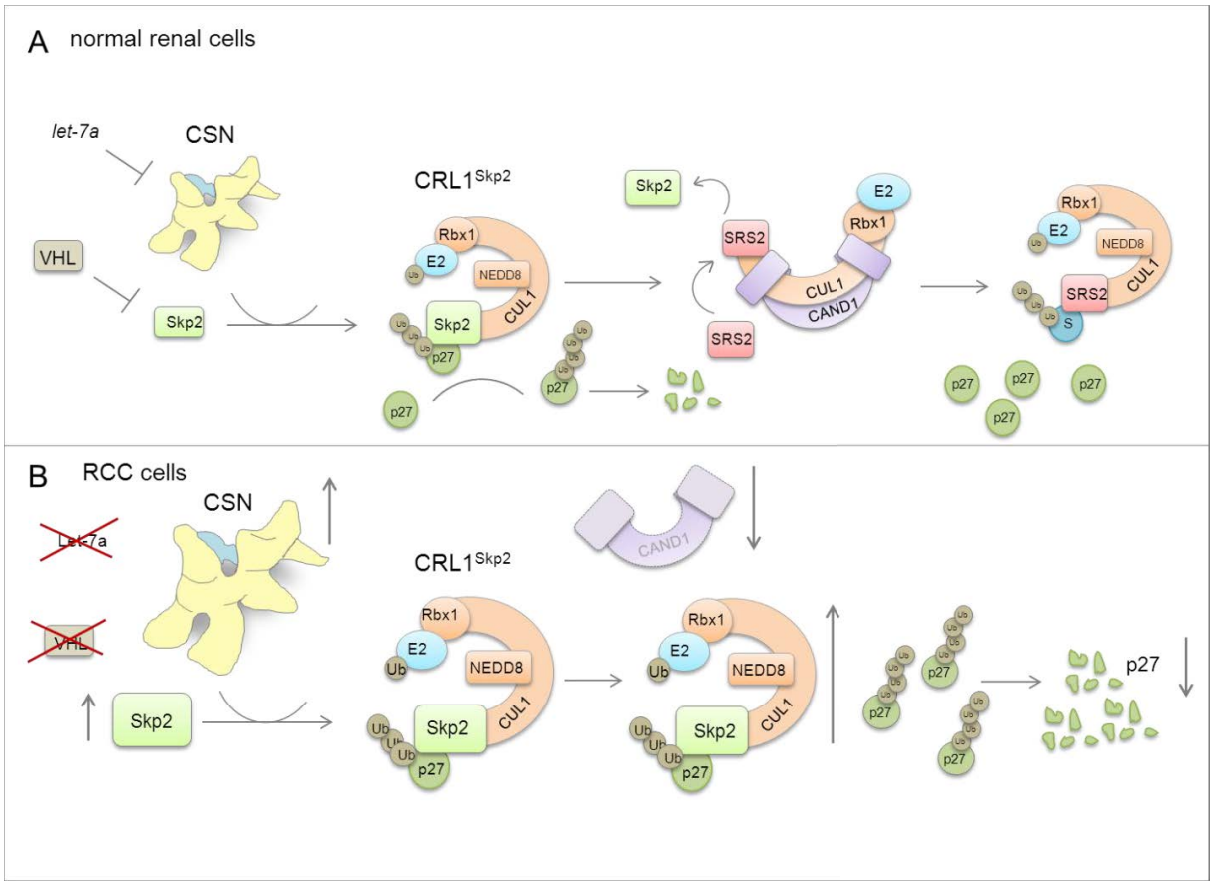

Fig. 28: Model of CAND1-Skp2-p27 axis in normal renal cells (A) compared to RCCs (B).

Skp2 is the most thoroughly studied among the FBPs (Uddin et al., 2015). The 45 kDa nuclear protein functions jointly with adapter protein Skp1 as the SRS of CRL1. The FBP was found to be involved in cell cycle progression. Skp2 knockout MEFs grew significantly slower implying a critical contribution of Skp2 to cell proliferation. In addition, MEFs with reduced Skp2 levels

presented with amplified expression of p27 providing the first genetic evidence that Skp2 is involved in p27 degradation (Nakayama et al., 2000; Zhu, 2010). Several studies hypothesized Skp2 to function as an oncoprotein by targeting and reducing levels of p27 and other tumorsupressors. Skp2 is involved in the pathogenesis of various cancers (for review see (Gstaiger et al., 2001; Uddin et al., 2015). In line with high levels of Skp2 protein displayed in 786-O cells, Skp2 was also found upregulated in a RCC tissue cohort of a TMA study along with reduced levels of p27 and Cks1 (Langner et al., 2004; Liu et al., 2008). In the present study, 4 RCC patients out of a 20 cohort were observed with higher Skp2 levels and associated with metastasis status (M1) according to clinicopathological data. Apart from regulation of important Cdk inhibitors, Skp2 was also found to be involved in metastasis formation in lymphomic (Latres et al., 2001), gastric (Wei et al., 2013), colon (Chen et al., 2014) and colorectal carcinomas (Bochis et al., 2015). Moreover, increased Skp2 levels in 786-O cells were also associated with cell migration and cell invasion. Lu *et al.* could demonstrate that Skp2 overexpression had a significant promotion effect on invasion and migration in 786-O cells (Lu et al., 2014). These effects were reversed by Skp2 silencing inducing subsequent p27 and cyclin E upregulation. Skp2 overexpression directly increased the expression of matrix metallo-proteases MMP-2 and MMP-9 and decreased TIMP-1, suggesting a possible mechanism by which Skp2 is involved in cell invasion (Lu et al., 2014). Taken together, the above presented findings point to a deregulation of CSN, CAND1 and Skp2 levels in RCC and their joint involvement in renal tumorigenesis. However, the reason of upregulation of Skp2 in 786-O cells compared to Skp2 levels in ACHN, A498 and Caki-1 cells is still unclear. Furthermore, an unusual double band of the Skp2 target p27 was found in the Western blot analysis of 786-O cells, which was identified in this study as p27V109G and p27I119T.

4.2 Characterization of p27 mutants in 786-O cells

The primary tumor cell line 786-O displayed an interesting unusual p27 double band in Western blot analysis. Primary assumptions regarding their origin focused on protein post-translational modification. CRL substrates are often modified prior to substrate recognition by SRS via phosphorylation. Several p27 phosphorylation sites and their corresponding kinases have been identified (Fig. 29, upper part). Each active phosphorylation residue enables p27-explicit functions. Skp2 along with Cks1 specifically recognizes $p27^{Thr187}$ in a phosphorylation-dependent manner (Carrano et al., 1999). p27 phosphorylation on the three specific residues

S10 (by hKIS, Akt and MAPK kinase), T157 and T198 (by Akt kinase) promotes translocation from the cell nucleus to the cytoplasm (Roy and Banerjee, 2015).

Moreover, oncogenic kinases Src and Abl phosphorylate p27 at tyrosine Y74 and Y88 leading to impaired inhibition of Cdks by of p27. However, contrary to initial expectation, posttranslational phosphorylation was not responsible for the shift of the two p27 forms from 786-O cells in SDS PAGE analysis. Dephosphorylation experiments did not show any reduction of the p27 upper migrating band. Ectopically expressed His-tagged p27wt in 786-O cells remained a single protein band. Based on these findings posttranslational modification as a reason for p27 protein migration pattern in 786-O cells is very unlikely, but it cannot be ruled out completely.

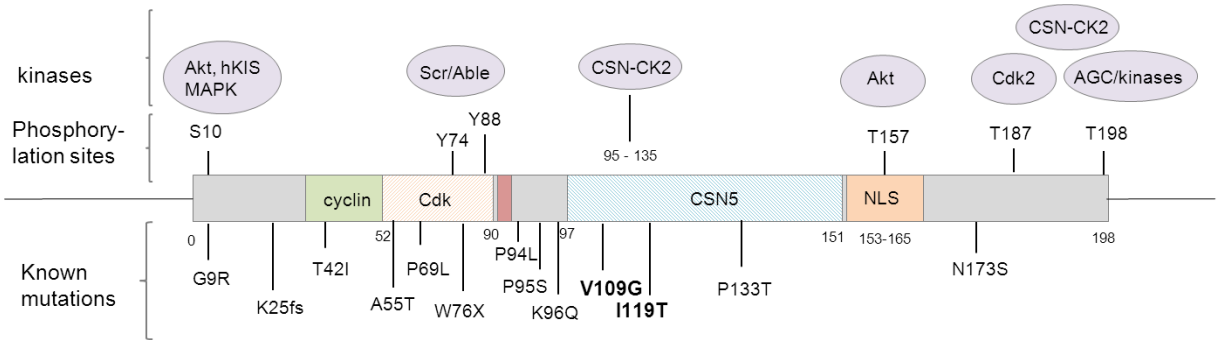

Fig. 29: Scheme of p27 functional domains. The upper part focuses on phosphorylation sites of p27 and their involved kinases. In the lower panel selected identified missense mutations are displayed.

In order to reveal the molecular basis of the specific p27 appearance in 786-O cells, p27 protein immunoprecipitates were analyzed by mass spectrometry. Comparison of p27wt and p27 upper and lower protein bands exposed a single point mutation in each of the two p27 proteins: p27V109G and p27I119T. Both point mutations were validated by sequencing of p27 cDNA from 786-O and A498 cells. Several missense mutations have been identified in p27 protein including p27V109G and p27I119T (Fig. 29, lower panel) and are associated with different carcinoma types (Tab. 20). p27V109G is an already known single nucleotide polymorphism (SNP) (rs2066827) found in various tumors (for review see (Wei et al., 2012)). Further, p27I119 is registered as SNP rs142833529. Obviously, the Valine to Glycine exchange results in a slightly faster gel migration whereas the Isoleucine to Threonine substitution in a slower

migration of the p27 mutant in SDS-PAGE as compared to p27wt. The unique migration pattern of p27I119T was also found by Tichomirowa and co-workers in pituitary adenoma tissue. Confirming my findings, the migration of the upper p27 mutant band was not affected by kinase inhibitors treatment suggesting no migration caused by phosphorylation of p27. However, glycosylation was not ruled out by the authors and might explain their observation of a more stable p27I119T (Tichomirowa et al., 2012).

Tab. 20: Selected missense mutation in p27 protein and their associated tumor types.

Protein change	Tumor type	Reference
T42I,N173S	Small bowel neuroendocrine tumors	(Maxwell et al., 2015)
A55T, **V109G**	Multiple endocrine Neoplasia 1	(Longuini et al., 2014)
W76X, P95S, P69L**, V109G**	Multiple endocrine Neoplasia 4	(Molatore et al., 2010)
K96Q, **I119T**	AIP- isolated pituitary Adenoma	(Tichomirowa et al., 2012)
G9R, P133T	Sporadic parathyroid adenoma	(Costa-Guda et al., 2011)
F80Q, P94L	Hairy cell leukemia	(Robak and Smolewski, 2015)

Homeostasis of p27 is finely regulated by multiple proteins on transcriptional and translational levels and via protein degradation (for review see (Chu et al., 2008)). Cycloheximide chase experiments revealed a downregulation of both p27wt and p27 variants, in 786-O and A498 cells. Protein degradation was rescued by proteasome inhibitor MG132 application demonstrating 26S proteasome-dependent proteolysis. The data confirm the degradation of p27V109G and p27I119T by the UPS. During G1 phase p27 proteolysis rises dramatically and p27 levels are reduced five- to eightfold in G0 to S phase cells (Nakayama and Nakayama, 2006). Whereas the half-life of p27 in G1 phase lasts approx. 2.5 h, it was found to be less than 15 min during S-phase (Connor et al., 2003). The cells used in our study were asynchronous. Half-life of p27wt and p27 mutants amounts 0.75-1 h and these results are in line with other recent findings (Fernandez et al., 2015). Moreover, CAND1 knockdown in 786-O cells revealed increased Skp2 levels accompanied by reduced p27 mutant levels indicating $CRL1^{Skp2}$-mediated degradation. In 1999, Carrano and co-workers first showed that Skp2 is required for ubiquitination of p27 (Carrano et al., 1999). Later, targeting p27 for degradation was found to be regulated by two pathways. In G0 or early G1 phase Skp2 and cyclin E levels are low and p27 degradation is mediated by KPC complexes (for review see (Chu et al., 2008)). Following mitogenic stimulation amounts of both proteins rise leading to rapid p27 degradation.

Whether ubiquitination of p27V109G and p27I119 occurs only via $CRL1^{Skp2}$ in 786-O cells or also through other mechanism is currently not clear.

A plethora of proteins bind to p27 in order to regulate protein stability and to promote several pathways (Fig. 30). In recent years, an increasing number of p27 interactors were identified like CSN5, Grb2, RhoA, Rac, Stathmin, 14-3-3, Jak2, HIPK and HSC70 (Borriello et al., 2015). The amino acid exchange in the two p27 variants might interfere with protein-protein interactions, leading to an altered p27 pathway network. As shown in Fig. 30, codons 109 and 119 do not lie neither within the well-characterized Cdk binding region (amino acids 22-106) nor NLS (amino acids 153-165) of p27 protein (Borriello et al., 2015). However, even single amino acid exchanges can provoke protein conformational changes and indirectly affect protein interaction. Interestingly, both codons are localized within the binding region to CSN5 (amino acids 97-151) and CSN associated kinases (amino acids 101-113) (Tomoda et al., 2002). FLAG pulldown analysis in A498 cells using generated FLAG-p27wt, FLAG-pV109G and FLAG- p27I119T constructs revealed binding partners of the CSN-CRL pathway. Both p27 variants and p27wt were found to precipitate with cullins (CUL1, CUL3), the CSN and Skp2. Contrary to initial expectation p27V109G and p27I119T bind to the CSN5 with no significant difference when compared to p27wt. However, the analysis only shows binding of both p27 variants to the CSN subunit but not their putative impact on CSN function. In this context, it has been suggested that p27 or p27-Skp2 modules inhibit CSN-mediated deneddylation (Bornstein et al., 2006; Schmaler and Dubiel, 2010; Emberley et al., 2012) as an important regulatory step in the CSN-CRL pathway. Subsequent mass spectrometry analysis of FLAG pulldown eluates showed slight variation in cyclin and cdk binding towards p27 protein.

As an exception, cyclin D3 was only found bound to p27V109G, but not to the other mutant or p27wt. In thyroid cancer cells, cyclin D3 supports maintenance of p27 in the cytoplasm of thyroid tumor cells. In normal thyroid cells more than 70% of p27 was detected in the nuclear compartment, whereas in tumor cells p27 was essentially confined in the cytoplasmic compartment co-localized with cyclin D3 (Baldassarre et al., 1999). Cytoplasmic p27 is less efficient in inhibiting the progression to S-phase of the cell cycle, probably resulting from the inability to bind and inhibit nuclear Cdk2. Interestingly, the mutant p27V109G was found in thyroid cancers (Pasquali et al., 2011; Barbieri et al., 2014). P27V109G-cyclin D3 binding might shuttle the mutant into the cytoplasm and contribute to cell cycle progression also in renal

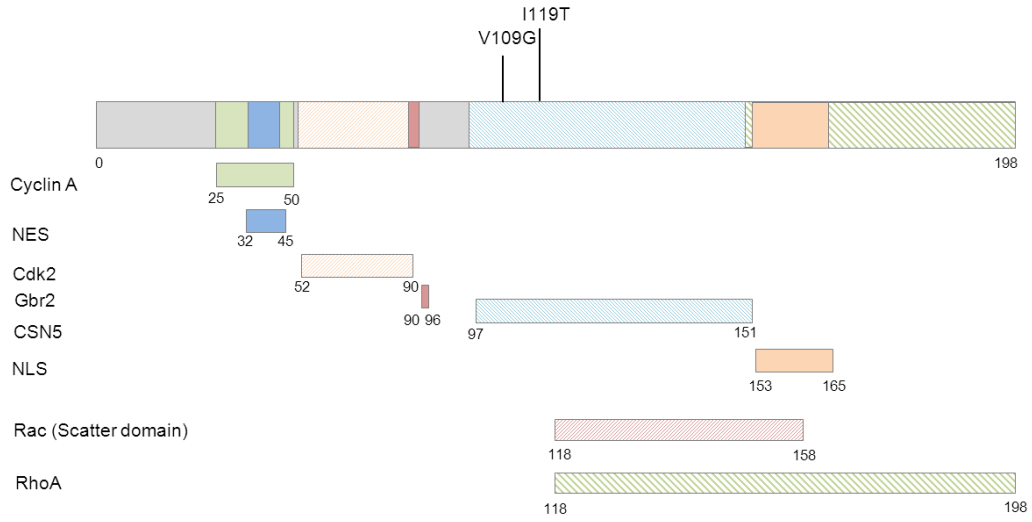

Fig. 30: Scheme of the main p27 structural domains with indicated binding regions. NES = nuclear export sequence, NLS = nuclear localization sequence, Gbr = Growth factor receptor-bound protein 2.

cancer cells. Nevertheless, cyclin E, essential for p27 function and stability, did bind to all three p27 types. Future studies should focus on additional prominent p27 binding cyclins and cdks. Inhibition of Cdks interfers with cell proliferation, and changes within the p27 protein might result in deregulation of proliferating cells. In this context, 786-O cells harboring both p27 mutants were found to grow 2-3 fold faster than p27wt possessing A498 cells. The presence of the two mutated p27 variants in 786-O cells might increase the cell proliferating effect additively in these RCC cells. Sekyia and co-workers observed similar results in pituitary adenomas cells (Sekiya et al., 2014). Genotyping a large cohort of patients with sporadic endocrine tumors revealed the first association of p27V109G with a group of pituitary adenomas ($p < 0.01$), especially ACTH-secreting tumors ($p < 0.005$) but not GH3-secreting tumors. Using AtT20 cells, a corticotropin mouse cell line ectopically overexpressing the p27V109G variant, the authors observed an increase of colony formation and cell growth rate compared to p27wt (Sekiya et al., 2014). Both RCC and endocrine cancers belong to the group of adenomas, tumors of epithelial tissue with glandular origin or glandular characteristics. P27V109G might play an important role in these tumors. Further investigations are needed to elucidate the molecular basis of these interesting findings to understand the exact mechanisms of how p27V109G and p27I119T are involved in altered proliferation of RCC cells.

4.3 p27V109G and p27I119T in cancer

In the past decades, several SNPs have been identified in the human *CDKN1B* gene and have attracted attention regarding their involvement in tumorigenesis. The SNPs rs2066827 (p27V109G) and rs142833529 (p27I119T) were already described in various tumors. It is unknown whether the two p27 mutants also play an important role in renal tumorigenesis. No study has confirmed the existence of p27V109G and p27I119T mutants in RCC patients so far. In a small cohort of 20 RCC patients, Western blot analysis of RCC tissues lysates revealed the presence of a p27 double band, potentially the p27V109G and p27I119T mutants. A genotyping assay was established to investigate the prevalence and relevance in a larger representative cohort of 71 RCC tissues. The variant p27V109G was found heterozygously (GT allele) in 42.5% of the RCC patient cDNAs, whereas the homozygous variant (GG allele) was present in 1 patient cDNA (1.4%). No significant association was found between the p27 polymorphism and RCC tumor grade ($p = 0.800$) or pT stadium ($p = 0.608$). However, for future studies a larger group of patients should be examined to confirm these correlation tendencies. In order to compare these here presented findings of p27V109G in RCC patients to a healthy control group, rs2066827 results from the *1000 Genomes Project* were considered.

The *1000 Genomes Project* aims to find genetic variants that have frequencies of at least 1% in the populations studied and make it quickly available to the worldwide scientific community (Abecasis et al., 2012). The p27V109G variant was found in 36% of the whole sequenced population, clearly qualifying it as polymorphism. Interesting to note, the rs2066827 varies strongly among the population subtypes: Asian (6%), African (78%), European (24%), North American (22%) and South American (32%). Considering these subpopulation variations for rs2066827, the p27V109G variant was detected in 42.5% of the European RCCs cases compared to 24% in the European healthy control population. These findings were found to be significant ($p = 0.002$) and might be a future discrimination tool for RCC patients. The p27I119T was observed associated with three diseases so far; myelo-proliferative disorder, familial isolated pituitary adenoma (FIPA) and prostate cancer (Tab. 21).

In hematological neoplasia, gene mutations of p27 are rarely described and might be an important discriminating tool. A decade ago, Pappa and co-workers reported on a novel point mutation in *CDKN1B* gene identified in a case of unclassified myelo-proliferative syndrome. A T to C transversion, resulting in an isoleucine to threonine substitution at codon 119 was found. The authors suggest an active OH^- group on the threonine may affect protein conformation (Pappa et al., 2005). Unfortunately, the patient died during the study and no intact tissue was

Tab. 21: Impact of p27I119T on cancerogenesis of different tumor types. (FIPA = familial isolated pituitary adenoma)

Disease	Incidence	Association with disease?	p27I119T impact	Reference
Myeloproliferative disorder	1 patient	**Yes**	unknown	(Pappa et al., 2005)
Acromegaly (FIPA)	1.13% of FIFA patients	**Yes**	may play role in tumor predisposition	(Tichomirowa et al., 2012)
Prostate cancer	not defined	**Yes**	increased risk of hereditary prostate carcinoma	(Chang et al., 2004)

available for further analysis. A larger cohort is needed to validate the presence of p27I119T in patients with myelo-proliferative syndromes and additional functional studies are required to evaluate its role in the pathogenesis. The SNP p27I119T was also detected in FIPA cases (Tichomirowa et al., 2012). FIPAs belong to pituitary adenomas in a familial setting, but in the absence of MEN1. 15-20% of the cases harbor mutations in the aryl hydrocarbon receptor (AIP). The *CDKN1B* gene was screened in 88 FIPA *AIP* mutation-negative patient tissues in order to expose additional potential genetic causes. The two new germline changes p27K96Q and p27I119T were revealed in the study (Tichomirowa et al., 2012). As shown above, further functional analyses were performed to learn more about the function of these two variants in FIPA, suggesting that p27I119T might play a role in tumor predisposition.

Over a decade ago, Chang and co-workers also found the p27 variant in hereditary prostate cancer (Chang et al., 2004). *CDKN1B* gene was screened in 96 probands from HPC families for p27 germline mutations in prostate cancer tissue and a total of ten sequence variants were identified. Three out of four SNPs in the coding sequence caused amino acid changes. A total of ten sequence variations were identified in different parts of the *CDNK1B* gene including three in the coding sequence causing the amino acid changes; p27E86D, p27V109G and p27I119T. The variant p27I119T was found in one patient only. Hereby Chang and co-workers confirmed the in the present thesis described observation on the low frequency of this variation. The authors suggest missense changes might alter the interaction between p27 and CSN5 due to the location in the interaction surface. As shown above, protein binding studies could not validate this hypothesis. Interestingly, the variant p27I119T was found along with the variant p27V109G (Chang et al., 2004) similar to findings in 786-O cells. The combination of both

variants might be responsible for the faster growth rate of prostate cancer cells. The p27V109G variant was also found to be associated with an increased risk of advanced prostate cancer in a European-American population (Kibel et al., 2003). Almost 25% of the patients harbored the heterozygous GT allele (p27V109G/p27wt) and were strongly associated in those patients with under the median age of diagnosis, with androgen-independent disease and high-risk genotypes of *CDKN1A* and *CDKN1B* gene, respectively. In addition to studies in Caucasian males, Huang and co-workers investigated the p27V109G in an Asian cohort. The frequency of the G allele in Taiwanese males appeared to be low (2.1%) and did not significantly associate with prostate cancer risk (Huang et al., 2008). However, according to *1000 Genomes Project* data the incidence of rs2066827 within the Asian control population is extremely low in general (6%) (Abecasis et al., 2012) and might not be comparable to the Caucasian data. After its discovery in prostate carcinoma, the p27 variant was also found in various other tumors entities later on. Whereas common solid cancers such as lung, stomach and liver cancer are rarely associated with the SNP, p27V109G is noticeable often described in endocrine tissue carcinomas influencing their outcome (Tab. 22).

For non-endocrine tumors, the variant p27V109G was also found in squamous cell carcinoma of the head and neck (SCCHN) tumorigenesis (Li et al., 2004), breast cancer (Ma et al., 2006; Naidu et al., 2007; Spurdle et al., 2009) and endometriosis (Camargo-Kosugi et al., 2009). The p27V109G variant does not play a major role in the etiology of SCCHN, though it may contribute to subsets of those tumors. The risk was significantly associated among men, current alcohol users and patients with oral cavity cancer (Li et al., 2004). Five studies investigated the p27 variant incidence in breast cancer including two recent meta-analyses (Xiang et al., 2013; Jia et al., 2014). Their data suggests no association between p27V109G alone and breast cancer risk. However, one study showed the variant is associated with lymph node metastases (Naidu et al., 2007). Therefore, it may not be a marker for determining the breast cancer risk but a potential genetic marker for tumor prognosis. For endometriosis the distribution of genotype and allele frequencies of p27V109G polymorphism differed significantly between the endometriosis cases and healthy women ($p = 0.016$ and 0.002). Women who had at least one mutated allele presented 2-fold chances for endometriosis development (Camargo-Kosugi et al., 2009). Further experiments are needed to completely understand the role of p27V109G in SCCHN, breast cancer and endometriosis. Another female organ disease associated with the p27V109G variant is epithelial ovarian cancer (ECO). While the p27V109G incidences vary between 5 and 35% in most tumors, 51% of the ECO patients harbor p27V109G (Gayther et al., 2007; Mohamed et al., 2013). ECO is one of the most

Tab. 22: Impact of p27V109G on cancerogenesis of different tumor types (sMTC = sporadic medullary thyroid carcinoma, SCCHN = Squamous cell cancer of the head and neck, MEN1 = Multiple endocrine neoplasia 1, SET = sporadic endocrine tumors)

Tumor type	Association with cancer?	p27V109G impact	Reference
Prostate cancer	**Yes**	Increased risk of advanced prostate carcinoma	(Kibel et al., 2003)
	Yes	Increased risk of hereditary prostate carcinoma	(Chang et al., 2004)
	No	None	(Huang et al., 2008)
SCCHN	**Yes**	Increased risk in at-risk subgroups or subsets	(Li et al., 2004)
Endometriosis	**Yes**	increased risk of endometriosis	(Camargo-Kosugi et al., 2009)
Ovarian cancer	**Yes**	Yes, moderate risk for ovarian cancer susceptibility	(Mohamed et al., 2013)
	Yes	decreased risk	(Gayther et al., 2007)
Breast cancer	No	None	(Spurdle et al., 2009)
	No	Increased risk of lymph node metastases	(Naidu et al., 2007)
	No	None	(Ma et al., 2006)
	No	None	(Jia et al., 2014)
	No	None	(Xiang et al., 2013)
Oral squamous cell, prostate, breast cancer, and pancreatic cancer	No, not overall cancer risk (but prostate cancer) decreased risk of prostate cancer		(Wei et al., 2012)
sMTC	**Yes**	decreased risk	(Pasquali et al., 2011)
	Yes	increased risk	(Barbieri et al., 2014)
SET	**Yes**	associated with pituitary adenomas	(Sekiya et al., 2014)
MEN1	**Yes**	Yes, disease modifier for the MEN1 syndrome	(Longuini et al., 2014)

commonly diagnosed cancers worldwide, but its etiology is still largely unknown. Goode *et al.* tagged common variation in 11cell cycle genes and could reveal an association between the p27V109G polymorphism and reduced EOC risk (Goode et al., 2009). Another recent study evaluated the role of SNPs in three genes; XRCC2 (R188H), ERCC2 (K751Q) and CDKN1B (V109G), which come with moderate risk for EOC susceptibility in Egyptian women, and identified these three gene variants as important candidate genes for susceptibility to ovarian cancer (Mohamed et al., 2013).

The here gathered data did not show fully consistent results within different studies published over the past years. A total of 8 eligible studies with 3591 cases and 3799 controls were comprised in a meta-analysis to comprehensively assess the correlation between the p27V109G polymorphism and the cancer risk (Wei et al., 2012). They included 4 types of cancer (pancreatic, prostate, breast cancer and SCCHN) and also embedded studies analyzed above (Kibel et al., 2003; Li et al., 2004; Ma et al., 2006; Naidu et al., 2007; Huang et al., 2008). The p27V109G polymorphism did not associate with the breast cancer risk, but it seemed to be associated with a decreased prostate cancer risk (Wei et al., 2012). However, the search for relevant studies for this meta-analysis was performed in 2011 and does not include recent studies involving mainly endocrine tumors, which showed a strong association between p27V109G and endocrine tumorigenesis. Furthermore, two older tumor studies were excluded from the study also revealing an association of rs2066827 with tumor risk or correlation with favorable disease progression (Chang et al., 2004; Pasquali et al., 2011). In its current state, it is impossible to exclude a p27V109G association with overall tumor risk completely. Future meta-analyses need to be performed to answer open questions and to clarify possible links between p27V109G and tumorigenesis.

Interesting to note, the SNP rs2066827 was found to be strongly associated with endocrine tumors such as thyroid cancers, sporadic medullary thyroid cancer (sMTC) and multiple endocrine neoplasia type 1 (MEN1). In sMTC the p27V109G allele (GG+GT allele combined) was found in 46% of the cancer patients and correlates with more favorable disease progression than the p27 (TT allele) (Pasquali et al., 2011). The variant is considered a new promising prognostic marker in sMTC as it positively correlates post-operative with biochemical remission and a normal range of calcitonin levels, a hormone responsible for regulating calcium blood levels (Fragu, 2007). The molecular basis of p27V109G involvement in calcitonin level regulation remains to be discovered. Moreover, somatic mutations in the gene encoding for the receptor tyrosine kinase RET were significantly associated with a more aggressive behavior especially in p27wt bearing patients (Pasquali et al., 2011). These findings are in line with a study from Joshi *et al.* which demonstrated downregulation of p27 by a RET mutant mediating repression of p27 mRNA expression (Joshi et al., 2007). Barbieri and co-workers could confirm the presence of p27V109G by 37.8% in sMTC patient group not harboring the sMTC promoting *RET* gene mutation. They could determine a relative contribution of p27V109G to the risk of developing MTC by 8% according to a stepwise regression analysis (Barbieri et al., 2014). These findings are contrary to Pasquali *et al.* and suggest an involvement of p27V109G in the tumorigenesis of sMTC without *RET* gene mutation. Landa *et al.* included other subtypes of sporadic thyroid carcinoma in their case

control study and could not find any significant association for rs2066827 with any of the thyroid cancer subtypes analyzed (Landa et al., 2010). Therefore, the p27V109G variant might be specifically involved in sMTC progression, but not in other thyroid cancer subtypes. As described above, another study investigated the p27V109G variant in a variety of sporadic endocrine tumors. The authors found an interesting association in pituitary adenomas, in particular ACTH-secreting pituitary adenomas (Sekiya et al., 2014). In line with results from Longuini *et al.*, they observed a significant over-representation of the T allele in patients with sporadic counterpart of MEN1-component neoplasia (Longuini et al., 2014). In contrast to the p27wt, the p27 variant seems to promote cell growth and proliferation. This specific molecular phenotype was only found in corticotrophe cells but not in somatotrophe cells suggesting a possible future discrimination factor for pituitary adenomas.

In multiple endocrine neoplasia type 1 (MEN1) a strong association between p27V109G presence and disease progression was found (Longuini et al., 2014; Sekiya et al., 2014). MEN syndromes are inherited as autosomal-dominant disorders and encounter several syndromes including neoplasias of endocrine glands such as parathyroid hyperplasia, pituitary adenoma, medullary thyroid cancer and pancreatic tumors as well as non-endocrine tumors (Falchetti et al., 2009; Marini et al., 2015). The four subtypes MEN1-4 have been described. In MEN1 the pituitary, parathyroidic and pancreatic tissue is affected. Initially germline p27 mutations were identified in patients with MEN4, also called MEN1-like syndrome (Falchetti et al., 2009). Mutations in the *MEN1* gene were identified in 70-95% of MEN1 patients (Gaudray and Weber, 2009; Marini et al., 2015). Interestingly, immunoprecipitation studies revealed that the MEN1 gene product menin directly associates with regions of the p27 promoter and regulates p27 protein expression in pancreatic β-cells, suggesting that MEN1 and p27 might share a common endocrine tumorigenic pathway (Karnik et al., 2005). Therefore, truncation of menin protein resulting in loss of function was postulated to lead to decreased p27 mRNA levels. Longuini *et al.* investigated patients harboring the MEN1-mutation and found significant differences in p27V109G allele frequencies between controls and MEN1 patients. The T allele (p27wt) was over-represented and the presence of at least 1 T allele was strongly associated with higher number of affected neoplastic glands in patients carrying truncating MEN1 mutations. In contrast to other studies, these results show that the variant G allele might protect against thyroid cancer development (Longuini et al., 2014). Nevertheless, the authors revealed the first strong genotype-phenotype correlation found in the MEN1 syndrome and could identify rs2066827 as a genetic variant that influences the clinical manifestation of MEN1 adult patients carrying MEN1 truncating mutations.

Taken together, both p27 variants were found in different tumor entities and were partly associated with tumor progression. P27I119T was found in 3 malignancy types only, whereas p27V109G was observed in various cancer types throughout the past decades. The variant does not play a major role in the etiology of most tumors. However, it was found in some tumor subtypes exclusively and therefore might be a useful future discrimination tool. Interesting to note, endocrine tumors were found to be associated with p27V109G. RCC and endocrine tumor belong both to adenomas suggesting similar pathways involved, which should be investigated in the future.

5. Conclusions and Outlook

Due to point mutations in protein coding sequences, tumor cells must deal with numerous unfolded proteins. They require more effective protein quality control than normal growing cells. Consequently, targeting components of the UPS are a promising approach for tumor therapy (Deshaies, 2014). In the present thesis, the CSN-CRL pathway was studied in order to identify possible new targets for the treatment of renal cancers. Immunohistochemistry results did not show an overexpression of a single CSN subunit in ccRCC. However, it seems that the CSN holo complex is upregulated in analyzed ccRCC tissues, probably resulting from the increased burden of unfolded proteins and DNA damage in these cells (Feist et al., 2014). Western blot analysis of four RCC cell lines revealed a deregulation of the CAND1-Skp2-p27 axis in 786-O cells. The cell line harbors a unique combination of two p27 mutants, increased Skp2 and decreased CAND1 levels. CAND1 was investigated in a larger cohort of RCC patients revealing that the combination of high levels of cytosolic CAND1 and low levels of nuclear CAND1 significantly reduces the overall survival rate in ccRCC patients. At the moment it is not clear whether p27V109G and p27I119T are directly responsible for the altered CAND1 and Skp2 expression. Although both p27 mutants and p27wt are degraded by $CRL1^{Skp2}$, they might challenge the UPS by slight conformational changes. The here analyzed protein-protein interactions of the two p27mut including binding to the CSN, Skp2, Cdks, and cyclin A revealed mostly unchanged interactions when compared to p27wt. Most notably, 786-O cells grow 3-fold faster than A496 cells expressing p27wt. This effect might be due to impaired functions of the p27V109G and p27I119T mutants to act as a cell cycle control proteins. Interestingly, the variant p27I119T was found along with the variant p27V109G in prostate cancer cells (Chang et al., 2004) similar to our findings in 786-O cells. The combination of both p27 variants might be responsible for the faster growth rate of these cancer cells. However, the exact mechanism has yet to be discovered.

Furthermore, the mutant p27V109G was identified in RCC tissues by Western blotting and a specifically developed genotyping assay. According to the detected frequency of occurrence (42.5%), the p27 variant has to be considered as SNP in RCCs. The polymorphism rs2066827 (p27V109G) and the polymorphism rs142833529 (p27I119T) have already been described in the literature regarding prostate and other cancers. However, whether tumorigenesis of renal cancers or other cancer types is directly associated with p27V109G and/or p27I119T have to be elucidated through future experiments. Interestingly, p27V109G was found in specific tumor subtypes, mainly endocrine tumors. The p27 mutant might serve as a discrimination factor and

is possibly involved in yet unknown RCC tumorigenesis pathways. In RCC the therapeutic opportunities are limited since RCC patients cannot be treated with conventional chemotherapy and radiation (Corn, 2007). As shown in this work and below, the CSN-CRL pathway might be a useful target for the treatment of renal cancers. Selected compounds which especially target the CSN-CRL pathway are summarized in Fig. 31 and Tab. 23. A growing body of literature implicates the potential of some compounds targeting the UPS including E1s, E2s and the 26S-proteasome (for review see (Bedford et al., 2011)). Bortezomib was found to be affective in multiple melanoma and mantel cell lymphoma and the first drug approved by the Food and Drug Administration (FDA) (for review see (Kouroukis et al., 2014)). Also noteworthy is the discovery of compound PYR-41, blocking ubiquitination of TRAF6 and thereby impeding the degradation of p53 and IκBα (Yang et al., 2007). PYR-41 killed transformed p53-expressing cells implying that the compound is an effective E1 inhibitor for treatments of human cancers (Liu et al., 2015). Furthermore, inhibition of the E2 enzyme Cdc34 by the compound CC0651 suppressed cell proliferation and led to accumulation of p27 in human cancer cell lines (Harper and King, 2011). Another recent approach are Protacs (proteolysis-targeting chimaeric molecules). These are small molecules that promote the binding of E3 ligases and their targets, inducing their ubiquitination and subsequent degradation (Bulatov and Ciulli, 2015).

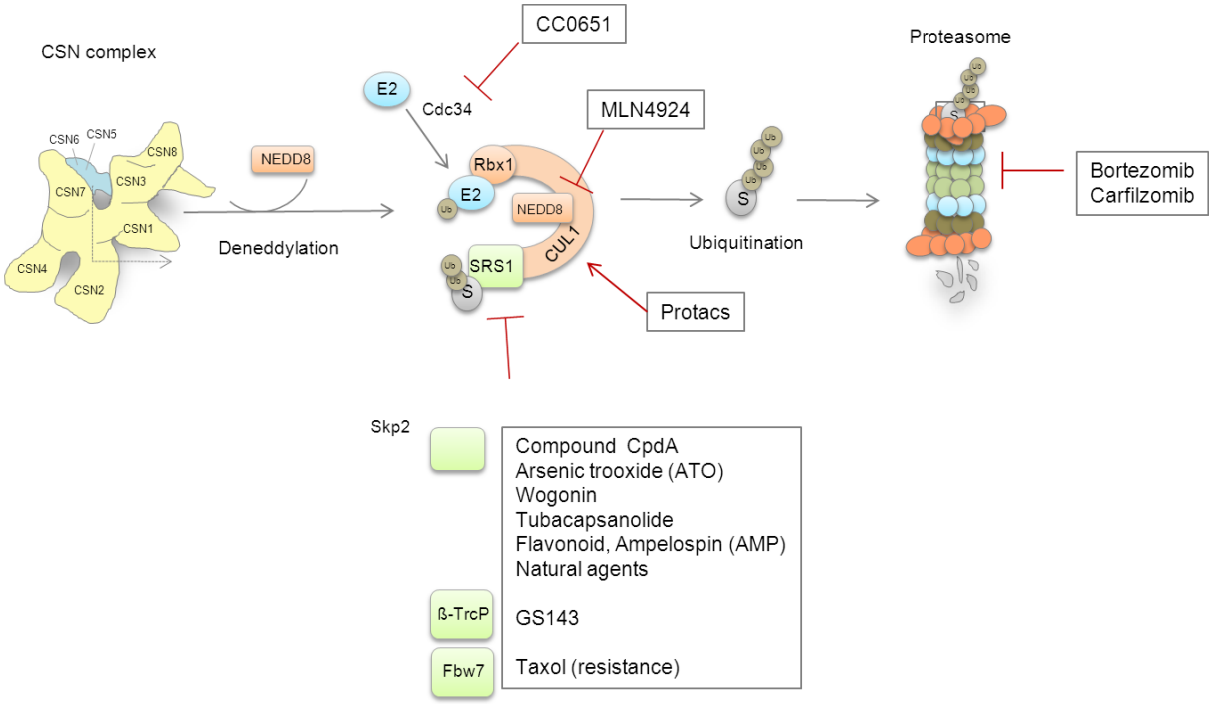

Fig. 31: The CSN-CRL pathway as drug potential target.

In contrast, inhibition of CRL activity is triggered by MLN4924 (Soucy et al., 2010). The compound is a potent and selective inhibitor of NAE (NEDD8-activating enzyme), an E1 that is involved in the neddylation of cullins, and rescues tumor suppressor proteins from degradation. However, most troubling is the lack of specificity of these inhibitors. The developed drugs affect a pool of essential proteins along with targeted protein substrates, causing severe side-effects. Inhibiting a single E3 ligase/SRS seems to be a better approach f treating human cancers (Tab. 23). Recently, well-studied FBPs such as Skp2, β-TrCP and Fbw7 evolved as potential drug targets (for review see (Uddin et al., 2015)). Skp2 and β-TrCP mainly function as oncoproteins, whereas Fbw7 was found to be a well-known tumor suppressor. The FBP recognizes several oncoproteins and ubiquitinates them for proteasomal degradation. Fbw7 is frequently mutated or depleted in numerous human cancers. Consequently, restoring Fbw7 levels is a promising approach for cancer therapy (Liu et al., 2015).

Tab. 23: Selected components targeting the CSN-CRL pathway. NAE = NEDD8-activating enzyme

Target	Compound	Function	Reference
Proteasome	Bortezomib, Carfilzomib	Blocks 26S-proteasome, effective in multiple melanomas and mantel cell lymphoma	(Kouroukis et al., 2014)
E1s	PYR-41	Blocks ubiquitination of TRAF6, prevents degradation of p53 and IκBα	(Yang et al., 2007)
Cdc34 (E2)	CC0651	Inhibitor, leads to accumulation of Skp2 target p27	(Zhong et al., 2012)
Cullins	Protacs	Promote binding of CRLs to target oncoprotein	(Bulatov and Ciulli, 2015)
NAE (E1)	MLN4924	Suppresses NEA activity	(Soucy et al., 2010)
β-TrCP	GS143	Inhibits β-TrCP and substrate interaction	(Blees et al., 2012)
	Erioflorin	Stabilizes β-TrCP substrate PCDC4	(Schmid et al., 2008)
Fbw7	Oridonin	Triggers Fbw7-mediated c-myc degradation	(Huang et al., 2012)
Skp2	Compound CpdA	Blocks recruitment of Skp2 to CRL 1 complex	(Chen et al., 2008)
	CG-12	Downregulate Skp2, while upregulating FBP β-TrCP	(Wang et al., 2012a)
	Compound #25	Prevents Skp1 association and $CRL1^{Skp2}$ formation	(Chan et al., 2014)
	Natural agents (curcumin, Vitamin D3, quercetin)	Inhibit the expression of Skp2 in human cancers	(Huang et al., 2008)

The compound Oridonin was found to induce cell cycle arrest and apoptosis in a myeloid leukemia cell line by triggering Fbw7-mediated c-myc degradation (Huang et al., 2012). The FBP β-TrCP was found to play a dual role in cancers due to its multiple specific substrates. Overexpression as well as loss of β-TrCP has been observed in a variety of human cancers (Liu et al., 2015). Therefore, targeting the FBP highly depends on the defined tumor subset. In this context, Erioflorin a potent small molecule was observed to stabilize the β-TrCP substrate PDCD4 (Schmid et al., 2008), whereas compound GS143 blocks the interaction between the FBP and its substrates (Blees et al., 2012). In the past decade, the crucial FBP Skp2 was considered as a potential drug target in breast cancer (Signoretti et al., 2002 Wang, 2012a), prostate cancer (Wang et al., 2012b), colon cancer (Jung et al., 2015), pituitary tumors (Wang et al., 2010), colorectal cancer (Bochis et al., 2015) and neuroblastoma (Evans et al., 2015). Consequently, specific small molecule inhibitors evolved to interfere with Skp2-mediated p27 degradation or $CRL1^{Skp2}$ assembly (Chen et al., 2008; Wu et al., 2012). High-throughput screening studies identified the small molecule inhibitor CpdA (Compound A), which blocks recruitment of Skp2 to the CRL complex (Chen et al., 2008). Interestingly, CpdA was able to overcome chemotherapy resistance, an issue often found during treatment of RCC patients. In addition, a novel energy restriction-mimic agent CG-12 was found to downregulate Skp2, while upregulating FBP β-TrCP These findings revealed a by then unknown Skp2-β-TrCP feedback loop (Wang et al., 2012b). However, both groups did not further examine whether their small molecules exhibit antitumor activity (Chan et al., 2014).

As yet, it is unknown whether these compounds could be used for cancer treatment. Chan and co-workers found another potent Skp2 inhibitor using high-throughput in silico screening of large and diverse chemical libraries (Chan et al., 2013). Compound #25 (SZL-P1-41) binds Skp2 FBP domain and thereby prevents Skp1 association and $CRL1^{Skp2}$ formation, but not the formation of other CRL complexes. Application of the compound *in vitro* augments p27-mediated apoptosis and senescence, whilst it impairs Akt-driven glycolysis. Its efficiency was validated and is not only limited to restricting tumor progression in lung and prostate cancer (Chan et al., 2013). Another group revealed a cross-talk between Skp2 and the mTOR pathway. An interesting interplay between the FBP and mTOR inhibitor Rapamycin was found. Phosphorylation of Skp2 via Akt is impaired by Rapamycin, leading to reduced Skp2 levels (Shanmugasundaram et al., 2013). Moreover, Skp2 silencing increased the sensitivity of tumor cells towards Rapamycin *in vitro* and *in vivo* (Totary-Jain et al., 2012). Therefore, Skp2 expression levels are an important predictor for mTOR inhibitor-sensitivity in cancer patients and additional targeting of the FBP is an attractive approach for future therapies.

Taken together, the CSN-CRL pathway might be a useful target for the treatment of renal cancers in the future. More studies are necessary to identify drugs that target selected segments of the CSN-CRL pathway specifically also for the treatment of RCCs. As shown in the present study, the CAND1-Skp2-p27 axis is altered in 786-O cells. Changed CAND1 levels and Skp2 expression should be addressed in future studies. Moreover, potent Skp2 inhibitors should also be considered to be tested in RCC cell lines. Skp2 silencing might interfere with high proliferation of RCC cells and could also increase the sensitivity of cancer cells towards Rapamycin, an mTOR inhibitor often used for RCC treatment. The presence of both p27 variants accompanied with a high proliferation rate in 786-O cells are interesting findings and their connection to tumorigenesis will be addressed in future experiments in RCCs and also in other types of cancers.

6. References

Abecasis, G.R., Auton, A., Brooks, L.D., DePristo, M.A., Durbin, R.M., Handsaker, R.E., Kang, H.M., Marth, G.T., McVean, G.A., Consortium, G.P., 2012. An integrated map of genetic variation from 1,092 human genomes. Nature 491, 56-65.

Adam, J., Hatipoglu, E., O'Flaherty, L., Ternette, N., Sahgal, N., Lockstone, H., Baban, D., Nye, E., Stamp, G.W., Wolhuter, K., Stevens, M., Fischer, R., Carmeliet, P., Maxwell, P.H., Pugh, C.W., Frizzell, N., Soga, T., Kessler, B.M., El-Bahrawy, M., Ratcliffe, P.J., Pollard, P.J., 2011. Renal cyst formation in Fh1-deficient mice is independent of the Hif/Phd pathway: roles for fumarate in KEAP1 succination and Nrf2 signaling. Cancer Cell 20, 524-537.

Admin, 2015. Biology (OpenStax import by section) copyright by Lumen learning, in: x (Ed.), https://courses.candelalearning.com/osbiosec/, x ed. x, x, p. x.

Baldassarre, G., Belletti, B., Bruni, P., Boccia, A., Trapasso, F., Pentimalli, F., Barone, M.V., Chiappetta, G., Vento, M.T., Spiezia, S., Fusco, A., Viglietto, G., 1999. Overexpressed cyclin D3 contributes to retaining the growth inhibitor p27 in the cytoplasm of thyroid tumor cells. J Clin Invest 104, 865-874.

Barbash, O., Zamfirova, P., Lin, D.I., Chen, X., Yang, K., Nakagawa, H., Lu, F., Rustgi, A.K., Diehl, J.A., 2008. Mutations in Fbx4 inhibit dimerization of the SCF(Fbx4) ligase and contribute to cyclin D1 overexpression in human cancer. Cancer Cell 14, 68-78.

Barberis, M., De Gioia, L., Ruzzene, M., Sarno, S., Coccetti, P., Fantucci, P., Vanoni, M., Alberghina, L., 2005. The yeast cyclin-dependent kinase inhibitor Sic1 and mammalian p27Kip1 are functional homologues with a structurally conserved inhibitory domain. Biochem J 387, 639-647.

Barbieri, R.B., Bufalo, N.E., Secolin, R., Assumpção, L.V., Maciel, R.M., Cerutti, J.M., Ward, L.S., 2014. Polymorphisms of cell cycle control genes influence the development of sporadic medullary thyroid carcinoma. Eur J Endocrinol 171, 761-767.

Bech-Otschir, D., Seeger, M., Dubiel, W., 2002. The COP9 signalosome: at the interface between signal transduction and ubiquitin-dependent proteolysis. J Cell Sci 115, 467-473.

Bedford, L., Lowe, J., Dick, L.R., Mayer, R.J., Brownell, J.E., 2011. Ubiquitin-like protein conjugation and the ubiquitin-proteasome system as drug targets. Nat Rev Drug Discov 10, 29-46.

Beli, P., Lukashchuk, N., Wagner, S.A., Weinert, B.T., Olsen, J.V., Baskcomb, L., Mann, M., Jackson, S.P., Choudhary, C., 2012. Proteomic investigations reveal a role for RNA processing factor THRAP3 in the DNA damage response. Mol Cell 46, 212-225.

Berthold, J., Schenková, K., Ramos, S., Miura, Y., Furukawa, M., Aspenström, P., Rivero, F., 2008. Characterization of RhoBTB-dependent Cul3 ubiquitin ligase complexes--evidence for an autoregulatory mechanism. Exp Cell Res 314, 3453-3465.

Besson, A., Dowdy, S.F., Roberts, J.M., 2008. CDK inhibitors: cell cycle regulators and beyond. Dev Cell 14, 159-169.

Blain, S.W., Montalvo, E., Massagué, J., 1997. Differential interaction of the cyclin-dependent kinase (Cdk) inhibitor p27Kip1 with cyclin A-Cdk2 and cyclin D2-Cdk4. J Biol Chem 272, 25863-25872.

Blees, J.S., Bokesch, H.R., Rubsamen, D., Schulz, K., Milke, L., Bajer, M.M., Gustafson, K.R., Henrich, C.J., McMahon, J.B., Colburn, N.H., Schmid, T., Brune, B., 2012. Erioflorin stabilizes the tumor suppressor Pdcd4 by inhibiting its interaction with the E3-ligase beta-TrCP1. PLoS One 7, e46567.

Bochis, O.V., Irimie, A., Pichler, M., Berindan-Neagoe, I., 2015. The role of Skp2 and its substrate CDKN1B (p27) in colorectal cancer. Journal of gastrointestinal and liver diseases : JGLD 24, 225-234.

Boh, B.K., Smith, P.G., Hagen, T., 2011. Neddylation-induced conformational control regulates cullin RING ligase activity in vivo. J Mol Biol 409, 136-145.

Bornstein, G., Ganoth, D., Hershko, A., 2006. Regulation of neddylation and deneddylation of cullin1 in SCFSkp2 ubiquitin ligase by F-box protein and substrate. Proc Natl Acad Sci U S A 103, 11515-11520.

Boron, W.F.B.E.L., 2012. Medical physiology: a cellular and molecular approach, Updated second edition.

Borriello, A., Bencivenga, D., Della Ragione, F., 2015. The unpredictable consequences of CDKN1B/p27Kip1 mutations in cancer. Cell Cycle 14, 2865-2866.

Bosu, D.R., Kipreos, E.T., 2008. Cullin-RING ubiquitin ligases: global regulation and activation cycles. Cell Div 3, 7.

Brugarolas, J., 2013. PBRM1 and BAP1 as novel targets for renal cell carcinoma. Cancer journal 19, 324-332.

Buczek, M., Escudier, B., Bartnik, E., Szczylik, C., Czarnecka, A., 2014. Resistance to tyrosine kinase inhibitors in clear cell renal cell carcinoma: from the patient's bed to molecular mechanisms. Biochim Biophys Acta 1845, 31-41.

Bulatov, E., Ciulli, A., 2015. Targeting Cullin-RING E3 ubiquitin ligases for drug discovery: structure, assembly and small-molecule modulation. Biochem J 467, 365-386.

Camargo-Kosugi, C.M., da Silva, I.D., Sato, H., D'Amora, P., Carvalho, C.V., Nogueira-de-Souza, N.C., Girão, M.J., Schor, E., 2009. The V109G polymorphism in the p27 gene is associated with endometriosis. Eur J Obstet Gynecol Reprod Biol 145, 180-183.

Carbone, M., Yang, H., Pass, H.I., Krausz, T., Testa, J.R., Gaudino, G., 2013. BAP1 and cancer. Nat Rev Cancer 13, 153-159.

Carrano, A.C., Eytan, E., Hershko, A., Pagano, M., 1999. SKP2 is required for ubiquitin-mediated degradation of the CDK inhibitor p27. Nat Cell Biol 1, 193-199.

Chamovitz, D.A., Wei, N., Osterlund, M.T., von Arnim, A.G., Staub, J.M., Matsui, M., Deng, X.W., 1996. The COP9 complex, a novel multisubunit nuclear regulator involved in light control of a plant developmental switch. Cell 86, 115-121.

Chan, C.H., Morrow, J.K., Li, C.F., Gao, Y., Jin, G., Moten, A., Stagg, L.J., Ladbury, J.E., Cai, Z., Xu, D., Logothetis, C.J., Hung, M.C., Zhang, S., Lin, H.K., 2013. Pharmacological inactivation of Skp2

SCF ubiquitin ligase restricts cancer stem cell traits and cancer progression. Cell 154, 556-568.

Chan, C.H., Morrow, J.K., Zhang, S., Lin, H.K., 2014. Skp2: a dream target in the coming age of cancer therapy. Cell Cycle 13, 679-680.

Chang, B.L., Zheng, S.L., Isaacs, S.D., Wiley, K.E., Turner, A., Li, G., Walsh, P.C., Meyers, D.A., Isaacs, W.B., Xu, J., 2004. A polymorphism in the CDKN1B gene is associated with increased risk of hereditary prostate cancer. Cancer Res 64, 1997-1999.

Chen, G., Li, G., 2010. Increased Cul1 expression promotes melanoma cell proliferation through regulating p27 expression. Int J Oncol 37, 1339-1344.

Chen, H., Mo, X., Yu, J., Huang, S., Huang, Z., Gao, L., 2014. Interference of Skp2 effectively inhibits the development and metastasis of colon carcinoma. Molecular medicine reports 10, 1129-1135.

Chen, L.C., Manjeshwar, S., Lu, Y., Moore, D., Ljung, B.M., Kuo, W.L., Dairkee, S.H., Wernick, M., Collins, C., Smith, H.S., 1998. The human homologue for the Caenorhabditis elegans cul-4 gene is amplified and overexpressed in primary breast cancers. Cancer Res 58, 3677-3683.

Chen, P., Yao, G.D., 2015. The role of cullin proteins in gastric cancer. Tumour Biol 10.1007/s13277-015-4154-z.

Chen, Q., Xie, W., Kuhn, D.J., Voorhees, P.M., Lopez-Girona, A., Mendy, D., Corral, L.G., Krenitsky, V.P., Xu, W., Moutouh-de Parseval, L., Webb, D.R., Mercurio, F., Nakayama, K.I., Nakayama, K., Orlowski, R.Z., 2008. Targeting the p27 E3 ligase SCF(Skp2) results in p27- and Skp2-mediated cell-cycle arrest and activation of autophagy. Blood 111, 4690-4699.

Choueiri, T.K., 2011. VEGF inhibitors in metastatic renal cell carcinoma: current therapies and future perspective. Curr Clin Pharmacol 6, 164-168.

Choueiri, T.K., Vaishampayan, U., Rosenberg, J.E., Logan, T.F., Harzstark, A.L., Bukowski, R.M., Rini, B.I., Srinivas, S., Stein, M.N., Adams, L.M., Ottesen, L.H., Laubscher, K.H., Sherman, L., McDermott, D.F., Haas, N.B., Flaherty, K.T., Ross, R., Eisenberg, P., Meltzer, P.S., Merino, M.J., Bottaro, D.P., Linehan, W.M., Srinivasan, R., 2013. Phase II and biomarker study of the dual MET/VEGFR2 inhibitor foretinib in patients with papillary renal cell carcinoma. J Clin Oncol 31, 181-186.

Christmann, M., Schmaler, T., Gordon, C., Huang, X., Bayram, O., Schinke, J., Stumpf, S., Dubiel, W., Braus, G.H., 2013. Control of multicellular development by the physically interacting deneddylases DEN1/DenA and COP9 signalosome. PLoS Genet 9, e1003275.

Chu, I.M., Hengst, L., Slingerland, J.M., 2008. The Cdk inhibitor p27 in human cancer: prognostic potential and relevance to anticancer therapy. Nat Rev Cancer 8, 253-267.

Chua, Y.S., Boh, B.K., Ponyeam, W., Hagen, T., 2011. Regulation of cullin RING E3 ubiquitin ligases by CAND1 in vivo. PLoS One 6, e16071.

Cihalova, D., Staud, F., Ceckova, M., 2015. Interactions of cyclin-dependent kinase inhibitors AT-7519, flavopiridol and SNS-032 with ABCB1, ABCG2 and ABCC1 transporters and their potential to overcome multidrug resistance in vitro. Cancer Chemother Pharmacol 76, 105-116.

Connor, M.K., Kotchetkov, R., Cariou, S., Resch, A., Lupetti, R., Beniston, R.G., Melchior, F., Hengst, L., Slingerland, J.M., 2003. CRM1/Ran-mediated nuclear export of p27(Kip1) involves a nuclear export signal and links p27 export and proteolysis. Mol Biol Cell 14, 201-213.

Cope, G.A., Deshaies, R.J., 2003. COP9 signalosome: a multifunctional regulator of SCF and other cullin-based ubiquitin ligases. Cell 114, 663-671.

Cope, G.A., Suh, G.S., Aravind, L., Schwarz, S.E., Zipursky, S.L., Koonin, E.V., Deshaies, R.J., 2002. Role of predicted metalloprotease motif of Jab1/Csn5 in cleavage of Nedd8 from Cul1. Science 298, 608-611.

Corn, P.G., 2007. Role of the ubiquitin proteasome system in renal cell carcinoma. BMC Biochem 8 Suppl 1, S4.

Costa-Guda, J., Marinoni, I., Molatore, S., Pellegata, N.S., Arnold, A., 2011. Somatic mutation and germline sequence abnormalities in CDKN1B, encoding p27Kip1, in sporadic parathyroid adenomas. The Journal of clinical endocrinology and metabolism 96, E701-706.

Curti, B.J., BRP; Javeed, M; Makhoul, I; Sachdeva, K; Hu, W; Perry, M; Talavera, F, 2014. Renal Cell Carcinoma. Medscape Reference WebMD.

Czarnecka, A.M., Kawecki, M., Lian, F., Korniluk, J., Szczylik, C., 2015. Feasibility, efficacy and safety of tyrosine kinase inhibitor treatment in hemodialyzed patients with renal cell cancer: 10 years of experience. Future Oncol 11, 2267-2282.

De Mulder, P.H., 2007. Targeted therapy in metastatic renal cell carcinoma. Ann Oncol 18 Suppl 9, 98-102.

Delahunt, B., Egevad, L., Samaratunga, H., Martignoni, G., Nacey, J.N., Srigley, J.R., 2015. Gleason and Fuhrman no longer make the grade. Histopathology 10.1111/his.12803.

Deng, X.W., Dubiel, W., Wei, N., Hofmann, K., Mundt, K., 2000. Unified nomenclature for the COP9 signalosome and its subunits: an essential regulator of development. Trends Genet 16, 289.

Denti, S., Fernandez-Sanchez, M.E., Rogge, L., Bianchi, E., 2006. The COP9 signalosome regulates Skp2 levels and proliferation of human cells. J Biol Chem 281, 32188-32196.

Deshaies, R.J., 2014. Proteotoxic crisis, the ubiquitin-proteasome system, and cancer therapy. BMC Biol 12, 94.

Deshaies, R.J., Joazeiro, C.A., 2009. RING domain E3 ubiquitin ligases. Annu Rev Biochem 78, 399-434.

Dessau, M., Halimi, Y., Erez, T., Chomsky-Hecht, O., Chamovitz, D.A., Hirsch, J.A., 2008. The Arabidopsis COP9 signalosome subunit 7 is a model PCI domain protein with subdomains involved in COP9 signalosome assembly. Plant Cell 20, 2815-2834.

Dietrich, S., Zenz, T., 2015. BRAF inhibitor therapy in HCL. Best practice & research. Clinical haematology 28, 246-252.

Donovan, J., Slingerland, J., 2000. Transforming growth factor-beta and breast cancer: Cell cycle arrest by transforming growth factor-beta and its disruption in cancer. Breast cancer research : BCR 2, 116-124.

Dubiel, D., Gierisch, M.E., Huang, X., Dubiel, W., Naumann, M., 2013. CAND1-dependent control of cullin 1-RING Ub ligases is essential for adipogenesis. Biochim Biophys Acta 1833, 1078-1084.

Dubiel, D., Ordemann, J., Pratschke, J., Dubiel, W., Naumann, M., 2015a. CAND1 exchange factor promotes Keap1 integration into cullin 3-RING ubiquitin ligase during adipogenesis. Int J Biochem Cell Biol 66, 95-100.

Dubiel, D., Rockel, B., Naumann, M., Dubiel, W., 2015b. Diversity of COP9 signalosome structures and functional consequences. FEBS Lett 589, 2507-2513.

Duda, D.M., Borg, L.A., Scott, D.C., Hunt, H.W., Hammel, M., Schulman, B.A., 2008. Structural insights into NEDD8 activation of cullin-RING ligases: conformational control of conjugation. Cell 134, 995-1006.

Duda, D.M., Scott, D.C., Calabrese, M.F., Zimmerman, E.S., Zheng, N., Schulman, B.A., 2011. Structural regulation of cullin-RING ubiquitin ligase complexes. Current opinion in structural biology 21, 257-264.

Echalier, A., Pan, Y., Birol, M., Tavernier, N., Pintard, L., Hoh, F., Ebel, C., Galophe, N., Claret, F.X., Dumas, C., 2013. Insights into the regulation of the human COP9 signalosome catalytic subunit, CSN5/Jab1. Proc Natl Acad Sci U S A 110, 1273-1278.

Emberley, E.D., Mosadeghi, R., Deshaies, R.J., 2012. Deconjugation of Nedd8 from Cul1 is directly regulated by Skp1-F-box and substrate, and the COP9 signalosome inhibits deneddylated SCF by a noncatalytic mechanism. J Biol Chem 287, 29679-29689.

Enchev, R.I., Scott, D.C., da Fonseca, P.C., Schreiber, A., Monda, J.K., Schulman, B.A., Peter, M., Morris, E.P., 2012. Structural Basis for a Reciprocal Regulation between SCF and CSN. Cell Rep 2, 616-627.

Evans, L., Chen, L., Milazzo, G., Gherardi, S., Perini, G., Willmore, E., Newell, D.R., Tweddle, D.A., 2015. SKP2 is a direct transcriptional target of MYCN and a potential therapeutic target in neuroblastoma. Cancer Lett 363, 37-45.

Falchetti, A., Marini, F., Luzi, E., Giusti, F., Cavalli, L., Cavalli, T., Brandi, M.L., 2009. Multiple endocrine neoplasia type 1 (MEN1): not only inherited endocrine tumors. Genet Med 11, 825-835.

Fang, L., Wang, X., Yamoah, K., Chen, P.L., Pan, Z.Q., Huang, L., 2008. Characterization of the Human COP9 Signalosome Complex Using Affinity Purification and Mass Spectrometry. J Proteome Res 10.1021/pr800574c.

Fay, A.P., Signoretti, S., Choueiri, T.K., 2014. MET as a target in papillary renal cell carcinoma. Clin Cancer Res 20, 3361-3363.

Feist, M., Huang, X., Muller, J.M., Rau, B., Dubiel, W., 2014. Can hyperthermic intraperitoneal chemotherapy efficiency be improved by blocking the DNA repair factor COP9 signalosome? Int J Colorectal Dis 29, 673-680.

Ferlay, J., Steliarova-Foucher, E., Lortet-Tieulent, J., Rosso, S., Coebergh, J.W., Comber, H., Forman, D., Bray, F., 2015. Reprint of: Cancer incidence and mortality patterns in Europe: Estimates for 40 countries in 2012. Eur J Cancer 51, 1201-1202.

Fernandez, S., Risolino, M., Mandia, N., Talotta, F., Soini, Y., Incoronato, M., Condorelli, G., Banfi, S., Verde, P., 2015. miR-340 inhibits tumor cell proliferation and induces apoptosis by targeting multiple negative regulators of p27 in non-small cell lung cancer. Oncogene 34, 3240-3250.

Fero, M.L., Rivkin, M., Tasch, M., Porter, P., Carow, C.E., Firpo, E., Polyak, K., Tsai, L.H., Broudy, V., Perlmutter, R.M., Kaushansky, K., Roberts, J.M., 1996. A syndrome of multiorgan hyperplasia with features of gigantism, tumorigenesis, and female sterility in p27(Kip1)-deficient mice. Cell 85, 733-744.

Flick, K., Kaiser, P., 2013. Set them free: F-box protein exchange by Cand1. Cell research 23, 870-871.

Fragu, P., 2007. Calcitonin's fantastic voyage: from hormone to marker of a genetic disorder. Gesnerus 64, 69-92.

Frescas, D., Pagano, M., 2008. Deregulated proteolysis by the F-box proteins SKP2 and beta-TrCP: tipping the scales of cancer. Nat Rev Cancer 8, 438-449.

Gaudray, P., Weber, G., 2009. Genetic background of MEN1: from genetic homogeneity to functional diversity. Adv Exp Med Biol 668, 17-26.

Gayther, S.A., Song, H., Ramus, S.J., Kjaer, S.K., Whittemore, A.S., Quaye, L., Tyrer, J., Shadforth, D., Hogdall, E., Hogdall, C., Blaeker, J., DiCioccio, R., McGuire, V., Webb, P.M., Beesley, J., Green, A.C., Whiteman, D.C., Goodman, M.T., Lurie, G., Carney, M.E., Modugno, F., Ness, R.B., Edwards, R.P., Moysich, K.B., Goode, E.L., Couch, F.J., Cunningham, J.M., Sellers, T.A., Wu, A.H., Pike, M.C., Iversen, E.S., Marks, J.R., Garcia-Closas, M., Brinton, L., Lissowska, J., Peplonska, B., Easton, D.F., Jacobs, I., Ponder, B.A., Schildkraut, J., Pearce, C.L., Chenevix-Trench, G., Berchuck, A., Pharoah, P.D., Group, A.O.C.S., Consortium, O.C.A., 2007. Tagging single nucleotide polymorphisms in cell cycle control genes and susceptibility to invasive epithelial ovarian cancer. Cancer Res 67, 3027-3035.

Genschik, P., Sumara, I., Lechner, E., 2013. The emerging family of CULLIN3-RING ubiquitin ligases (CRL3s): cellular functions and disease implications. Embo J 32, 2307-2320.

Goode, E.L., Fridley, B.L., Vierkant, R.A., Cunningham, J.M., Phelan, C.M., Anderson, S., Rider, D.N., White, K.L., Pankratz, V.S., Song, H., Hogdall, E., Kjaer, S.K., Whittemore, A.S., DiCioccio, R., Ramus, S.J., Gayther, S.A., Schildkraut, J.M., Pharaoh, P.P., Sellers, T.A., 2009. Candidate gene analysis using imputed genotypes: cell cycle single-nucleotide polymorphisms and ovarian cancer risk. Cancer Epidemiol Biomarkers Prev 18, 935-944.

Greene, F.L., Sobin, L.H., 2002. The TNM system: our language for cancer care. Journal of surgical oncology 80, 119-120.

Grimmler, M., Wang, Y., Mund, T., Cilensek, Z., Keidel, E.M., Waddell, M.B., Jäkel, H., Kullmann, M., Kriwacki, R.W., Hengst, L., 2007. Cdk-inhibitory activity and stability of p27Kip1 are directly regulated by oncogenic tyrosine kinases. Cell 128, 269-280.

Gstaiger, M., Jordan, R., Lim, M., Catzavelos, C., Mestan, J., Slingerland, J., Krek, W., 2001. Skp2 is oncogenic and overexpressed in human cancers. Proc Natl Acad Sci U S A 98, 5043-5048.

Guérinier, T., Millan, L., Crozet, P., Oury, C., Rey, F., Valot, B., Mathieu, C., Vidal, J., Hodges, M., Thomas, M., Glab, N., 2013. Phosphorylation of p27(KIP1) homologs KRP6 and 7 by SNF1-related protein kinase-1 links plant energy homeostasis and cell proliferation. Plant J 75, 515-525.

Gummlich, L., Kaehne, T., Naumann, M., Kilic, E., Jung, K., Dubiel, W., 2016. New Insights into the Mechanism of COP9 Signalosome-Cullin-RING Ubiquitin-Ligase Pathway Deregulation in Urological Cancers. Int Rev Cell Mol Biol (accepted).

Gummlich, L., Rabien, A., Jung, K., Dubiel, W., 2013. Deregulation of the COP9 signalosome-cullin-RING ubiquitin-ligase pathway: mechanisms and roles in urological cancers. Int J Biochem Cell Biol 45, 1327-1337.

Gusmaroli, G., Figueroa, P., Serino, G., Deng, X.W., 2007. Role of the MPN subunits in COP9 signalosome assembly and activity, and their regulatory interaction with Arabidopsis Cullin3-based E3 ligases. The Plant cell 19, 564-581.

Hannss, R., Dubiel, W., 2011. COP9 signalosome function in the DDR. FEBS Lett 585, 2845-2852.

Harper, J.W., King, R.W., 2011. Stuck in the middle: drugging the ubiquitin system at the e2 step. Cell 145, 1007-1009.

Heinzelmann, J., Henning, B., Sanjmyatav, J., Posorski, N., Steiner, T., Wunderlich, H., Gajda, M.R., Junker, K., 2011. Specific miRNA signatures are associated with metastasis and poor prognosis in clear cell renal cell carcinoma. World J Urol 29, 367-373.

Heo, J., Eki, R., Abbas, T., 2015. Deregulation of F-box proteins and its consequence on cancer development, progression and metastasis. Seminars in cancer biology 10.1016/j.semcancer.2015.09.015.

Hershko, A., Ciechanover, A., 1998. The ubiquitin system. Annu Rev Biochem 67, 425-479.

Hetfeld, B.K., Helfrich, A., Kapelari, B., Scheel, H., Hofmann, K., Guterman, A., Glickman, M., Schade, R., Kloetzel, P.M., Dubiel, W., 2005. The zinc finger of the CSN-associated deubiquitinating enzyme USP15 is essential to rescue the E3 ligase Rbx1. Curr Biol 15, 1217-1221.

Hoeller, D., Dikic, I., 2009. Targeting the ubiquitin system in cancer therapy. Nature 458, 438-444.

Hofmann, K., Bucher, P., 1998. The PCI domain: a common theme in three multiprotein complexes. Trends Biochem Sci 23, 204-205.

Huang, H.L., Weng, H.Y., Wang, L.Q., Yu, C.H., Huang, Q.J., Zhao, P.P., Wen, J.Z., Zhou, H., Qu, L.H., 2012. Triggering Fbw7-mediated proteasomal degradation of c-Myc by oridonin induces cell growth inhibition and apoptosis. Mol Cancer Ther 11, 1155-1165.

Huang, S.P., Yu, C.C., Liu, C.C., Wu, T.T., Huang, C.H., Wu, M.T., 2008. CDKN1B V109G polymorphism frequency and prostate cancer risk in Taiwan. Urol Int 81, 36-40.

Huang, X., Wagner, E., Dumdey, R., Peth, A., Berse, M., Dubiel, W., 2006. Phosphorylation by COP9 signalosome-associated CK2 promotes degradation of p27 during the G1 cell cycle phase. Israel Journal of Chemistry 46, 231-238.

Ishida, N., Kitagawa, M., Hatakeyama, S., Nakayama, K., 2000. Phosphorylation at serine 10, a major phosphorylation site of p27(Kip1), increases its protein stability. J Biol Chem 275, 25146-25154.

James, M.K., Ray, A., Leznova, D., Blain, S.W., 2008. Differential modification of p27Kip1 controls its cyclin D-cdk4 inhibitory activity. Mol Cell Biol 28, 498-510.

Jia, Z.M., Liu, Y., Cui, S.Y., 2014. Lack of association between cyclin-dependent kinase inhibitor 1B rs2066827 polymorphism and breast cancer susceptibility. Tumour Biol 35, 5527-5531.

Jin, D., Li, B., Deng, X.W., Wei, N., 2014. Plant COP9 signalosome subunit 5, CSN5. Plant science : an international journal of experimental plant biology 224, 54-61.

Joseph, R.W., Kapur, P., Serie, D.J., Eckel-Passow, J.E., Parasramka, M., Ho, T., Cheville, J.C., Frenkel, E., Rakheja, D., Brugarolas, J., Parker, A., 2014. Loss of BAP1 protein expression is an independent marker of poor prognosis in patients with low-risk clear cell renal cell carcinoma. Cancer 120, 1059-1067.

Joshi, P.P., Kulkarni, M.V., Yu, B.K., Smith, K.R., Norton, D.L., van Veelen, W., Höppener, J.W., Franklin, D.S., 2007. Simultaneous downregulation of CDK inhibitors p18(Ink4c) and p27(Kip1) is required for MEN2A-RET-mediated mitogenesis. Oncogene 26, 554-570.

Jung, C., Hong, J.Y., Bae, S.Y., Kang, S.S., Park, H.J., Lee, S.K., 2015. Antitumor Activity of Americanin A Isolated from the Seeds of Phytolacca americana by Regulating the ATM/ATR Signaling Pathway and the Skp2-p27 Axis in Human Colon Cancer Cells. Journal of natural products 10.1021/acs.jnatprod.5b00743.

Kapur, P., Christie, A., Raman, J.D., Then, M.T., Nuhn, P., Buchner, A., Bastian, P., Seitz, C., Shariat, S.F., Bensalah, K., Rioux-Leclercq, N., Xie, X.J., Lotan, Y., Margulis, V., Brugarolas, J., 2014. BAP1 immunohistochemistry predicts outcomes in a multi-institutional cohort with clear cell renal cell carcinoma. J Urol 191, 603-610.

Karnik, S.K., Hughes, C.M., Gu, X., Rozenblatt-Rosen, O., McLean, G.W., Xiong, Y., Meyerson, M., Kim, S.K., 2005. Menin regulates pancreatic islet growth by promoting histone methylation and expression of genes encoding p27Kip1 and p18INK4c. Proc Natl Acad Sci U S A 102, 14659-14664.

Kibel, A.S., Suarez, B.K., Belani, J., Oh, J., Webster, R., Brophy-Ebbers, M., Guo, C., Catalona, W.J., Picus, J., Goodfellow, P.J., 2003. CDKN1A and CDKN1B polymorphisms and risk of advanced prostate carcinoma. Cancer Res 63, 2033-2036.

Kim, C.J., Song, J.H., Cho, Y.G., Kim, Y.S., Kim, S.Y., Nam, S.W., Yoo, N.J., Lee, J.Y., Park, W.S., 2007. Somatic mutations of the beta-TrCP gene in gastric cancer. APMIS 115, 127-133.

Koh, M.Y., Spivak-Kroizman, T.R., Powis, G., 2010. HIF-1alpha and cancer therapy. Recent results in cancer research. Fortschritte der Krebsforschung. Progres dans les recherches sur le cancer 180, 15-34.

Korzeniewski, N., Hohenfellner, M., Duensing, S., 2012. CAND1 promotes PLK4-mediated centriole overduplication and is frequently disrupted in prostate cancer. Neoplasia 14, 799-806.

Kouroukis, T.C., Baldassarre, F.G., Haynes, A.E., Imrie, K., Reece, D.E., Cheung, M.C., 2014. Bortezomib in multiple myeloma: systematic review and clinical considerations. Current oncology 21, e573-603.

Kwok, S.F., Piekos, B., Misera, S., Deng, X.W., 1996. A complement of ten essential and pleiotropic arabidopsis COP/DET/FUS genes is necessary for repression of photomorphogenesis in darkness. Plant physiology 110, 731-742.

LaBaer, J., Garrett, M.D., Stevenson, L.F., Slingerland, J.M., Sandhu, C., Chou, H.S., Fattaey, A., Harlow, E., 1997. New functional activities for the p21 family of CDK inhibitors. Genes Dev 11, 847-862.

Langner, C., von Wasielewski, R., Ratschek, M., Rehak, P., Zigeuner, R., 2004. Biological significance of p27 and Skp2 expression in renal cell carcinoma. A systematic analysis of primary and metastatic tumour tissues using a tissue microarray technique. Virchows Arch 445, 631-636.

Latif, F., Tory, K., Gnarra, J., Yao, M., Duh, F.M., Orcutt, M.L., Stackhouse, T., Kuzmin, I., Modi, W., Geil, L., 1993. Identification of the von Hippel-Lindau disease tumor suppressor gene. Science 260, 1317-1320.

Latres, E., Chiarle, R., Schulman, B.A., Pavletich, N.P., Pellicer, A., Inghirami, G., Pagano, M., 2001. Role of the F-box protein Skp2 in lymphomagenesis. Proc Natl Acad Sci U S A 98, 2515-2520.

Leal, J.F., Fominaya, J., Cascón, A., Guijarro, M.V., Blanco-Aparicio, C., Lleonart, M., Castro, M.E., Ramon Y Cajal, S., Robledo, M., Beach, D.H., Carnero, A., 2008. Cellular senescence bypass screen identifies new putative tumor suppressor genes. Oncogene 27, 1961-1970.

Lee, J.E., Sweredoski, M.J., Graham, R.L., Kolawa, N.J., Smith, G.T., Hess, S., Deshaies, R.J., 2011a. The steady-state repertoire of human SCF ubiquitin ligase complexes does not require ongoing Nedd8 conjugation. Mol Cell Proteomics 10, M110.006460.

Lee, M.H., Zhao, R., Phan, L., Yeung, S.C., 2011b. Roles of COP9 signalosome in cancer. Cell Cycle 10, 3057-3066.

Leppert, U., Henke, W., Huang, X., Müller, J.M., Dubiel, W., 2011. Post-transcriptional fine-tuning of COP9 signalosome subunit biosynthesis is regulated by the c-Myc/Lin28B/let-7 pathway. J Mol Biol 409, 710-721.

Li, G., Sturgis, E.M., Wang, L.E., Chamberlain, R.M., Spitz, M.R., El-Naggar, A.K., Hong, W.K., Wei, Q., 2004. Association between the V109G polymorphism of the p27 gene and the risk and progression of oral squamous cell carcinoma. Clin Cancer Res 10, 3996-4002.

Liakopoulos, D., Doenges, G., Matuschewski, K., Jentsch, S., 1998. A novel protein modification pathway related to the ubiquitin system. EMBO J 17, 2208-2214.

Linehan, W.M., 2012. Genetic basis of kidney cancer: role of genomics for the development of disease-based therapeutics. Genome Res 22, 2089-2100.

Lingaraju, G.M., Bunker, R.D., Cavadini, S., Hess, D., Hassiepen, U., Renatus, M., Fischer, E.S., Thoma, N.H., 2014. Crystal structure of the human COP9 signalosome. Nature 512, 161-165.

Liu, J., Shaik, S., Dai, X., Wu, Q., Zhou, X., Wang, Z., Wei, W., 2015. Targeting the ubiquitin pathway for cancer treatment. Biochim Biophys Acta 1855, 50-60.

Liu, Z., Fu, Q., Lv, J., Wang, F., Ding, K., 2008. Prognostic implication of p27Kip1, Skp2 and Cks1 expression in renal cell carcinoma: a tissue microarray study. J Exp Clin Cancer Res 27, 51.

Ljungberg, B., Bensalah, K., Canfield, S., Dabestani, S., Hofmann, F., Hora, M., Kuczyk, M.A., Lam, T., Marconi, L., Merseburger, A.S., Mulders, P., Powles, T., Staehler, M., Volpe, A., Bex, A., 2015. EAU guidelines on renal cell carcinoma: 2014 update. Eur Urol 67, 913-924.

Longuini, V.C., Lourenço, D.M., Sekiya, T., Meirelles, O., Goncalves, T.D., Coutinho, F.L., Francisco, G., Osaki, L.H., Chammas, R., Alves, V.A., Siqueira, S.A., Schlesinger, D., Naslavsky, M.S., Zatz, M., Duarte, Y.A., Lebrão, M.L., Gama, P., Lee, M., Molatore, S., Pereira, M.A., Jallad, R.S., Bronstein, M.D., Cunha-Neto, M.B., Liberman, B., Fragoso, M.C., Toledo, S.P., Pellegata, N.S., Toledo, R.A., 2014. Association between the p27 rs2066827 variant and tumor multiplicity in patients harboring MEN1 germline mutations. Eur J Endocrinol 171, 335-342.

Lopez-Beltran, A., Scarpelli, M., Montironi, R., Kirkali, Z., 2006. 2004 WHO classification of the renal tumors of the adults. Eur Urol 49, 798-805.

Lu, H., Cao, X., Zhang, H., Sun, G., Fan, G., Chen, L., Wang, S., 2014. Imbalance between MMP-2, 9 and TIMP-1 promote the invasion and metastasis of renal cell carcinoma via SKP2 signaling pathways. Tumour Biol 35, 9807-9813.

Lyapina, S., Cope, G., Shevchenko, A., Serino, G., Tsuge, T., Zhou, C., Wolf, D.A., Wei, N., Deshaies, R.J., 2001. Promotion of NEDD-CUL1 conjugate cleavage by COP9 signalosome. Science 292, 1382-1385.

Ma, H., Jin, G., Hu, Z., Zhai, X., Chen, W., Wang, S., Wang, X., Qin, J., Gao, J., Liu, J., Wei, Q., Shen, H., 2006. Variant genotypes of CDKN1A and CDKN1B are associated with an increased risk of breast cancer in Chinese women. Int J Cancer 119, 2173-2178.

Mao, J.H., Perez-Losada, J., Wu, D., Delrosario, R., Tsunematsu, R., Nakayama, K.I., Brown, K., Bryson, S., Balmain, A., 2004. Fbxw7/Cdc4 is a p53-dependent, haploinsufficient tumour suppressor gene. Nature 432, 775-779.

Marini, F., Giusti, F., Brandi, M.L., 2015. Genetic test in multiple endocrine neoplasia type 1 syndrome: An evolving story. World J Exp Med 5, 124-129.

Maxwell, J.E., Sherman, S.K., Li, G., Choi, A.B., Bellizzi, A.M., O'Dorisio, T.M., Howe, J.R., 2015. Somatic alterations of CDKN1B are associated with small bowel neuroendocrine tumors. Cancer genetics 10.1016/j.cancergen.2015.08.003.

Maynard, M.A., Evans, A.J., Shi, W., Kim, W.Y., Liu, F.F., Ohh, M., 2007. Dominant-negative HIF-3 alpha 4 suppresses VHL-null renal cell carcinoma progression. Cell Cycle 6, 2810-2816.

Meir, M., Galanty, Y., Kashani, L., Blank, M., Khosravi, R., Fernandez-Avila, M.J., Cruz-Garcia, A., Star, A., Shochot, L., Thomas, Y., Garrett, L.J., Chamovitz, D.A., Bodine, D.M., Kurz, T., Huertas, P., Ziv, Y., Shiloh, Y., 2015. The COP9 signalosome is vital for timely repair of DNA double-strand breaks. Nucleic Acids Res 43, 4517-4530.

Meister, C., Kolog Gulko, M., Kohler, A.M., Braus, G.H., 2015. The devil is in the details: comparison between COP9 signalosome (CSN) and the LID of the 26S proteasome. Current genetics 10.1007/s00294-015-0525-7.

Miller, R.M., 2015. Kidney (Renal Cell) Carcinoma, http://www.aboutcancer.com/kidney_basic.htm, 15.11.2015.

Mohamed, F.Z., Hussien, Y.M., AlBakry, M.M., Mohamed, R.H., Said, N.M., 2013. Role of DNA repair and cell cycle control genes in ovarian cancer susceptibility. Mol Biol Rep 40, 3757-3768.

Molatore, S., Marinoni, I., Lee, M., Pulz, E., Ambrosio, M.R., degli Uberti, E.C., Zatelli, M.C., Pellegata, N.S., 2010. A novel germline CDKN1B mutation causing multiple endocrine tumors: clinical, genetic and functional characterization. Human mutation 31, E1825-1835.

Moore, L.E., Nickerson, M.L., Brennan, P., Toro, J.R., Jaeger, E., Rinsky, J., Han, S.S., Zaridze, D., Matveev, V., Janout, V., Kollarova, H., Bencko, V., Navratilova, M., Szeszenia-Dabrowska, N., Mates, D., Schmidt, L.S., Lenz, P., Karami, S., Linehan, W.M., Merino, M., Chanock, S., Boffetta, P., Chow, W.H., Waldman, F.M., Rothman, N., 2011. Von Hippel-Lindau (VHL) inactivation in sporadic clear cell renal cancer: associations with germline VHL polymorphisms and etiologic risk factors. PLoS Genet 7, e1002312.

Moran-Jones, K., Brown, L.M., Samimi, G., 2015. INC280, an orally available small molecule inhibitor of c-MET, reduces migration and adhesion in ovarian cancer cell models. Sci Rep 5, 11749.

Murata, T., Takayama, K., Katayama, S., Urano, T., Horie-Inoue, K., Ikeda, K., Takahashi, S., Kawazu, C., Hasegawa, A., Ouchi, Y., Homma, Y., Hayashizaki, Y., Inoue, S., 2010. miR-148a is an androgen-responsive microRNA that promotes LNCaP prostate cell growth by repressing its target CAND1 expression. Prostate Cancer Prostatic Dis 13, 356-361.

Naidu, R., Har, Y.C., Taib, N.A., 2007. P27 V109G Polymorphism is associated with lymph node metastases but not with increased risk of breast cancer. J Exp Clin Cancer Res 26, 133-140.

Nakayama, K., Nagahama, H., Minamishima, Y.A., Matsumoto, M., Nakamichi, I., Kitagawa, K., Shirane, M., Tsunematsu, R., Tsukiyama, T., Ishida, N., Kitagawa, M., Nakayama, K., Hatakeyama, S., 2000. Targeted disruption of Skp2 results in accumulation of cyclin E and p27(Kip1), polyploidy and centrosome overduplication. EMBO J 19, 2069-2081.

Nakayama, K.I., Nakayama, K., 2006. Ubiquitin ligases: cell-cycle control and cancer. Nat Rev Cancer 6, 369-381.

Network, C.G.A.R., 2013. Comprehensive molecular characterization of clear cell renal cell carcinoma. Nature 499, 43-49.

New, 2015. Renal Cell Carcinoma Staging, http://www.newhealthadvisor.com, 17.11.2015.

Ooi, A., Dykema, K., Ansari, A., Petillo, D., Snider, J., Kahnoski, R., Anema, J., Craig, D., Carpten, J., Teh, B.T., Furge, K.A., 2013. CUL3 and NRF2 mutations confer an NRF2 activation phenotype in a sporadic form of papillary renal cell carcinoma. Cancer Res 73, 2044-2051.

Pappa, V., Papageorgiou, S., Papageorgiou, E., Panani, A., Boutou, E., Tsirigotis, P., Dervenoulas, J., Economopoulos, T., Raptis, S., 2005. A novel p27 gene mutation in a case of unclassified myeloproliferative disorder. Leuk Res 29, 229-231.

Pasquali, D., Circelli, L., Faggiano, A., Pancione, M., Renzullo, A., Elisei, R., Romei, C., Accardo, G., Coppola, V.R., De Palma, M., Ferolla, P., Grimaldi, F., Colao, A., Colantuoni, V., 2011. CDKN1B V109G polymorphism a new prognostic factor in sporadic medullary thyroid carcinoma. Eur J Endocrinol 164, 397-404.

Patard, J.J., Pignot, G., Escudier, B., Eisen, T., Bex, A., Sternberg, C., Rini, B., Roigas, J., Choueiri, T., Bukowski, R., Motzer, R., Kirkali, Z., Mulders, P., Bellmunt, J., 2011. ICUD-EAU International Consultation on Kidney Cancer 2010: treatment of metastatic disease. Eur Urol 60, 684-690.

Patil, M.A., Gütgemann, I., Zhang, J., Ho, C., Cheung, S.T., Ginzinger, D., Li, R., Dykema, K.J., So, S., Fan, S.T., Kakar, S., Furge, K.A., Büttner, R., Chen, X., 2005. Array-based comparative genomic hybridization reveals recurrent chromosomal aberrations and Jab1 as a potential target for 8q gain in hepatocellular carcinoma. Carcinogenesis 26, 2050-2057.

Petroski, M.D., Deshaies, R.J., 2005. Function and regulation of cullin-RING ubiquitin ligases. Nat Rev Mol Cell Biol 6, 9-20.

Pierce, N.W., Lee, J.E., Liu, X., Sweredoski, M.J., Graham, R.L., Larimore, E.A., Rome, M., Zheng, N., Clurman, B.E., Hess, S., Shan, S.O., Deshaies, R.J., 2013. Cand1 promotes assembly of new SCF complexes through dynamic exchange of F box proteins. Cell 153, 206-215.

Pulvino, M., Chen, L., Oleksyn, D., Li, J., Compitello, G., Rossi, R., Spence, S., Balakrishnan, V., Jordan, C., Poligone, B., Casulo, C., Burack, R., Shapiro, J.L., Bernstein, S., Friedberg, J.W.,

Deshaies, R.J., Land, H., Zhao, J., 2015. Inhibition of COP9-signalosome (CSN) deneddylating activity and tumor growth of diffuse large B-cell lymphomas by doxycycline. Oncotarget 6, 14796-14813.

Ray, D., Cuneo, K.C., Rehemtulla, A., Lawrence, T.S., Nyati, M.K., 2015. Inducing Oncoprotein Degradation to Improve Targeted Cancer Therapy. Neoplasia 17, 697-703.

Robak, T., Smolewski, P., 2015. New mutation in hairy cell leukemia. Blood 126, 930-931.

Rockel, B., Schmaler, T., Huang, X., Dubiel, W., 2014. Electron microscopy and in vitro deneddylation reveal similar architectures and biochemistry of isolated human and Flag-mouse COP9 signalosome complexes. Biochem Biophys Res Commun 450, 991-997.

Roe, J.S., Kim, H.R., Hwang, I.Y., Cho, E.J., Youn, H.D., 2011. von Hippel-Lindau protein promotes Skp2 destabilization on DNA damage. Oncogene 30, 3127-3138.

Roy, A., Banerjee, S., 2015. p27 and leukemia: cell cycle and beyond. J Cell Physiol 230, 504-509.

Rozen, S., Tieri, A., Ridner, G., Stark, A.K., Schmaler, T., Ben-Nissan, G., Dubiel, W., Sharon, M., 2013. Exposing the subunit diversity within protein complexes: a mass spectrometry approach. Methods 59, 270-277.

Saha, A., Deshaies, R.J., 2008. Multimodal activation of the ubiquitin ligase SCF by Nedd8 conjugation. Mol Cell 32, 21-31.

Sarikas, A., Hartmann, T., Pan, Z.Q., 2011. The cullin protein family. Genome biology 12, 220.

Schang, L.M., 2005. Advances on cyclin-dependent kinases (CDKs) as novel targets for antiviral drugs. Curr Drug Targets Infect Disord 5, 29-37.

Schmaler, T., Dubiel, W., 2010. Control of Deneddylation by the COP9 Signalosome. Subcell Biochem 54, 57-68.

Schmid, T., Jansen, A.P., Baker, A.R., Hegamyer, G., Hagan, J.P., Colburn, N.H., 2008. Translation inhibitor Pdcd4 is targeted for degradation during tumor promotion. Cancer Res 68, 1254-1260.

Schmidt, L., Duh, F.M., Chen, F., Kishida, T., Glenn, G., Choyke, P., Scherer, S.W., Zhuang, Z., Lubensky, I., Dean, M., Allikmets, R., Chidambaram, A., Bergerheim, U.R., Feltis, J.T., Casadevall, C., Zamarron, A., Bernues, M., Richard, S., Lips, C.J., Walther, M.M., Tsui, L.C., Geil, L., Orcutt, M.L., Stackhouse, T., Lipan, J., Slife, L., Brauch, H., Decker, J., Niehans, G., Hughson, M.D., Moch, H., Storkel, S., Lerman, M.I., Linehan, W.M., Zbar, B., 1997. Germline and somatic mutations in the tyrosine kinase domain of the MET proto-oncogene in papillary renal carcinomas. Nat Genet 16, 68-73.

Schmidt, M.W., McQuary, P.R., Wee, S., Hofmann, K., Wolf, D.A., 2009a. F-Box-Directed CRL Complex Assembly and Regulation by the CSN and CAND1. Molecular Cell 35, 586-597.

Schmidt, M.W., McQuary, P.R., Wee, S., Hofmann, K., Wolf, D.A., 2009b. F-box-directed CRL complex assembly and regulation by the CSN and CAND1. Mol Cell 35, 586-597.

Schweitzer, K., Naumann, M., 2015. CSN-associated USP48 confers stability to nuclear NF-kappaB/RelA by trimming K48-linked Ub-chains. Biochim Biophys Acta 1853, 453-469.

Seeger, M., Kraft, R., Ferrell, K., Bech-Otschir, D., Dumdey, R., Schade, R., Gordon, C., Naumann, M., Dubiel, W., 1998. A novel protein complex involved in signal transduction possessing similarities to 26S proteasome subunits. FASEB J 12, 469-478.

Sekiya, T., Bronstein, M.D., Benfini, K., Longuini, V.C., Jallad, R.S., Machado, M.C., Goncalves, T.D., Osaki, L.H., Higashi, L., Viana-Jr, J., Kater, C., Lee, M., Molatore, S., Francisco, G., Chammas, R., Naslavsky, M.S., Schlesinger, D., Gama, P., Duarte, Y.A., Lebrão, M.L., Zatz, M., Meirelles, O., Liberman, B., Fragoso, M.C., Toledo, S.P., Pellegata, N.S., Toledo, R.A., 2014. p27 variant and corticotropinoma susceptibility: a genetic and in vitro study. Endocr Relat Cancer 21, 395-404.

Shanmugasundaram, K., Block, K., Nayak, B.K., Livi, C.B., Venkatachalam, M.A., Sudarshan, S., 2013. PI3K regulation of the SKP-2/p27 axis through mTORC2. Oncogene 32, 2027-2036.

Siegel, R.L., Miller, K.D., Jemal, A., 2016. Cancer statistics, 2016. CA Cancer J Clin 10.3322/caac.21332.

Signoretti, S., Di Marcotullio, L., Richardson, A., Ramaswamy, S., Isaac, B., Rue, M., Monti, F., Loda, M., Pagano, M., 2002. Oncogenic role of the ubiquitin ligase subunit Skp2 in human breast cancer. J Clin Invest 110, 633-641.

Singh, A., Misra, V., Thimmulappa, R.K., Lee, H., Ames, S., Hoque, M.O., Herman, J.G., Baylin, S.B., Sidransky, D., Gabrielson, E., Brock, M.V., Biswal, S., 2006. Dysfunctional KEAP1-NRF2 interaction in non-small-cell lung cancer. PLoS Med 3, e420.

Singhal, S., Amin, K.M., Kruklitis, R., DeLong, P., Friscia, M.E., Litzky, L.A., Putt, M.E., Kaiser, L.R., Albelda, S.M., 2003. Alterations in cell cycle genes in early stage lung adenocarcinoma identified by expression profiling. Cancer Biol Ther 2, 291-298.

Skaar, J.R., Pagan, J.K., Pagano, M., 2013. Mechanisms and function of substrate recruitment by F-box proteins. Nat Rev Mol Cell Biol 14, 369-381.

Skaar, J.R., Pagan, J.K., Pagano, M., 2014. SCF ubiquitin ligase-targeted therapies. Nat Rev Drug Discov 13, 889-903.

Soucy, T.A., Dick, L.R., Smith, P.G., Milhollen, M.A., Brownell, J.E., 2010. The NEDD8 Conjugation Pathway and Its Relevance in Cancer Biology and Therapy. Genes Cancer 1, 708-716.

Spirin, K.S., Simpson, J.F., Takeuchi, S., Kawamata, N., Miller, C.W., Koeffler, H.P., 1996. p27/Kip1 mutation found in breast cancer. Cancer Res 56, 2400-2404.

Spurdle, A.B., Deans, A.J., Duffy, D., Goldgar, D.E., Chen, X., Beesley, J., Easton, D.F., Antoniou, A.C., Peock, S., Cook, M., Nathanson, K.L., Domchek, S.M., MacArthur, G.A., Chenevix-Trench, G., kConFaB, Collaborators, E.S., 2009. No evidence that CDKN1B (p27) polymorphisms modify breast cancer risk in BRCA1 and BRCA2 mutation carriers. Breast Cancer Res Treat 115, 307-313.

Su, D., Singer, E.A., Srinivasan, R., 2015. Molecular pathways in renal cell carcinoma: recent advances in genetics and molecular biology. Curr Opin Oncol 27, 217-223.

Su, D., Stamatakis, L., Singer, E.A., Srinivasan, R., 2014. Renal cell carcinoma: molecular biology and targeted therapy. Curr Opin Oncol 26, 321-327.

Suarez, B.K., Lin, J., Burmester, J.K., Broman, K.W., Weber, J.L., Banerjee, T.K., Goddard, K.A., Witte, J.S., Elston, R.C., Catalona, W.J., 2000. A genome screen of multiplex sibships with prostate cancer. Am J Hum Genet 66, 933-944.

Tichomirowa, M.A., Lee, M., Barlier, A., Daly, A.F., Marinoni, I., Jaffrain-Rea, M.L., Naves, L.A., Rodien, P., Rohmer, V., Faucz, F.R., Caron, P., Estour, B., Lecomte, P., Borson-Chazot, F., Penfornis, A., Yaneva, M., Guitelman, M., Castermans, E., Verhaege, C., Wémeau, J.L., Tabarin, A., Fajardo Montañana, C., Delemer, B., Kerlan, V., Sadoul, J.L., Cortet Rudelli, C., Archambeaud, F., Zacharieva, S., Theodoropoulou, M., Brue, T., Enjalbert, A., Bours, V., Pellegata, N.S., Beckers, A., 2012. Cyclin-dependent kinase inhibitor 1B (CDKN1B) gene variants in AIP mutation-negative familial isolated pituitary adenoma kindreds. Endocr Relat Cancer 19, 233-241.

Tomlinson, I.P., Alam, N.A., Rowan, A.J., Barclay, E., Jaeger, E.E., Kelsell, D., Leigh, I., Gorman, P., Lamlum, H., Rahman, S., Roylance, R.R., Olpin, S., Bevan, S., Barker, K., Hearle, N., Houlston, R.S., Kiuru, M., Lehtonen, R., Karhu, A., Vilkki, S., Laiho, P., Eklund, C., Vierimaa, O., Aittomäki, K., Hietala, M., Sistonen, P., Paetau, A., Salovaara, R., Herva, R., Launonen, V., Aaltonen, L.A., Consortium, M.L., 2002. Germline mutations in FH predispose to dominantly inherited uterine fibroids, skin leiomyomata and papillary renal cell cancer. Nat Genet 30, 406-410.

Tomoda, K., Kubota, Y., Arata, Y., Mori, S., Maeda, M., Tanaka, T., Yoshida, M., Yoneda-Kato, N., Kato, J.Y., 2002. The cytoplasmic shuttling and subsequent degradation of p27Kip1 mediated by Jab1/CSN5 and the COP9 signalosome complex. J Biol Chem 277, 2302-2310.

Totary-Jain, H., Sanoudou, D., Dautriche, C.N., Schneller, H., Zambrana, L., Marks, A.R., 2012. Rapamycin resistance is linked to defective regulation of Skp2. Cancer Res 72, 1836-1843.

Uddin, S., Bhat, A.A., Krishnankutty, R., Mir, F., Kulinski, M., Mohammad, R.M., 2015. Involvement of F-BOX proteins in progression and development of human malignancies. Seminars in cancer biology 10.1016/j.semcancer.2015.09.008.

Uhle, S., Medalia, O., Waldron, R., Dumdey, R., Henklein, P., Bech-Otschir, D., Huang, X., Berse, M., Sperling, J., Schade, R., Dubiel, W., 2003. Protein kinase CK2 and protein kinase D are associated with the COP9 signalosome. EMBO J 22, 1302-1312.

Uhlen, M., Fagerberg, L., Hallstrom, B.M., Lindskog, C., Oksvold, P., Mardinoglu, A., Sivertsson, A., Kampf, C., Sjostedt, E., Asplund, A., Olsson, I., Edlund, K., Lundberg, E., Navani, S., Szigyarto, C.A., Odeberg, J., Djureinovic, D., Takanen, J.O., Hober, S., Alm, T., Edqvist, P.H., Berling, H., Tegel, H., Mulder, J., Rockberg, J., Nilsson, P., Schwenk, J.M., Hamsten, M., von Feilitzen, K., Forsberg, M., Persson, L., Johansson, F., Zwahlen, M., von Heijne, G., Nielsen, J., Ponten, F., 2015. Proteomics. Tissue-based map of the human proteome. Science 347, 1260419.

Varela, I., Tarpey, P., Raine, K., Huang, D., Ong, C.K., Stephens, P., Davies, H., Jones, D., Lin, M.L., Teague, J., Bignell, G., Butler, A., Cho, J., Dalgliesh, G.L., Galappaththige, D., Greenman, C., Hardy, C., Jia, M., Latimer, C., Lau, K.W., Marshall, J., McLaren, S., Menzies, A., Mudie, L., Stebbings, L., Largaespada, D.A., Wessels, L.F., Richard, S., Kahnoski, R.J., Anema, J., Tuveson, D.A., Perez-Mancera, P.A., Mustonen, V., Fischer, A., Adams, D.J., Rust, A., Chan-on, W., Subimerb, C., Dykema, K., Furge, K., Campbell, P.J., Teh, B.T., Stratton, M.R., Futreal, P.A., 2011. Exome sequencing identifies frequent mutation of the SWI/SNF complex gene PBRM1 in renal carcinoma. Nature 469, 539-542.

Wang, H., Bauzon, F., Ji, P., Xu, X., Sun, D., Locker, J., Sellers, R.S., Nakayama, K., Nakayama, K.I., Cobrinik, D., Zhu, L., 2010. Skp2 is required for survival of aberrantly proliferating Rb1-deficient cells and for tumorigenesis in Rb1+/- mice. Nat Genet 42, 83-88.

Wang, S.S., Gu, Y.F., Wolff, N., Stefanius, K., Christie, A., Dey, A., Hammer, R.E., Xie, X.J., Rakheja, D., Pedrosa, I., Carroll, T., McKay, R.M., Kapur, P., Brugarolas, J., 2014. Bap1 is essential for kidney function and cooperates with Vhl in renal tumorigenesis. Proc Natl Acad Sci U S A 111, 16538-16543.

Wang, Z., Fukushima, H., Inuzuka, H., Wan, L., Liu, P., Gao, D., Sarkar, F.H., Wei, W., 2012a. Skp2 is a promising therapeutic target in breast cancer. Front Oncol 1.

Wang, Z., Gao, D., Fukushima, H., Inuzuka, H., Liu, P., Wan, L., Sarkar, F.H., Wei, W., 2012b. Skp2: a novel potential therapeutic target for prostate cancer. Biochim Biophys Acta 1825, 11-17.

Webber, C., Gospodarowicz, M., Sobin, L.H., Wittekind, C., Greene, F.L., Mason, M.D., Compton, C., Brierley, J., Groome, P.A., 2014. Improving the TNM classification: findings from a 10-year continuous literature review. Int J Cancer 135, 371-378.

Wei, F., Xu, J., Tang, L., Shao, J., Wang, Y., Chen, L., Guan, X., 2012. p27(Kip1) V109G polymorphism and cancer risk: a systematic review and meta-analysis. Cancer Biother Radiopharm 27, 665-671.

Wei, M.H., Toure, O., Glenn, G.M., Pithukpakorn, M., Neckers, L., Stolle, C., Choyke, P., Grubb, R., Middelton, L., Turner, M.L., Walther, M.M., Merino, M.J., Zbar, B., Linehan, W.M., Toro, J.R., 2006. Novel mutations in FH and expansion of the spectrum of phenotypes expressed in families with hereditary leiomyomatosis and renal cell cancer. J Med Genet 43, 18-27.

Wei, N., Chamovitz, D.A., Deng, X.W., 1994. Arabidopsis COP9 is a component of a novel signaling complex mediating light control of development. Cell 78, 117-124.

Wei, N., Deng, X.W., 1998. Characterization and purification of the mammalian COP9 complex, a conserved nuclear regulator initially identified as a repressor of photomorphogenesis in higher plants. Photochem Photobiol 68, 237-241.

Wei, N., Deng, X.W., 2003. The COP9 signalosome. Annu Rev Cell Dev Biol 19, 261-286.

Wei, N., Serino, G., Deng, X.W., 2008. The COP9 signalosome: more than a protease. Trends Biochem Sci 33, 592-600.

Wei, Z., Jiang, X., Liu, F., Qiao, H., Zhou, B., Zhai, B., Zhang, L., Zhang, X., Han, L., Jiang, H., Krissansen, G.W., Sun, X., 2013. Downregulation of Skp2 inhibits the growth and metastasis of gastric cancer cells in vitro and in vivo. Tumour Biol 34, 181-192.

Welcker, M., Clurman, B.E., 2008. FBW7 ubiquitin ligase: a tumour suppressor at the crossroads of cell division, growth and differentiation. Nat Rev Cancer 8, 83-93.

Wu, L., Grigoryan, A.V., Li, Y., Hao, B., Pagano, M., Cardozo, T.J., 2012. Specific small molecule inhibitors of Skp2-mediated p27 degradation. Chemistry & biology 19, 1515-1524.

Xiang, H., Li, H., Ge, W., Wu, W., Gao, M., Wang, W., Hong, L., Jiang, D., Zhang, C., 2013. Association of CDKN1B gene polymorphisms with susceptibility to breast cancer: a meta-analysis. Mol Biol Rep 40, 6371-6377.

Yan, T., Wunder, J.S., Gokgoz, N., Gill, M., Eskandarian, S., Parkes, R.K., Bull, S.B., Bell, R.S., Andrulis, I.L., 2007. COPS3 amplification and clinical outcome in osteosarcoma. Cancer 109, 1870-1876.

Yang, Y., Kitagaki, J., Dai, R.M., Tsai, Y.C., Lorick, K.L., Ludwig, R.L., Pierre, S.A., Jensen, J.P., Davydov, I.V., Oberoi, P., Li, C.C., Kenten, J.H., Beutler, J.A., Vousden, K.H., Weissman, A.M., 2007. Inhibitors of ubiquitin-activating enzyme (E1), a new class of potential cancer therapeutics. Cancer Res 67, 9472-9481.

Yogosawa, S., Kayukawa, K., Kawata, T., Makino, Y., Inoue, S., Okuda, A., Muramatsu, M., Tamura, T., 1999. Induced expression, localization, and chromosome mapping of a gene for the TBP-interacting protein 120A. Biochem Biophys Res Commun 266, 123-128.

Zhong, H.J., Ma, V.P., Cheng, Z., Chan, D.S., He, H.Z., Leung, K.H., Ma, D.L., Leung, C.H., 2012. Discovery of a natural product inhibitor targeting protein neddylation by structure-based virtual screening. Biochimie 94, 2457-2460.

Zhu, L., 2010. Skp2 knockout reduces cell proliferation and mouse body size: and prevents cancer? Cell research 20, 605-607.

7. Appendix

7.1 List of Abbreviations

aa	amino acid
APS	Ammonium persulfate
BAP1	BRCA1 associated protein 1
bp	base pair
BSA	Bovine serum albumin
C	Cytosolic
CAND1	Cullin-Associated and Neddylation-Dissociated 1
Cdk	Cyclin dependent kinase
CHX	Cycloheximide
CRL	Cullin Ring Ligases
CSN	COP9 signalosome
DMSO	Dimethylsulfoxide
E3	E3 ligase
FBP	F-box protein
FCS	Fetal calf serum
FFPE	Formalin-fixed, paraffin-embedded tissue
FIPA	Familial isolated pituitary adenoma
G	Tumor grade
HIF-1α	Hypoxia inducible factor 1α
IP	Immunoprecipitation
MEN1	Multiple endocrine neoplasia 1
MS	Mass spectrometry
N	Nuclear
NEDD8	Neural precursor cell expressed, developmentally down-regulated 8
Nrf2	Nuclear factor (erythroid-derived 2)-like 2
p27I119T	p27 protein mutated on position 119 leading to isoleucin to threonin exchange
p27mut	p27 protein mutants
p27V109G	p27 protein mutated on position 109 leading to valin to glycin exchange
p27wt	p27 wild type protein
PD	Pull down
pT	Pathological tumor stage
RCC	Renal cell carcinoma
RING	Really interesting new gene
S	Substrate
SDS-PAGE	Sodium auryl sulphate Polyacrylamid gelelectrophorese
Skp2	S-phase kinase-associated protein
SNP	Single nucleotide polymorphism
TMA	Tissue Micro Array
Ub	Ubiquitin
UPS	Ubiquitin Proteasome System
VHL	von Hippel Lindau protein

7.2 List of Figures

7.3 List of Tables

7.4 Declaration

Eidesstattliche Erklärung

Hiermit erkläre ich, die Dissertation selbstständig und nur unter Verwendung der angegebenen Hilfen und Hilfsmittel angefertigt zu haben. Ich habe mich anderwärts nicht um einen Doktorgrad beworben und besitze einen entsprechenden Doktorgrad nicht. Ich erkläre die Kenntnisnahme der dem Verfahren zugrunde liegenden Promotionsordnung der Lebenswissenschaftlichen Fakultät der Humboldt-Universität zu Berlin vom 05. März 2015.

Linda Gummlich

Berlin, Januar 2016

7.5 Bibliography

Publications

Gummlich L, Rabien A, Jung K, Dubiel W. Deregulation of the COP9 signalosome-cullin-RING ubiquitin-ligase pathway with emphasis on urological cancers, *The International Journal of Biochemistry and Cell Biology*, 2013 Jul;45(7):1327-37.

Wotschowsky Z, **Gummlich L**, Liep J, Carsten S, Ergin K, Klaus J, Billaud J, Meyer H. Integrated microRNA and mRNA Signature Associated with the Transition from Locally Confiend to the Metastasized Clear Cell Renal Cell Carcinoma Exemplified by miR-146-5p. PLOS ONE (accepted January 2016)

Gummlich L, Jung K, Dubiel W. 'Insight into the mechanism for deregulation of COP9 signalosome-cullin-RING ubiquitin-ligase pathway in urological neoplasia'. *International Review of Cell and Molecular Biology.* (accepted December 2015)

Awards

Poster Award: **Gummlich L**, Kilic E, Jung K, Dubiel W. Deregulation of the CSN-CRL pathway during urological tumorigenesis? 5. Symposium "Urologische Forschung der Deutschen Gesellschaft für Urologie", Gießen, 14.-16.11.2013

Talks

Gummlich L, Kähne T, Jung K and Dubiel W. Two $p27^{Kip1}$ mutations in renal carcinoma and their possible link to the CSN-CRL pathway. *Making walls history - Overcoming treatment barriers in cancer Meeting*. Berlin, 05.-06.6.2015

Gummlich L, Jung K, Dubiel W. Two $p27^{Kip1}$ mutations in renal carcinoma and their possible link to the CSN-CRL pathway. *Annual DGF Meeting*, Berlin-Zeuthen, 06.-08.5.2015

Gummlich L, Kilic E, Jung K, Dubiel W. Characterization of the CSN-CRL pathway in urological cancers. *Annual DGF Meeting*, Berlin-Zeuthen, 22.-24.5.2013

Posters

Gummlich L, Kilic E, Jung K, Dubiel W. Two $p27^{Kip1}$ mutations in renal carcinoma and their possible link to the CSN-CRL pathway. **8. ZOMES-Konferenz**, Xiamen, China, 17.-21.11.2014

Gummlich L, Kilic E, Jung K, Dubiel W. Two $p27^{Kip1}$ mutations in renal carcinoma and their possible link to the CSN-CRL pathway**. 6. Symposium** "Urologische Forschung der Deutschen Gesellschaft für Urologie", Homburg, 13.-15.11.2014/ *Der Urologe* 1, 2015 118:128

Gummlich L, Kilic E, Jung K, Dubiel W. Deregulation of the CSN-CRL pathway during urological tumorigenesis? **5. Symposium** "Urologische Forschung der Deutschen Gesellschaft für Urologie", Gießen, 14-16.11.2013/ *Der Urologe* 1, 2014, 53:110

Gummlich L, Kilic E, Jung K, Dubiel W. Characterization of the CSN-CRL pathway in urological cancers. **The Ubiquitin Family Meeting**, Cold Spring Harbor, USA, 14.-18.5.2013

Gummlich L, Kilic E, Stephan C, Rabien A, Jung K, Dubiel W. COP9 signalosome and components of the CRL complex in urological cancers. **4. Symposium** "Urologische Forschung der Deutschen Gesellschaft für Urologie": Individualisierte Medizin: möglich, sinnvoll, machbar? Berlin, 08.-10.11.2012/ *Der Urologe* 1, 2013, 52:105

Gummlich L, Kilic E, Jung K, Dubiel W. COP9 Signalosopme and components of the CRL complex in urological cancer. **7. ZOMES-Konferenz**, München, 18.-21.9.2012